View metadata, citation and similar papers at core.ac.uk

brought to you by CORE

provided by University of Tennessee, Knoxville: Trace

University of Tennessee, Knoxville

TRACE: Tennessee Research and Creative Exchange

Doctoral Dissertations

Graduate School

5-2008

Contribution of Water and Energetics of Ligand Binding in the Catalytic Mechanism of R67 Dihydrofolate Reductase

Shaileja Chopra
University of Tennessee - Knoxville

Follow this and additional works at: https://trace.tennessee.edu/utk_graddiss

 Part of the Biochemistry, Biophysics, and Structural Biology Commons

Recommended Citation

Chopra, Shaileja, "Contribution of Water and Energetics of Ligand Binding in the Catalytic Mechanism of R67 Dihydrofolate Reductase. " PhD diss., University of Tennessee, 2008.
https://trace.tennessee.edu/utk_graddiss/337

This Dissertation is brought to you for free and open access by the Graduate School at TRACE: Tennessee Research and Creative Exchange. It has been accepted for inclusion in Doctoral Dissertations by an authorized administrator of TRACE: Tennessee Research and Creative Exchange. For more information, please contact trace@utk.edu.

To the Graduate Council:

I am submitting herewith a dissertation written by Shaileja Chopra entitled "Contribution of Water and Energetics of Ligand Binding in the Catalytic Mechanism of R67 Dihydrofolate Reductase." I have examined the final electronic copy of this dissertation for form and content and recommend that it be accepted in partial fulfillment of the requirements for the degree of Doctor of Philosophy, with a major in Biochemistry and Cellular and Molecular Biology.

Elizabeth E. Howell, Major Professor

We have read this dissertation and recommend its acceptance:

Ronald B. Wetzel, Engin H. Serpersu, John W. Koontz, Elias J. Fernandez

Accepted for the Council:

Carolyn R. Hodges

Vice Provost and Dean of the Graduate School

(Original signatures are on file with official student records.)

To the Graduate Council:

I am submitting herewith a dissertation written by Shaileja Chopra entitled "Contribution of Water and Energetics of Ligand Binding in the Catalytic Mechanism of R67 Dihydrofolate Reductase." I have examined the final electronic copy of this dissertation for form and content and recommend that it be accepted in partial fulfillment of the requirements for the degree of Doctor of Philosophy, with a major in Biochemistry, Cellular and Molecular Biology.

Elizabeth E. Howell

Major Professor

We have read this dissertation
and recommend its acceptance:

Ronald B. Wetzel

Engin H. Serpersu

John W. Koontz

Elias J. Fernandez

Accepted for the Council:

Carolyn R. Hodges

Vice Provost and Dean
of the Graduate School

(Original signatures are on file with official student records)

Contribution of Water and Energetics of Ligand Binding in the Catalytic Mechanism of R67 Dihydrofolate Reductase

A Dissertation
Presented for the
Doctor of Philosophy Degree,
The University of Tennessee, Knoxville

Shaileja Chopra
May 2008

Dedication

This thesis is dedicated to my mother, Mrs. Neelam Chopra for her prayers for my well-being and happiness, and to my father, Dr. Vinod Chopra for showing me the way.

Acknowledgements

I would like to express my gratitude to my advisor, Dr. Elizabeth Howell for giving me the opportunity to work in her lab. Under her guidance, not only did I gain the knowledge and skill to work in a research laboratory, but I also learned to be persistent in my efforts even in the most difficult of situations. I know these lessons will hold me in good stead in the future. I would also like to thank my committee members Dr. Ronald Wetzel, Dr. John Koontz, Dr. Engin Serpersu and Dr. Elias Fernandez for their valuable advice.

I would like to extend many thanks to the several past members of the Howell lab; notably Stephanie Hicks, Lori Stinnett, Derike Smiley, Michael Jackson and Brad Strader for their help during my time in the lab. I also want to thank Russ Dooling for his invaluable assistance with some of my experiments ands for making the lab atmosphere more fun and lively. I have always enjoyed our conversations, and will cherish them for a long time to come.

I am very grateful to my parents, Neelam and Vinod Chopra for their hard work and many sacrifices, without which I would not have been where I am today, and for always supporting all my decisions including the one for pursuing graduate studies in the United States. I also cannot thank my dear sister Swati enough for being my pillar of support throughout and for giving me a boost of energy and confidence every time I found myself feeling dejected.

I would like to acknowledge Dr. Subrata Tripathi at the Tata Institute of Fundamental Research, India for his guidance and for encouraging me to pursue graduate studies in the United States.

I made quite a few friends during the time spent at the University of Tennessee (UT), and I thank them all for their wonderful friendship, and for making me feel at home. Of them, I would like to

give special thanks to; Srilalitha Kuruganti, who has been a great friend and with whom I could discuss anything and everything. I would also like to thank Ashraf Jahangeer for introducing me to the various activities around the university and Shambhunath Choudhary for accompanying me to the lab for late night ITC experiments. These and several other friends made my stay in Knoxville so very memorable.

Lastly, a very special thank you to my husband and best friend, Sarat, who patiently tolerated my ranting on and about everything under the sun! Thank you for your love and support, and for being such a wonderful companion.

Abstract

R67 dihydrofolate reductase (DHFR) catalyzes the transfer of a hydride ion from NADPH to dihydrofolate (DHF) to produce tetrahydrofolate (THF). The enzyme is a homotetramer and its 222 symmetry allows for binding of both ligands to a single active site pore. A productive ternary complex is formed by the binding of one molecule of DHF and NADPH and inter-ligand cooperativity has been suggested to be essential for binding and catalysis. To gain further insight into the thermodynamics involved in the ground state and the transition state, temperature dependent studies on DHF binding and catalysis were performed. It was observed that binding of both NADPH and DHF is enthalpy driven. From van't Hoff plots, the change in enthalpy, entropy and free energy for NADPH binding to R67 DHFR in the ground state were determined. Similarly, the thermodynamics of DHF binding to the R67 DHFR-NADPH complex in the ground state were determined. Arrhenius plots were also employed to study the energetics of the transition state. A comparison of TdeltaS values (for DHF binding to R67 DHFR-NADPH complex) in both ground state and transition state indicates that TdeltaS is more negative in the transition state (–11.3 kcal/mol) as compared to the ground state (–5.4 kcal/mol). This indicates a reorientation of the substrate in the transition state.

The role of water in DHF and NADPH binding to R67 DHFR was also investigated. For this, the effect of osmotic pressure on the K_a /K_m of ligand binding, as well as the k_{cat} of the reaction was studied. It was observed that the k_{cat} of the reaction was not significantly affected, while the binding of ligands was affected with increasing osmolality. Specifically, binding of NADPH tightened as osmolality increased, while binding of DHF weakened with increasing osmolality, suggesting release of water upon NADPH binding and an uptake of water on DHF binding. Results from *in vivo* experiments on *E.coli* cells containing wild type and mutant clones of R67 DHFR were also consistent with *in vitro* experiments, suggesting that water is involved in ligand binding to R67 DHFR.

Preface

R67 Dihydrofolate reductase (DHFR) catalyzes the NADPH dependent reduction of dihydrofolate (DHF) to tetrahydrofolate (THF). The enzyme is a homotetramer with 222 symmetry that has a single active site pore 24 Å long and 18 Å wide traversing the length of the protein. The promiscuous binding surface of the active site can accommodate two ligands that enter the pore from opposite ends. Binding of two DHF or two NADPH molecules results in the formation of non-productive complexes, while a productive ternary complex is formed when one molecule of DHF and one molecule of NADPH bind. X-ray crystallography and NMR spectroscopy studies indicate that the pteridine ring of DHF adopts a fixed position, while the pABA-glutamate tail is disordered. Additionally, the cofactor NADPH binds in a relatively fixed position.

The first goal of this research was to investigate the thermodynamics of ligand binding in the ground state and transition state. For this, ligand binding and catalysis was monitored as a function of temperature. Binding of both NADPH and DHF is enthalpy driven. Also, recent primary isotope effect studies indicate hydride transfer is the rate-determining step. From van't Hoff plots, the ΔH, $T\Delta S$ and ΔG for NADPH binding to R67 DHFR in the ground state were determined to be -8.6 kcal/mol, -1.1 kcal/mol and –7.5 kcal/mol respectively. Similarly, ΔH, $T\Delta S$ and ΔG for DHF binding to the R67 DHFR•NADPH complex in the ground state were determined to be -13.3 kcal/mol, -5.4 kcal/mol and –7.9 kcal/mol respectively. Using Arrhenius plots, the activation energy associated with the transition state ($[\text{R67 DHFR}\bullet\text{NADPH}\bullet\text{DHF}]^{\ddagger}$) was determined to be 6.9 kcal/mol, corresponding to a ΔH of 6.3 kcal/mol. Also, $T\Delta S$ and ΔG associated with the transition state were –11.3 kcal/mol and 17.6 kcal/mol. A comparison of $T\Delta S$ values from both ground state and transition state indicates that $T\Delta S$ is more negative in the

transition state (–11.3 kcal/mol) as compared to the ground state (–5.4 kcal/mol), indicating a reorientation of the substrate in the transition state.

In order to understand the role of the glutamate tail of DHF, dihydropteroate (an analog of DHF lacking the para-aminobenzoyl-glutamate tail (pABA)) also was used. A weaker binding affinity was observed as compared to DHF ($\Delta\Delta G$ = 1.9 kcal/mol), along with a large loss in the binding enthalpy value ($\Delta\Delta H$ = 6.4 kcal/mol). Additionally, the k_{cat} value for dihydropteroate reduction is decreased 1600-fold compared to DHF usage. This result suggested that the pABA-glutamate tail of DHF is important for catalysis.

The second goal of this research was to investigate the role of water in DHF and NADPH binding to R67 DHFR. For this, the protein was subjected to osmotic pressure using different osmolytes. Steady state kinetics as well as isothermal titration calorimetry experiments were employed to determine the effect of osmotic pressure on the K_a of ligand binding as well as the k_{cat} of the reaction. It was observed that the k_{cat} of the reaction was not significantly affected with the addition of osmolytes. For NADPH binding, the K_a increased as osmolality went higher. Similar effects were observed using a range of osmolytes, where NADPH binding is accompanied by a net release of 38 water molecules. In contrast, DHF binding weakened as osmolality increased, suggesting that water stabilizes DHF binding. The net number of water molecules taken up by DHF binding varied, which may possibly be due to the different binding modes of the disordered pABA-glutamate tail. *In vivo* experiments were also used to probe the sensitivity of ligand binding to change in water activity. Using the antibacterial drug trimethoprim, as a selection for R67 DHFR, it was demonstrated that increasing concentrations of in media containing sorbitol resulted in decreased catalytic efficiency of *E.coli* cells containing wild type and mutant clones of

R67 DHFR. These results are consistent with *in vitro* experiments, suggesting that water is involved in ligand binding in R67 DHFR.

Table of Contents

List of Tables

Part II

Part III

Part IV

List of Figures

Part I

Part II

Part III

Part III

Figure **Page**

Part IV

Figure **Page**

List of Abbreviations and/or Symbols

DHFR	Dihydrofolate reductase
R67 DHFR	R67 Dihydrofolate reductase
TS	Thymidylate synthase
DHF	7, 8-Dihydrofolate
THF	5, 6, 7, 8-Tetrahydrofolate
pABA-glu	para-aminobenzoylglutamate
Fol	folate
DHP	7,8-Dihydropteroate
DHB	7,8 Dihydrobiopterin
PG2	Pteroyldi- γ-L-glutamate
PG5	Pteroylpenta- γ-L-glutamate
NADPH	Nicotinamide adenine dinucleotide phosphate (reduced form)
$NADP^+$	Nicotinamide adenine dinucleotide phosphate (oxidized form)
NMN	Nicotinamide mononucleotide
MTX	Methotrexate
TMP	Trimethoprim
PMT	Pyrimethamine
H	Hydrogen (^1H)
D	Deuterium (^2H)
EDTA	Ethyl-diamine-triacetic acid
HCl	Hydrochloric acid
PEG	Polyethylene glycol
HEPES	4-(2-Hydroxyethyl) piperazine-1-ethanesulfonic acid
MES	2-(*N*-morpholino)ethanesulfonic acid
Tris	Tris (hydroxymethyl) aminoethane
MTH/ MTA	100 mM Mes, 50 mM Tris, 100 mM acetic acid
TE	10 mM Tris, 1 mM EDTA
NMR	Nuclear magnetic resonance
MALDI	Matrix-assisted laser desorption ionization
ESI	Electrospray ionization
MS	Mass spectrometry
MD	Molecular dynamics
ITC	Isothermal titration calorimetry
FPLC	Fast pressure liquid chromatography
R.M.S.D.	Root mean square deviation
DMSO	Dimethyl sulfoxide
TMAO	Tri-methylamine-oxide
WHAM	Weighted histogram analysis method
QM	Quantum mechanics
MM	Molecular mechanics
$TS^‡$	Transition state
M	Molar
Mg	milligram (10^{-3} gram (g))
Ml	milliliter (10^{-3} liter (l))
Mm	millimeter (10^{-3} meter (m))

Mm	micrometer (10^{-6} m)
s/ sec	second; unit of time
°C	Degree Celsius
°K	Degree Kelvin
RT	Room temperature
Å	Angstrom (10^{-8} cm)
KDa	KiloDalton (10^{3} Da)
A	Alpha
B	Beta
γ	Gamma
D	Dielectric constant
Ps	Picoseconds
ρ	Density
η	Viscosity
η/ρ	Kinematic viscosity
V_{mol}	Molar volume
ΔC_p	Heat capacity
ASA	Solvent accessible surface area
ν_{H2O} and ν_S	Stoichiometric coefficients of water and osmolyte
Δn_w	Net number of waters taken up or released upon Binding.
K_d	Dissociation constant (Binding)
K_m	Michaelis Menten constant
K_i	Inhibition constant
k_{cat}	Catalytic rate constant
ε	Molar extinction coefficient

Part I: Introduction To R67 Dihydrofolate Reductase: An Overview Of The Structure And Function Of The Enzyme.

General Introduction To Dihydrofolate Reductases

Folic acid intake is essential during cell division and growth as it is required for nucleic acid synthesis in both prokaryotes and eukaryotes. One of the biologically active forms of folic acid is methylene-tetrahydrofolate which is used by thymidylate synthase to methylate dUMP to produce dTMP and dihydrofolate (DHF). The dTMP is then used for nucleic acid biosynthesis. Thus, a deficiency of folic acid hinders DNA synthesis and cell division. The DHF product is further reduced by dihydrofolate reductase (DHFR) to form tetrahydrofolate (THF). THF is essential for the synthesis of thymidylate, purine nucleosides, methionine and other metabolic intermediates. Due to its important metabolic role, DHFR has been extensively studied and is the target for a number of inhibitors (antifolates). For example, methotrexate is one of the anticancer drugs that have been developed to inhibit DHFR. Trimethoprim is another drug targeted against DHFR used in combination with sulfonamides to block nucleic acid biosynthesis.

R-Plasmid Dihydrofolate Reductases

Clinical studies have shown that certain strains of *Escherichia coli* and *Klebsiella aerogenes* can grow in the presence of high levels of trimethoprim. This resistance is imparted by plasmids called R-factors (*1*). On the basis of their sensitivity to TMP, seventeen different types of R-plasmid encoded DHFRs have been discovered so far, namely types I-XVII (*2*).

Of these, the type II R-plasmid encoded DHFRs provide the most resistance to trimethoprim and are also weakly inhibited by methotrexate. The type-II family has 3 members: R67, R388 and R751 DHFRs. They share greater than 78% sequence identity, differing from each other only at the N-terminus (first 21 residues) (*1*, *3*, *4*).

Structure Of Chromosomal DHFR

Chromosomal DHFR has a molecular weight of 18,000 Daltons and is a monomer (159 amino acids) with an eight–stranded β-sheet core and with 4 α-helices packing against the β-strands (figure 1A). There is a hinge region between two domains (*5-7*). The enzyme contains a single active site with specific binding pockets for the substrate, DHF, and the cofactor, NADPH. Some of the conserved active site residues include M20, P21, W22, D27, F31, R44, R57, G75, G96 and T113 (*8-10*). Of these, the M20 residue is present in a flexible loop that connects the A strand of the β-sheet with α-helix B (figure 1A). The conformational change of the loop from closed to occluded to open is a part of the catalytic cycle (*11, 12*). The reaction mechanism involves binding of DHF followed by transfer of a proton and hydride. This is then followed by the release of $NADP^+$, binding of NADPH and finally the release of THF (*13*). This catalytic cycle is therefore facilitated not only by the movement of the M20 loop, but also sub-domain movement (*14*).

Structure Of R67 DHFR

R67 DHFR is a 34 KDa protein that is active as a homotetramer (with each subunit of 78 amino acids) as shown in figure1B. At a low pH, the active homotetramer dissociates into 2 inactive dimers, indicating an equilibrium between the active homotetrameric form and the inactive dimeric form (*15*). The first crystal structure was of dimeric DHFR and a weak electron density was observed around the first 17 amino acids (*7*). Later, Narayana et al. solved the crystal structure at 1.7Å resolution with the first 16 amino acids cleaved off by chymotrypsin (pdb file 1VIE) (*16*). The N-terminal truncation however does not result in any loss of activity (*17*). The enzyme possesses 222 symmetry with a central pore that is 25Å long, 18Å wide and 12Å thick. This is unusual as there is only one active site per tetramer. Each subunit of the tetramer is a β-

Figure 1: Structures of Chromosomal (from *E.coli*) and R67 DHFR A) Structure of *E. coli* DHFR bound to the inhibitor methotrexate (MTX) and NADPH (PDB: 3DFR): The β-sheets are in yellow and the α-helices packing against them are in purple. The different loop regions (along with Met 20 loop) are represented in cyan. The aspartate 27 residue in the active site is shown in white. B) Ribbon diagram of R67 DHFR (PDB: IVIE). Four monomers (green, pink, ochre and violet) join to form a homotetramer, with a large active site pore in the center. The monomer-monomer interfaces occur between pink and green (or ochre and violet) subunits. The dimer-dimer interfaces occur between green and violet (or pink and ochre) subunits.

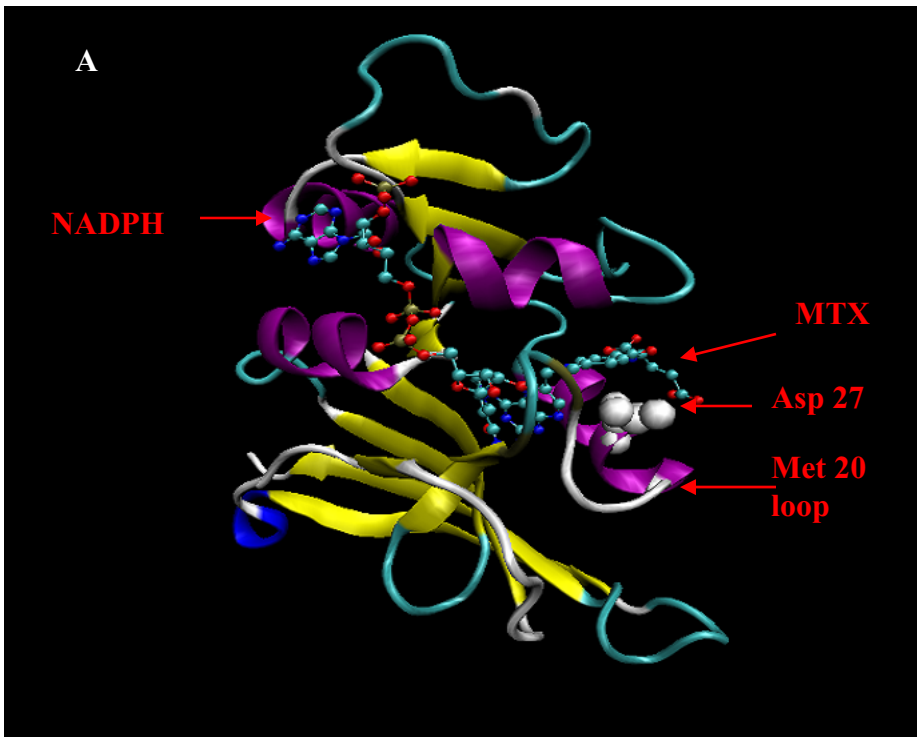
A
NADPH
MTX
Asp 27
Met 20
loop

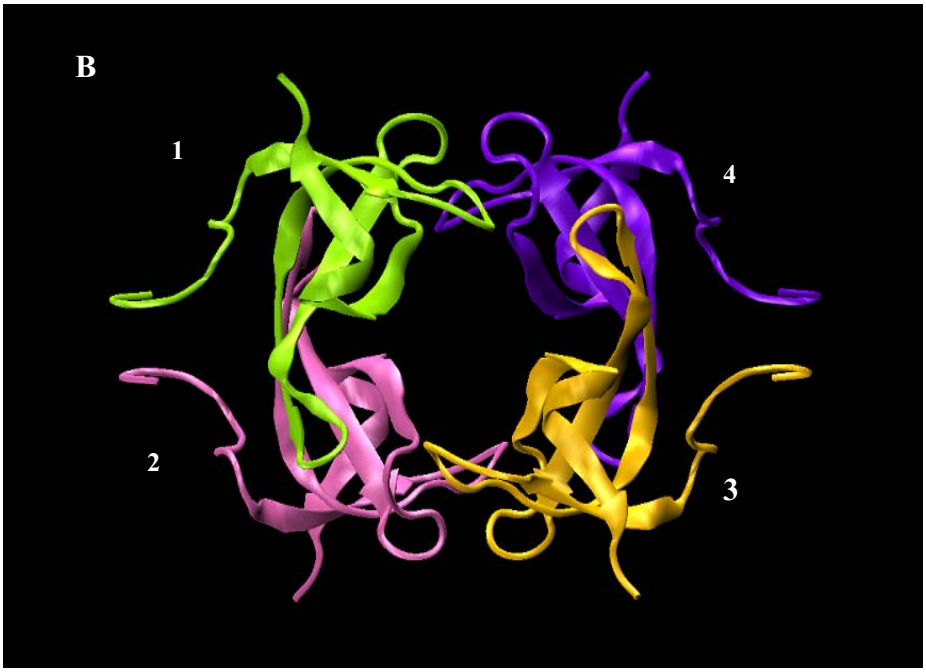
B
1
4
2
3

barrel made up of 5 antiparallel β-strands (residues 28-32, 38-47, 54-59, 65-70 and 74-76). The enzyme is dimer of dimers. The monomer-monomer interfaces are stabilized by an intersubunit 6-stranded β-barrel structure. The dimer-dimer interfaces are stabilized by loop-loop interactions. Symmetry related histidine 62 residues occur at these interfaces and their protonation leads to tetramer destabilization and dimer formation. The dimer-dimer interface is also stabilized by hydrogen bonding interactions between histidine 62 and related serine 59 residues (*15, 18*). Another crystal structure is the binary complex with folate (1VIF) (*16*). The Fourier map of the binary complex and apoenzyme are isomorphous which suggests that no conformational change occurs upon folate binding. The electron density was fit to two asymmetrically bound molecules of folate, the first with Fol1 bound with its *si* face exposed towards the center of the pore and the other orientation with Fol2 bound with its *si* face facing the protein surface. Fol1 describes a productive orientation as it agrees with the stereochemistry of the hydride transfer reaction.

The central, hourglass shaped pore is comprised of the loop region between β-strands of monomer 1 and 2 (residues 30-40), monomer 2 and 3 (residues 44-55) and the region of β-strand of monomer 4 (residues 63 to 74). Residues K32, A36, Y46, T51, G64, S64, V66, G67, I68 and Y69 from each subunit make up the active site pore. Of these, S65, V66, Q67, I68 and Y69 comprise 47% of the surface area of the active site pore. Gln67 and its symmetry related residues are present at the dimer-dimer interfaces and form the floor and ceiling of the pore. I68 and its symmetry related partners form interacting pairs at the sides of the pore.

Recently, another crystal structure of truncated apo R67 DHFR was solved by Narayana (*19*). This structure was solved at cryo-cooling conditions (100^{o}K) and had a resolution of 1.1 Å. The electron density of this structure agreed with the earlier structure at 277^{o}K. However, the side chains of S20, N21, R29, R31, K32, Q41, W45, Q67, L74, E75 and N78 residues appeared in

slightly different conformations, indicating flexibility in these regions. The volume of the central hourglass shaped pore is 2600 $Å^3$, with a total of 168 water molecules in the pore. These water molecules are well ordered and form a network of hydrogen bonds with an array of fixed pentagonal rings.

Ligand Binding To R67 DHFR

The 222 symmetry in the structure of R67 DHFR suggests that four identical sites could theoretically be used for binding of ligands. The ligand binding properties of R67 DHFR were evaluated using fluorescence anisotropy and isothermal titration calorimetry techniques (*20*). It was observed that R67 DHFR forms three different types of ligand complexes: either 2 NADPH molecules, or 2 DHF molecules, or one molecule of each NADPH and DHF (structures shown in figure 2A and 2B). This suggested that even though there are four identical binding sites, they cannot be occupied simultaneously due to steric hindrance. The binding of two DHF molecules exhibits positive cooperativity, whereas the binding of two NADPH molecules shows negative cooperativity (figure 2C). A productive complex is formed when 1 molecule of folate binds to a 1:1 mixture of R67 and NADPH (*21*).

To gain further insight into the ternary structure of R67 DHFR, Li et al. used transferred NOE (Nuclear Overhauser Effect) and Interligand NOE (ILOE) experiments with bound $NADP^+$ and folate (*22*). They found that the ribonicotinamide bond of cofactor adopts a *syn* conformation, while glycosidic bond of the adenosine moiety adopts an *anti* conformation. This is in contrast to all other reductases in which the ribonicotinamide bond adopts an anti conformation ((*23*) and references therein). Also, strong ILOEs were observed between the H4 and H5 protons of the nicotinamide ring and the H9 protons of folate. In order to determine the orientation of the

Figure 2: The structures of Folate and NADPH and the proposed binding mechanism of R67 DHFR A) Folate is comprised of the pteridine ring and para-amino benzoyl glutamate (pABA-glu) tail. In dihydrofolate (DHF), the C7-N8 double bond is reduced. B) The cofactor, NADPH, has the NMNH (nicotinamide mononucleotide) moiety that transfers a hydride (H_R) from C4 of the nicotinamide ring to C6 of DHF. C) Isothermal titration calorimetry (ITC) and time resolved fluorescence anisotropy experiments were used to determine the mechanism of binding of substrate (DHF) and cofactor (NADPH) to the enzyme. The preferred path is shown in bold, where NADPH binds to the enzyme followed by DHF (*20*).

A

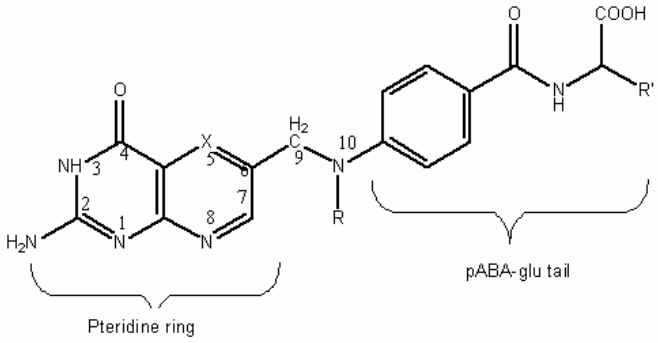
Pteridine ring
pABA-glu tail

B

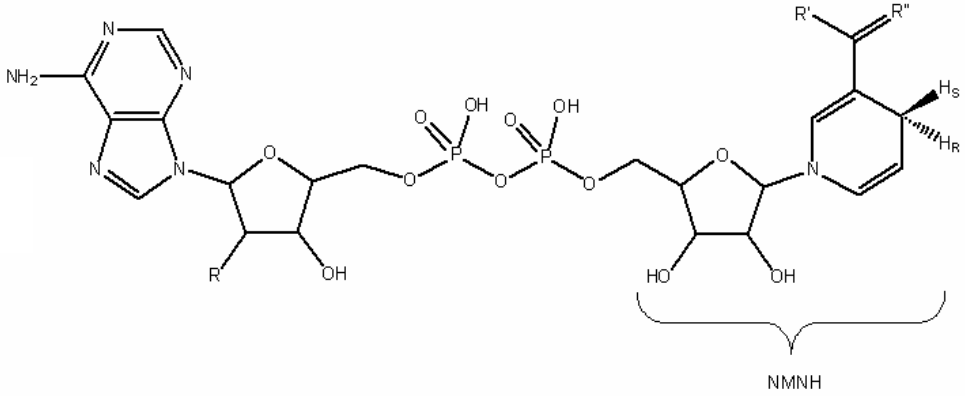
NMNH

C

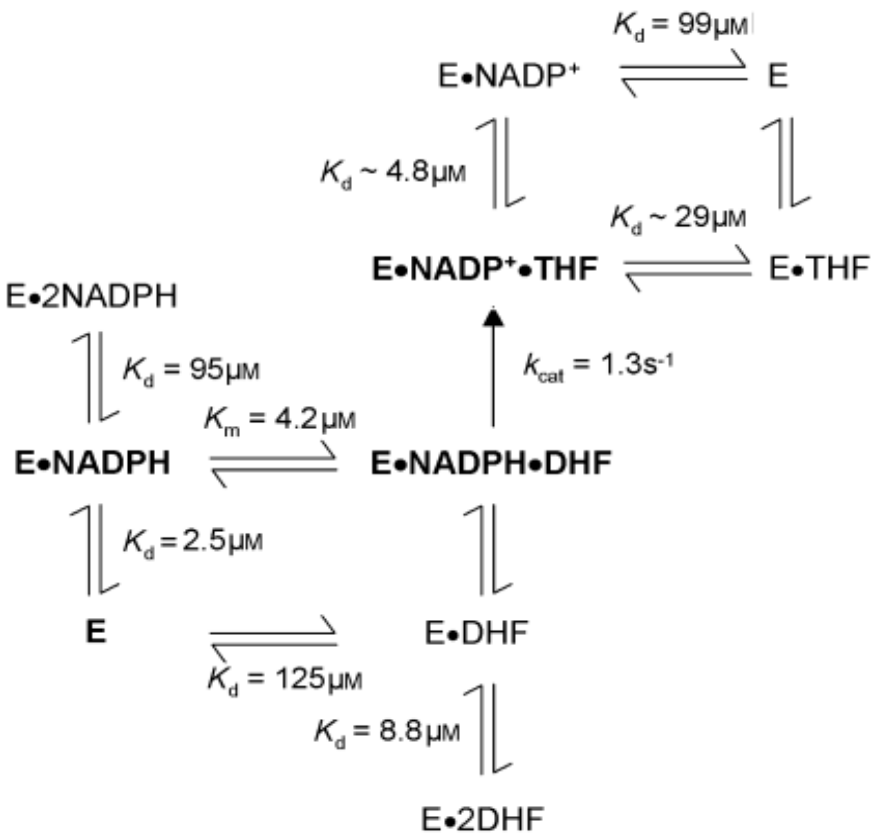
E•NADP+
E
E•NADP+•THF
E•THF
E•2NADPH
E•NADPH
E•NADPH•DHF
E
E•DHF
E•2DHF

substrate and cofactor in the active site, a folate analog 2-*d*eamino-2-*m*ethyl-5,8-*did*eaza*f*olate (DMDDF) was employed. The advantage of using this analog is that it contains more protons as compared to folate and would therefore increase the possibility of obtaining stronger NOE signals. The results suggest that folate and $NADP^+$ molecules enter from either side of the pore, and the pteridine and nicotinamide rings meet at the middle. Ring stacking is observed supporting an *endo* transition state geometry (*24*). This is in contrast to the chromosomal enzyme, where the ligands adopt an edge on or *exo* conformation (figure 3).

To gain further insight into the orientation of the bound cofactor, Pitcher et al. labeled R67 DHFR with ^{13}C and ^{15}N (*25*). Then using Heteronuclear single-quantum coherence spectroscopy (HSQC), changes in the chemical shifts of the amide groups upon titration of either folate or $NADP^+$ were determined. The general observation was that amides exhibiting the biggest chemical shift were the residues lining the active site pore. These include K32, K33, G35, E39, S59, E60, A61, G64, S65, V71, A72, A73 and L74 residues.

To obtain more information on the orientation of $NADP^+$ bound to the enzyme, transfer NOE experiments were also performed (*25*). While a direct observation of NOEs between $NADP^+$ and the enzyme was not observed (*25*), stronger NOEs were observed in the presence of folate (between the nicotinamide H4 and H5 protons and the H9 protons of folate). These results possibly suggest that the structure of $NADP^+$ would be more constrained in the presence of folate. It was also proposed that the adenine base of $NADP^+$ is positioned near the pore, while the phosphate group of the adenosine extends into the pore and forms interactions with a lysine 32 residue. This is consistent with R67 DHFR having a preference for binding to NADPH as compared to NADH. Another observation was that there was a slow conversion of $NADP^+$ to NAD^+ upon binding to the enzyme. This indicates that R67 DHFR possesses a phosphatase

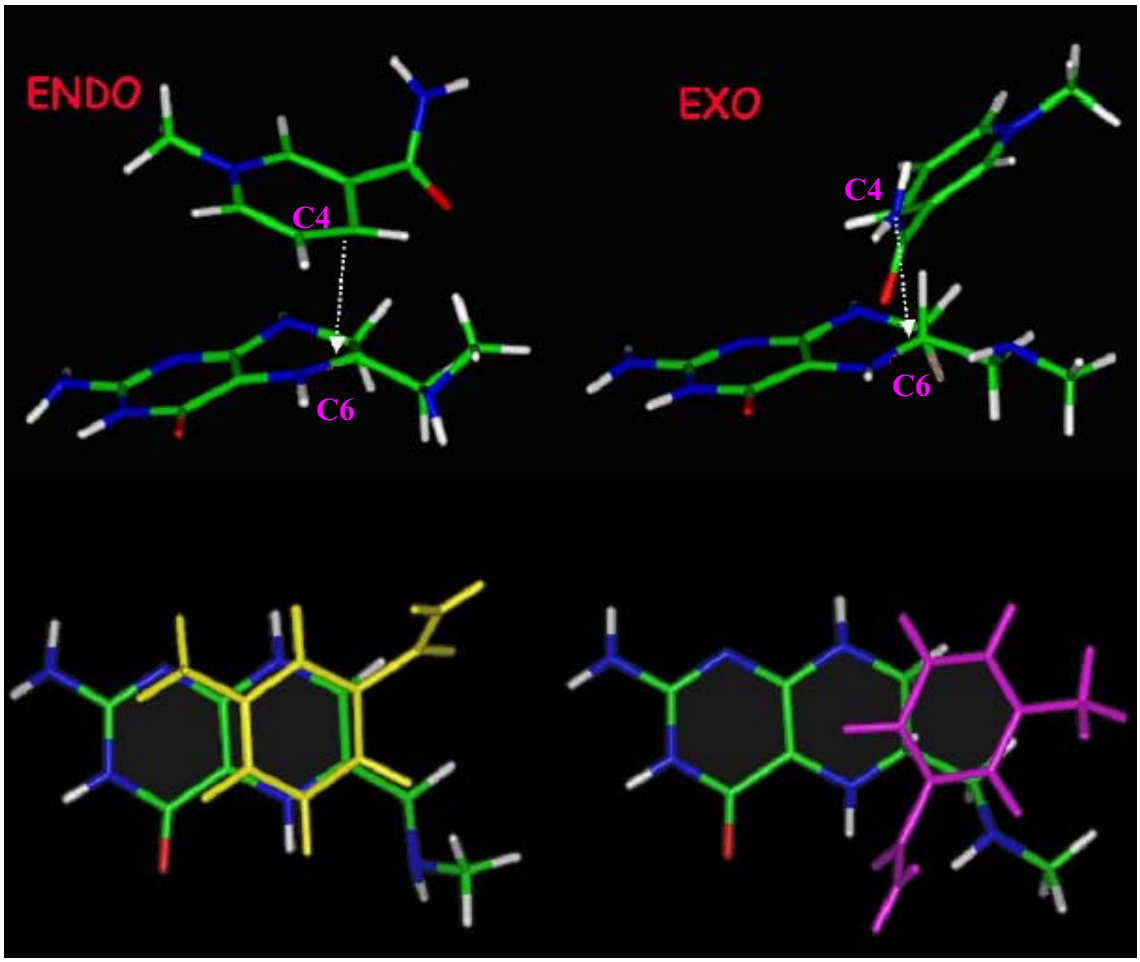

Figure 3: *Endo* (left) and *Exo* (right) orientations of the transition states. *Ab initio* quantum mechanical calculations have been used to determine the geometry of hydride transfer from the C4 (red) position of the nicotinamide ring to the C6 (magenta) position of the pteridine ring. Results obtained suggested that the *endo* transition state is more stable than the *exo* transition state by 2-8 kcal/mol (*26*). Maximum overlap of the nicotinamide ring (yellow) with the pteridine ring occurs in the *endo* transition state. Very little overlap between the nicotinamide ring (purple) and pteridine ring is seen in the *exo* transition state (*27*).

activity. Also, a transhydrogenase activity was observed, indirectly indicating that R67 DHFR can bind two cofactor molecules.

Since the orientation of NADPH in the active site pore was not well understood, the crystal structure of R67 DHFR with bound Fol1 (*16*) was used as a template to dock the nicotinamide ribose-phosphate moiety (NMNH) of NADPH (*26*). This study used the DOCK 4.0 program, which is based on utilizing van der Waals interactions for docking flexible ligands (*28, 29*). Another program, SLIDE (*30, 31*), was also employed, which takes into account ligand and protein side-chain flexibility as well as bound water molecules. First the NMNH moiety of NADPH was docked into the R67 DHFR•Fol1 complex (*20*). Eight out of the top ten docked NMNH conformers docked into the active site in an orientation consistent with previous experimental data (*24*). The top scoring conformers from both DOCK and SLIDE agreed with the ILOE data, which suggests that ligands bind in an extended conformation with no overlap of the tails (*24, 32*) (figure 4). Also, the transition state adopted by the R67 DHFR•Folate•NMNH docked complex is consistent with an *endo* conformation. From the model, several residues were proposed to interact with NMNH. Also a number of residues including A36, Y46, V66, Q67, I68 and Y69 were also predicted to serve dual binding roles. The amphipathic nature of these ligands can allow for making hydrophobic and hydrophilic contacts with the ligands.

Role Of Interligand Interactions In Catalysis

The folate•$NADP^+$•enzyme complex has been probed by NMR and the NOEs (intraligand and interligand) obtained indicate that the ligands bind in an extended conformation in the active site pore (*25*). In addition, stacking between the pteridine (of DHF) and nicotinamide (of NADPH) rings is observed. These interligand interactions appear to play a crucial role in facilitating the

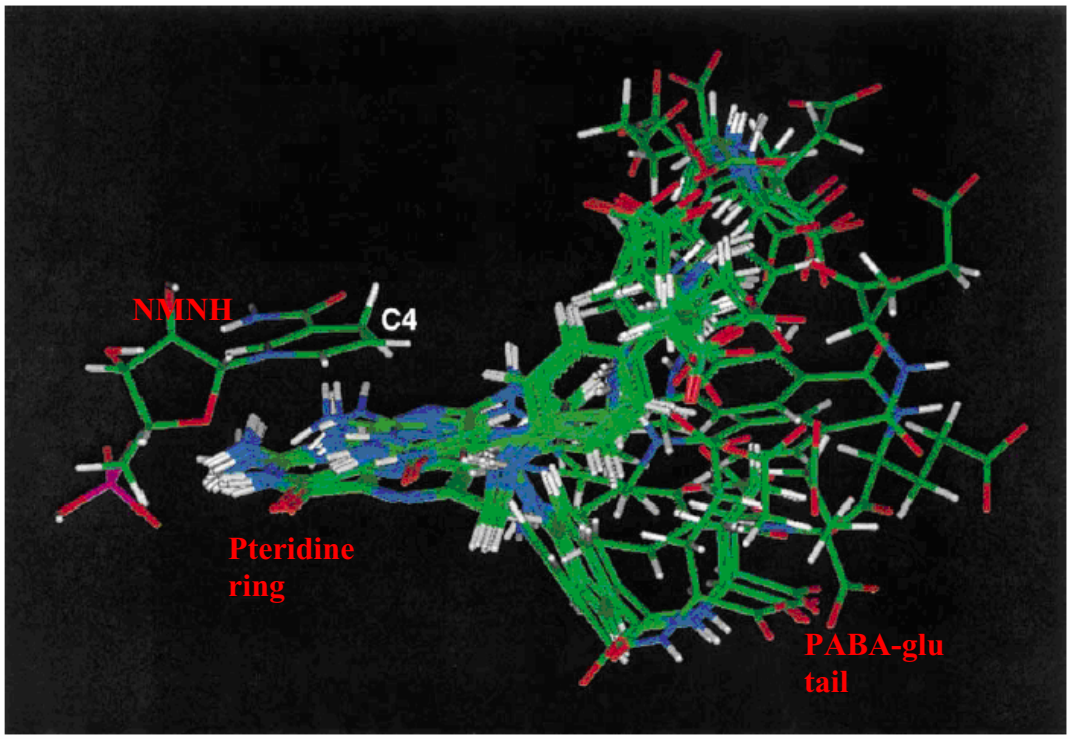

Figure 4: Docking of Folate into R67 DHFR•NMNH complex. The high scoring NMNH conformer (left) was used for generating a model of the ternary complex. The pteridine ring (middle) is mostly in a fixed conformation, which agrees with the Fol1 orientation in the crystal structure. On the other hand, the pABA-glu moiety can be seen to possess numerous potential orientations. For clarity, the enzyme is not shown.

formation of the ternary complex. *Ab initio* quantum mechanical calculations predict that the *endo* transition state is 2-8 kcal/mol more stable than the *exo* transition state (*33*). Also, NMR and docking results predict that R67 uses an *endo* transition state complex in its catalytic mechanism. Therefore, in this enzyme, interligand co-operativity is likely important in transition state formation.

Mechanism Of Hydride Transfer In R67 DHFR

Hydride transfer takes place from the H4 (*re*) atom of NADPH to the C6 atom of DHF. The *si* face of DHF receives the hydride from NADPH (*32*). In order to determine if hydride transfer is the rate-limiting step of the reaction, isotope effect studies were performed. NADPD isotope effects using a H62C mutant of R67 DHFR were used to determine ^{D}V (ratio of k_{cat} in the presence of NADPH and NADPD) at pHs 5.0 and 7.0. The ^{D}V at pH 5.0 was found to be 3.6 and the ^{D}V at pH 7.0 was found to be 3.3 (*34*). Therefore, hydride transfer is at least partially rate limiting for pH 5 to 7. More recent studies by Amnon Kohen indicate that hydride transfer is fully rate determining (personal communication).

Does R67 DHFR Possess A Proton Donor?

In order to determine if R67 possesses a proton donor, a pH profile of R67 DHFR activity was studied. At low pH, the activity of the enzyme decreased due to dimer formation (*34*). Therefore, an H62C mutant was generated so as to covalently link the tetramer at all pH values. A linear increase in activity was observed as the pH decreased to pH 4.5. This suggested that R67 DHFR does not possess a proton donor. The possibility that Y69 residue could be a potential proton donor was also ruled out since it did not show any evidence of a titration upto pH 10 (*34*). To further investigate this model, Raman spectroscopy with DHF bound to R67 DHFR•$NADP^{+}$ was

performed by Deng et al. (*35*). The pK_a for the N5 of bound DHF was less than 5, indicating minimal to no perturbation of its pK_a. Together, these results suggest that R67 DHFR does not possess a proton donor in its active site, but uses a preprotonated substrate to facilitate catalysis. Since the concentration of protonated DHF is low, so is the catalytic rate.

Critical Residues Lining The Active Site Pore

Based on the crystal structure, the residues in the pore have been identified, which include K32, K33, S34, G35, A36, Y46, T48, L50, T51, G64, S65, V66, Q67, I68, Y69, P70 and A73. Of these, S65, Q67, I68 and Y69 make up 47% of the surface in the pore. From the structure, the symmetry related Q67 residues pair with each other as do the I68 side chains. On the other hand, the S65 and Y69 residues are located further away from the 222 symmetry operator and do not form pair-wise interactions. Another critical residue is K32, which is present at the edge of the active site pore and which forms an electrostatic patch with other charged residues such as R31 and K33. Site directed mutagenesis of these residues was previously performed and the results obtained are described below:

1) ***Q67 residue:*** The crystal structure of R67 DHFR with bound folate shows that Q67 forms van der Waals interactions with the pteridine ring of folate (*16*). Also, the symmetry related Q67 residues present on the floor as well as the ceiling of the active site pore (figure 5) interact with their symmetry related partners via hydrogen bonds. To study the role of the Q67 residue, a Q67H mutant was generated (*36*). This mutant binds DHF 36-fold tighter and NADPH 110-fold tighter than the wild type enzyme (*17, 36*), however it is accompanied by severe substrate and cofactor inhibition. The effect of this mutant on binding and catalysis suggests that Q67 is directly involved in binding DHF and NADPH. A recent crystal structure of the R67 DHFR•DHF•$NADP^+$ complex by

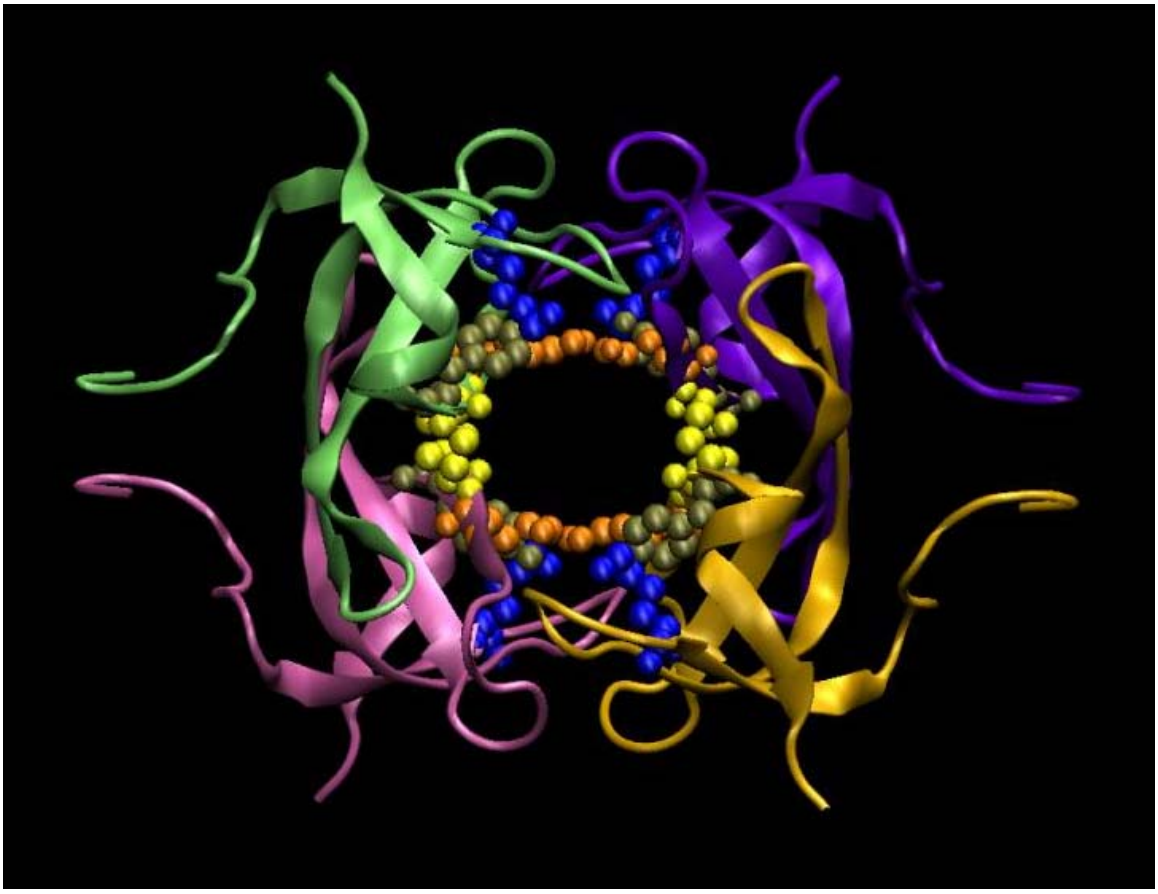

Figure 5: Important residues lining the active site pore of R67 DHFR (PDB: 1VIE). The monomers 1, 2, 3 and 4 are shown in green, pink ochre and violet respectively. Each monomer contains symmetry related K32 (blue), Q67 (orange), I68 (yellow) and Y69 (grey) residues. The K32 residues are present at the edge of the pore, while the Q67 residues form the floor and ceiling of the pore. Additionally, the I68 residues are present at the sides of the pore and the Y69 residues are located near the Q67 residues.

Krahn et al. suggests that binding of substrates causes a change in conformation of Q67 from an extended to a bent conformation (*37*). This also suggests that Q67 is a critical residue involved in ligand binding and catalysis. Therefore, the role of the Q67 residue was further studied using asymmetric mutations as described in the following section.

2) I68 residue: The I68 residues are present at the sides of the pore. From the R67 DHFR•DHF•$NADP^+$ structure (*37*), the N3 and O4 atoms of DHF form hydrogen bonds with the backbone atoms of I68. Also, hydrogen bonds are formed between the carboxamide group of NADPH and the backbone NH and O atoms of a symmetry related I68 residue. In order to study the role of this residue, I68M and I68L mutants were generated. Kinetic studies indicated that both mutants had similar effects. The K_m of DHF increased by ~4-fold and the K_m of NADPH increased ~9-fold. Also, the k_{cat} was decreased, especially in the case of the I68M mutant (*8, 38, 39*). These data suggest that I68 directly affects the binding of the ligands and consequently catalysis.

3) Y69 residue: The crystal structure of R67 DHFR in complex with DHF and $NADP^+$ suggests that two pairs of Y69 and Q67 residues together form an extended surface so as to tightly hold the substrate and cofactor in a favorable position for hydride transfer. Kinetic studies using the Y69F mutant show that the K_m of DHF is increased 11-fold and that of NADPH is increased 23-fold. Also, the k_{cat} of the reaction is 2-fold higher than that for the wild type enzyme (*38*). Introduction of non-conservative mutations such as Y69L affected the K_m of DHF and NADPH 31-fold and 23-fold respectively. Similarly, for the Y69H mutation K_m of DHF and NADPH was increased 8-fold and 59-fold respectively. Additionally, the k_{cat} values for Y69L and Y69H DHFRs decreased 8 and 93-fold respectively (as compared to the wild type enzyme) (*38, 39*). Therefore, the overall catalytic efficiency is decreased, which indicates a strong preference for a hydrophobic group (specifically aromatic groups) at that position. NMR studies also suggested that the chemical shift of Y69 is affected upon binding of $NADP^+$ (*25*). These results confirm that Y69 forms important

interactions with both the substrate and cofactor. Therefore, the Y69 residue is also critical in binding and catalysis.

4) K32 residue: The crystal structure of R67 DHFR indicates that the K32 residue is present at the edge of the active site pore (*16, 19*) (figure 5). Another crystal structure with R67 in complex with DHF and $NADP^+$ shows that two K32 residues interact with 2 phosphate moieties of NADPH and two other K32 residues bind to DHF, contributing to positioning and affinity. Also, Delphi predictions show that K32 helps form a positive electrostatic potential in and near the active site pore which aids in binding of negatively charged ligands (*26*). Mutation of K32 resulted in an inactive dimer, therefore the role of K32 was studied indirectly using salt effects (*40*). Using steady state kinetics, a log-log plot of k_{cat} versus ionic strength showed a slope of 0.9. This indicated that during catalysis, one ionic bond is broken. Other charged residues around lysine 32 include arginine 31, lysine 33 and glutamic acid 75 and they form a charged patch near the active site pore. Since the role of the K32 residue could not be directly studied by site directed mutagenesis, an alternate approach was employed in which the neighboring K33 residue was replaced with a methionine. Kinetic studies revealed that both the K_m and the k_{cat} were affected by 2 to 4 fold suggesting the K33 residue is only minimally involved in binding and catalysis. Therefore, to directly probe the role of the K32 residue, asymmetric mutants were generated and characterized by kinetics and binding studies (*41*). These results will be discussed in the following section on asymmetric mutations.

To summarize, mutagenesis and binding studies indicate that the enzyme possesses a promiscuous binding surface that is capable of binding to both folate and NADPH. In other words, catalysis in R67 DHFR does not depend on a single residue, but depends on the global environment of the active site. Therefore, R67 DHFR not only adopts a novel mechanism, but a simple approach to catalysis (*38*). Finally binding studies on these mutants using isothermal

titration calorimetry (ITC) also suggest that there is a linear correlation between the enthalpy change for the formation of a ternary complex and the catalytic efficiency of the enzyme (*39*). In other words, the positive cooperativity observed between the substrate and cofactor is correlated with the increasing exothermicity of the reaction. Other studies have also proposed that increased exothermicity (associated with non-covalent interactions) may result in closer contact distances (*42-44*).

Asymmetric Mutations

Non-conservative mutations in the R67 DHFR gene result in 4 mutations per active site pore and can cause a large cumulative effect. In order to study the effect of a single mutation on binding and catalysis, it is necessary to eliminate the constraints imposed by the 222 symmetry of the enzyme. For this reason, a tandem array of 4 gene copies was constructed to allow generation of asymmetric mutations. Briefly, four R67 DHFR gene copies were covalently linked in frame so as to obtain a quadruplicated gene product. The molecular weight of the protein product is four times the mass of the monomer and is proposed to have the same tertiary structure as wild type R67 DHFR, since it has similar kinetic and binding properties as compared to R67 DHFR (*20*). In addition, unique restriction sequences were engineered between gene copies to allow for mutation of a single gene copy, which can be inserted back into the tandem array (*45*). One limitation of early versions of the tandem gene array was that the N-terminal 17 residues are long enough to allow alternate ways for the domains to associate. If the domains are labeled 1, 2, 3 and 4, then they could form either a 1234 or a 1243 topology. In order to circumvent this problem, two additional mutations were inserted into the sequence based on the observation that H62 interacts with S59 from another monomer at the dimer-dimer interface in wild type R67 DHFR (*18*). Neither the H62L nor the S59A mutants were active. They were found to be stable dimers.

However, mixing of these two dimers resulted in complementation and heterotetramer formation and enzyme activity (*18*). Therefore, these mutations were introduced into gene copy 1 and gene copy 4 respectively so as to complement each other at the dimer-dimer interface. This resulted in a preferred topology. This construct was named 'Quad 3'. The kinetic parameters of Quad 3 (k_{cat} and K_m) as well as the binding parameters (*46*) are similar to those of the wild type enzyme (*47*), therefore this construct was used to study the role of the K32, Q67 and Y69 residues (*41, 47, 48*). Only the Q67 and K32 results are summarized below as they help build a multimutant of interest. The nomenclature used to describe the asymmetric mutants is as follows: the wild type residue (letter code) and its position in the monomeric amino acid sequence is specified first, followed by the residue to which it is being mutated. The domains have been numbered numerically where domain 1 occurs in the top left region and the domains increase in number in an anticlockwise manner. The domain in which the asymmetric mutant is generated, is then represented by the number after the colon. For example, Q67H: 1+4 indicates that glutamine is replaced by histidine in domains 1 and 4.

1) Q67 residue: Q67H homotetrameric mutant binds DHF and NADPH 36-fold and 100-fold more tightly than the wild type enzyme. However, the k_{cat} concurrently decreased 7-fold, which resulted in a 3.6-fold increase in the catalytic efficiency (*34*). This mutant also shows substrate and cofactor inhibition. Therefore, asymmetric mutants were generated to probe whether tight binding could be uncoupled from substrate and cofactor inhibition. A single mutant Q67H: 1 was generated as well as three double mutants, Q67H: 1+2, Q67H: 1+3 and Q67H: 1+4. Finally, a triple mutant Q67H: 1+2+3 and a quadruple mutant Q67H: 1+2+3+4 were also generated (*47*). Steady state kinetic studies as well as ITC studies were performed and it was observed that a single mutation had an effect on DHF binding. However, the catalysis of the reaction was not affected by the addition of the mutants. Also, it was observed that at least three mutations were required to see an effect on NADPH binding. The Q67H: 1+2 mutant showed cofactor inhibition

and the Q67H: 1+3 mutant showed both substrate and cofactor inhibition. However, the Q67H: 1+4 mutant showed no substrate or cofactor inhibition. A comparison of K_d values for formation of the various complexes indicated that as the number of mutations increased, the enzyme became unable to differentiate between productive and non-productive complexes, supporting a role for Q67 in interligand co-operativity patterns.

2) K32 residue: In order to directly study the role of the K32 residue, three different asymmetric constructs were generated. They included K32M: 1+2, K32M: 1+3 and K32M: 1+4 asymmetric mutants (*41*). The K32M: 1+2 and the K32M: 1+4 mutants placed two mutations on either side of the pore, although at different orientations. Kinetic studies of the K32M: 1+2 mutant indicated that the $K_{m(DHF)}$ and $K_{m(NADPH)}$ are increased by ~2-fold and ~4-fold respectively. Also, the k_{cat} is decreased ~4-fold. In the case of the K32M: 1+4 mutant, both the $K_{m(DHF)}$ and $K_{m(NADPH)}$ are increased by ~1.5-fold and the k_{cat} is decreased 8.5-fold. This suggested that R67 DHFR tolerates alternate positions of the pABA-glu tail of DHF. On the other hand, the K32M: 1+3 mutant, places these two mutations on the same side of the pore. The DHF K_m increased more than 50-fold, while the K_m of NADPH increased by about 37-fold (as compared to Quad 3), indicating a loss of ionic interactions of DHF with the K32 residues. Also surprisingly, the k_{cat} was enhanced 4-fold suggesting that removal of charge on one side of the pore enhances transition state formation. Therefore, the K32M asymmetric mutants helped provide more insight into the binding preference of DHF and NADPH to the active site.

Asymmetric Multimutants

The Q67H residues are present on the floor and ceiling of the active site pore and have been suggested to form interactions with the nearby Y69 residues so as to provide additional stacking interactions with the pteridine and nicotinamide rings (*37, 47*). Therefore various asymmetric

mutants of Q67H were evaluated as described above and in Smiley et al. (*47*). Of these, the Q67H: 1+4 mutant contains a pair of wild type Q67 residues on the floor, while a pair of Q67H residues is present on the ceiling of the active site. In contrast to the Q67H: 1+2 and Q67H: 1+3 mutants, this mutant shows neither substrate nor cofactor inhibition. Also, the binding of NADPH is tightened 5-fold in this mutant.

As described earlier, another important residue that has been studied using asymmetric mutations is the K32 residue (*41*). Hicks et al. have demonstrated that the K32M: 1+3 mutations, which are present on the same side of the pore, shows a very weak binding of substrate coupled with an increase in k_{cat} (*41*). The K32 residue is located about 8Å away from the Q67 residue in the active site pore and there is a possibility that mutations at Q67 could be additive with mutations at K32 (*49-52*). Therefore the question arises: can addition of the Q67H: 1+4 mutations compensate for the loss of K32 in the K32M: 1+3 mutant?

To investigate this, Q67H: 1+ 4 mutations were engineered into the K32M: 1+3 construct and the resultant construct was called $Q67H_{half}K32M_{half}$ (figure 6). Another construct was also generated which contained the Q67H mutation in all monomers, called $Q67H_{full}K32M_{half}$ (Feng and Howell, manuscript accepted). Kinetic and ITC studies showed that the binding of DHF was tightened 40-fold in $Q67H_{half}K32M_{half}$ as compared to the K32M: 1+3 'parent'. These results indicated that the Q67H mutations could compensate for the weak binding of the substrate due to the loss of the K32 residues. Another observation is that this mutant exhibits no DHF and NADPH inhibition. The $Q67H_{full}K32M_{half}$ mutant on the other hand is strongly inhibited by DHF, but not by NADPH. In other words, addition of the Q67H mutations to the $Q67H_{half}K32M_{half}$ does not rescue the binding of NADPH to the mutant K32M side of the pore. This provides strong evidence that NADPH binds to the wild type half of the pore. Additional support for this arises from the

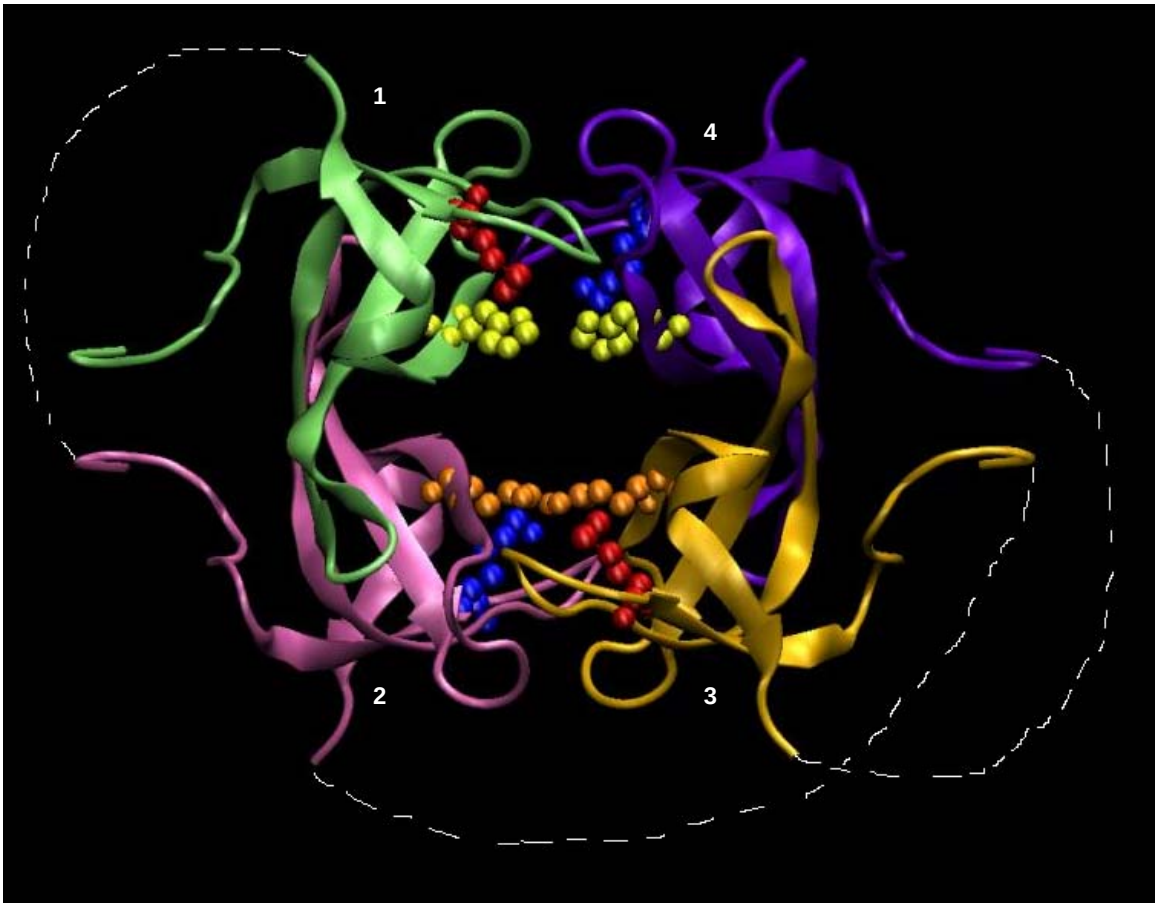

Figure 6: Ribbon structure of the Q67H$_{half}$K32M$_{half}$ mutant of R67 DHFR. Monomers 1, 2, 3 and 4 are shown in green, pink, ochre and violet respectively. The expected linkages between the monomers to form the Quad 3 construct are shown by the dashed lines. The Q67 residues (orange) are present on the ceiling and floor of the pore, and are mutated to histidines (yellow) in monomers 1 and 4. The K32 residues (blue) are located at the edge of the active site pore and are mutated to methionine (red) in monomers 1 and 3.

observation that the $k_{cat}/K_{m(NADPH)}$ for the K32M: 1+3, $Q67H_{half}K32M_{half}$ and the $Q67H_{full}K32M_{half}$ mutants remains relatively constant, suggesting that NADPH prefers binding to the wild type half of the pore. Finally, a strong salt dependence of NADPH binding also suggests the presence of two ionic interactions between the pyrophosphate bridge and the 2' phosphate with the symmetry related K32 residues (*40*).

NMR and crystallography studies have shown that the pABA-glu tail of DHF is disordered and docking studies predict that its carboxylate groups form intermittent contacts with K32 residues on the same side of the pore. Previously, ITC studies using analogs of folate showed that loss of the pABA-glu tail or the glutamic acid results in loss of binding enthalpy (*53*). This suggested that the binding enthalpy arises from the interaction between the K32 residues and the glutamic acid tail of DHF. However, in the case of the $Q67H_{half}K32M_{half}$ and the $Q67H_{full}K32M_{half}$ mutants, a binding enthalpy was observed, suggesting that loss of the ion pair or solvent separated ion pair between K32 and the glutamate tail did not have an effect on the binding enthalpy. One possibility is that water molecules entrapped in the active site provide an enthalpic contribution (*54, 55*). Another possibility is that interligand interactions between the pteridine and nicotinamide rings provide binding enthalpy.

Determination Of Critical Regions Of Substrate And Cofactor That Are Involved In Binding To R67 DHFR

Site directed mutagenesis has been employed to determine the critical residues that determine the binding and positioning of the substrate and cofactor in the active site (*38-41, 47, 48*). A parallel approach is to mutate / modify the substrate and/or cofactor, so as to identify the critical regions of DHF and NADPH that are involved in binding to R67 DHFR. These experiments were

performed by Jackson et al., wherein the binding affinity of different analogs of DHF/ Folate and NADPH were determined using steady state kinetics (K_i determination) and isothermal titration calorimetry studies (K_d determination) (*53*).

Analogs of Folate:

1) Folate analogs with truncations of the para- aminobenzoic acid glutamic acid (pABA-glu) tail: Biopterin lacks both the para-amino benzoic acid moiety and the glutamic acid moiety of folate (figure 7). The reduced form of this analog, 7,8 dihydrobiopterin (DHB), was used to determine its binding properties. An inhibition constant (K_i) of ~157 μM was obtained. However, no signal was obtained for the binary complex titration using ITC. Another analog, pteroic acid, contains the pteridine ring and the pABA moiety. However, it lacks the glutamate tail (figure 7). The K_i of pteroic acid is ~60 μM and an ITC signal was observed for a binary titration (binding of two molecules of ligand to protein). However, saturation was not achieved due to solubility problems. The reduced form, dihydropteroate had a K_i of ~27 μM. ITC studies with these analogs also showed that ternary complex (enzyme•NADPH•substrate) formation was weakened going from folate/DHF to pteroic acid/DHP to bioterin/DHB. Also, a decrease in binding enthalpy to ~-8 kcal/mol (for DHP binding to a NADPH•R67 DHFR complex) was observed, as compared to -12 kcal/mol (for DHF binding to a $NADP^+$•R67 DHFR complex). These results suggested that the pABA-glutamic acid tail of folate is important for binding to the enzyme. Further studies were also performed using these analogs to study the transition state formation as described later.

2) Substitution of the glutamic acid tail with a positively charged amino acid: Substitution of glutamic acid in the folate tail with histidine or ornithine (N^{α}-pteroyl-L-histidine or N^{α}-pteroyl-L-ornithine respectively) showed less than a 2-fold effect on binding by K_i determination. These studies suggested that the α-carboxylate moiety of DHF is not important

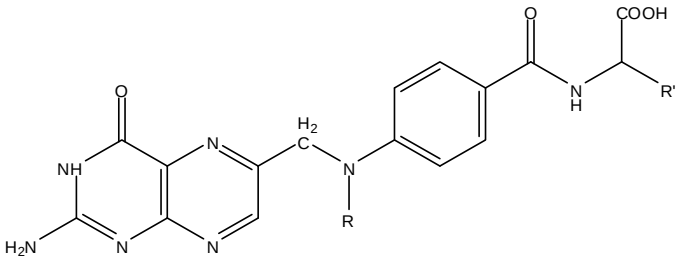

Folic Acid

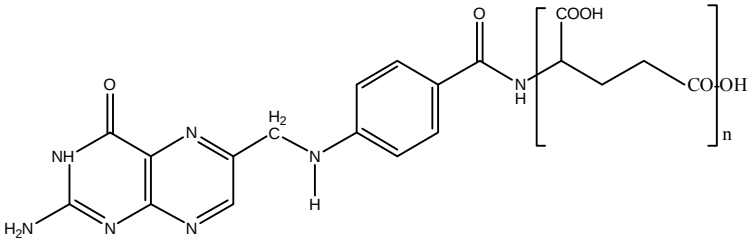

Pteroyl-diglutamate (PG2); n=2
Pteroyl-pentaglutamate (PG5); n=5

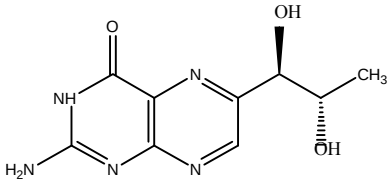

Biopterin

Figure 7: Structures of folic acid and its analogs used for binding studies. 7,8-Dihydrofolate, 7,8-dihydropteroic acid and 7,8-dihydrobiopterin are reduced across the C7-N8 bond. In N^{α}-pteroyl-L-histidine and N^{α}-pteroyl-L-ornithine, the glutamate moiety is replaced by histidine and ornithine, respectively (*53*). The acids are represented in their un-ionized forms.

(Continued)

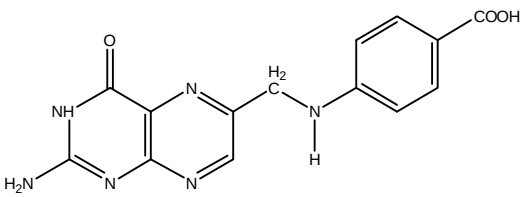

Pteroic acid

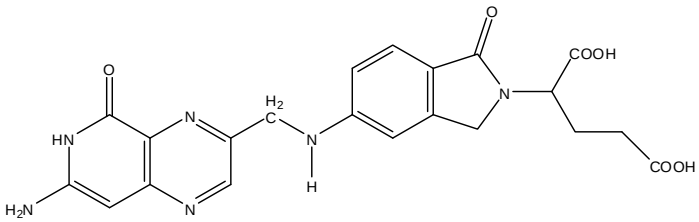

PT648 [(2S)-2-[5-[N-(2-amino-4(3H)-oxopyrido[2,3-d]pyrimidin-6-yl) methylamino[2,3-dihydro-1(3H) oxoisoindol-2-yl]aminopentane-1,5-dioic acid)]

Figure 7 (Continued): Structures of folic acid and its analogs used for binding studies.

in binding. If ionic interactions occur, then they likely exist between the α-carboxylate of DHF and K32.

3) Increasing the length of the glutamic acid tail or rotational restriction of tail: Little effect was observed on binding when the length of the glutamic acid tail was increased by addition of 1 or 4 glutamates (pteroyl γ-L di glutamate and pteroyl γ-L -penta glutamate). When the tail was substituted with a N5-deaza analog, which also contains a rotationally restricted glutamic acid tail as in the case of PT648 [(2S)-2-[5-[N- (2-amino-4 (3H)-oxopyrido [2,3-d] pyrimidin-6-yl) methylamino [2,3-dihydro-1 (3H)-oxoisoindol-2-yl] aminopentane-1, 5-dioic acid)], weaker binding was observed and the K_i increased 3-fold.

4) Substitution of the groups on the pteridine moiety: Aminopterin has a NH_2 group in place of the O4 atom in folate; it was not able to form a ternary complex. This suggested that the O4 group is important for binding.

In summary, studies with folate analogs showed that R67 DHFR has a strong preference for binding to the dihydro form of the substrate compared to folate or tetrahydrofolate. An important observation was that the keto form of folate displays stronger binding. Therefore, a neutral pteridine ring is required for binding to the enzyme. These atoms have been shown to form interactions with the NH and O backbone of I68 (*26*). Finally, removal of the pABA glu tail weakened binding and resulted in a low enthalpic signal.

Analogs of NADPH:

1) Importance of nicotinamide group: When an analog lacking the nicotinamide group was used to monitor binding, as in the case of ATP-ribose (figure 8), the K_d increased 64-fold. This result indicates that the nicotinamide ring is important for binding of the cofactor in the active site. Other analogs used to investigate the importance of this group were thio-NADPH and acetyl

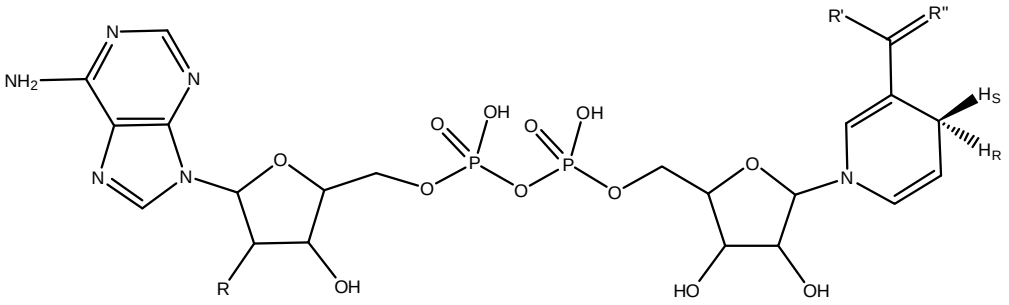

NADPH; R = OPO_3H_2, R' = NH_2, R" = O

NADH; R = OH, R' = NH_2, R" = O

Thio-NADPH; R = OPO_3H_2, R' = NH_2, R" = S

3-Acetylpyridine adenine dinucleotide phosphate (A_cPADPH); R = OPO_3H_2, R' = CH_3, R" = O

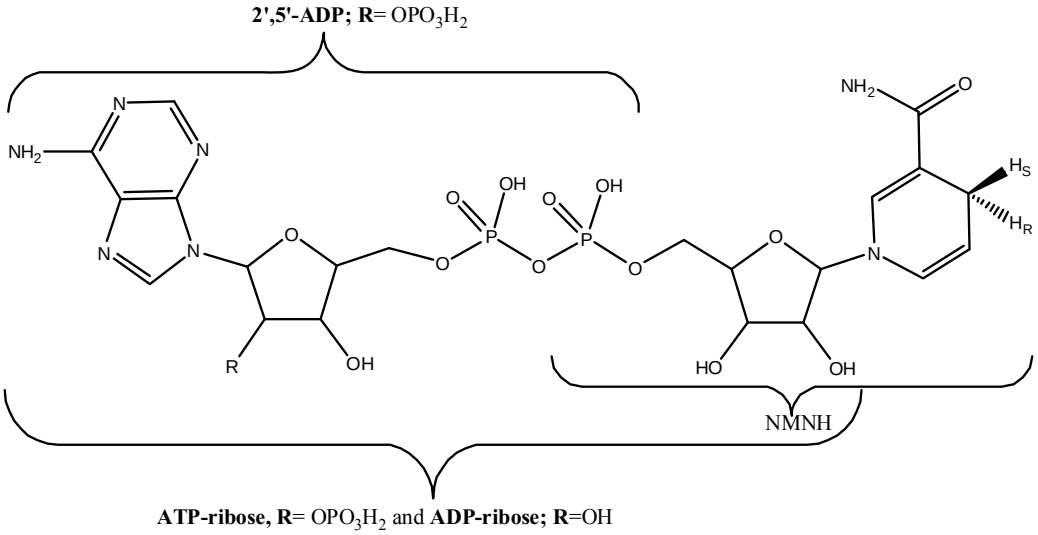

Figure 8: Structures of analogs of NADPH used in binding studies. The structures of NADPH, NADH, Thio-NADPH, A_cPADPH have been shown with respective substitutions on the R' and R" groups (*53*). Also shown are structures for 2', 5' adenosine phosphate, ADP-ribose and ATP-ribose.

pyridine adenine dinulceotide phosphate (A_cPADPH). Binary ITC titrations using these two compounds showed that binding of the first cofactor molecule is reduced by 3-fold and 33-fold respectively. Use of these analogs identified the importance of the carboxamide moiety in binding to R67 DHFR. Additionally, truncations of the cofactor to 2,5-diphosphosphoadenosine showed weakened binding.

2) 2'phosphate group of NADPH: To test the importance of the 2'phosphate group of NADPH, NADH was used as it lacks the 2' phosphate group (figure 8). A 14-fold weaker binding by this analog indicated the 2'phosphate group was important in binding. This is consistent with salt effect studies (*40, 41*). Additional experiments using ADP-ribose and 2', 5'diphosphoadenosine showed (110-fold and 250-fold weaker binding respectively) as compared to NADPH, which showed that the sugar and 2'phosphate groups are essential for binding.

Overall, the thermodynamic parameters obtained by ITC studies of substrate and cofactor analogs show that binding of the first molecule of NADPH is enthalpy driven, while binding of the second molecule of folate is enthalpy driven. These observations are similar to those observed by Bradrick (*20*).

Protonation Effects During Ligand Binding

To determine whether binding is accompanied by changes in protonation state, the ΔH change associated with formation of the 2 NADPH binary complex or 2 folate binary complex or the R67 DHFR•$NADP^+$•DHF ternary complex was monitored in different buffers.

If a pK_a perturbation occurs upon binding and is accompanied by proton release or uptake, then changes in enthalpy will be observed as represented below:

$$\Delta H_{observed} = \Delta H_{binding} + n\Delta H_{ionization} \quad (1)$$

where, $\Delta H_{binding}$ is the enthalpy change associated with binding, $\Delta H_{ionization}$ is the change in the heat of ionization and n is the number of protons involved (*55*).

Therefore, the binary and ternary ITC titrations were performed in different buffers, each possessing different heats of ionization. Results indicated that no enthalpy change was involved with binding of 2 NADPH molecules or DHF to enzyme•$NADP^+$. However, the enthalpy change associated with the binding of 2 folate molecules or folate to R67 DHFR•NADPH was found to vary in different buffers. Using equation 1, the $\Delta H_{binding}$ of folate to R67 DHFR•NADPH was found to be -13.1 Kcal/mol. Also, the $\Delta H_{observed}$ was plotted against the $\Delta H_{ionization}$. The plot obtained was linear and the slope of the plot gave an estimate of the number of protons involved in binding. A positive slope of 0.4 ± 0.05 was obtained which indicated proton uptake upon binding at pH 8.0 (*53*).

The pK_a of the N3 group of DHF is reported as 9.54 or more recently 10.8 (*56, 57*). This is much above the pH of ITC experiments (8.0) and is consistent with no perturbation of this group upon binding to R67 DHFR. Therefore, DHF binds to the active site without any proton uptake. On the other hand, the pK_a of the N3 group of folate is 8.38 (*56, 58*). This is near the pH of the experiment (8.0) and is consistent with folate binding to the enzyme with a partial proton uptake as R67 utilizes N3 and O4 atoms in binding folate (*37*).

Use Of Alternate Substrates To Study Ligand Binding And Catalysis

Folate analogs with truncations in the tail region showed that the binding is weakened in the absence of the glutamic acid tail and is further weakened if both the pABA moiety and the glutamic acid tail are removed. Salt effect studies have also shown that in going from the ground state to transition state, one ionic interaction is broken (*40*). Binding and kinetic studies with

dihydropteroic acid (DHP, folate analog lacking the glutamic acid tail) showed that the K_m is increased ~5-fold. Additionally, k_{cat} of the DHFR reaction using DHP as a substrate showed an approximately 1600-fold reduction in the k_{cat} as compared to the k_{cat} obtained using DHF (*59*). This suggested that the pABA glu tail is important for interacting with the K32 residue and consequently for correctly positioning the substrate in the active site.

Thermodynamics Of Ligand Binding In The Ground State And Transition State

To garner more information on how R67 DHFR facilitates transition state formation, the temperature dependence of binding (NADPH and DHF) and catalysis was monitored. Using the van't Hoff plot, the enthalpy of binding of DHF and/or NADPH in the ground state was determined to be –8.6 kcal/mol and –13.3 kcal/mol respectively. Additionally, an Arrhenius plot was used to obtain the activation energy and the corresponding enthalpy change of (6.3 kcal/mol at 25^{o}C) associated with transition state formation. The TΔS associated with ground state was also calculated to be –5.4 kcal/mol. This value of TΔS is less negative as compared to the TΔS in the ground state (-11.3 kcal/mol), indicating a reorientation of the substrate in the transition state. Similar results have been obtained using a poor substrate DHP (*53, 59*) . These results have been discussed in chapter 2.

Role Of Water In Ligand Binding In R67 DHFR?

Water is an essential component present in all living organisms. It forms an integral part of all biomolecular systems as it associates with proteins, carbohydrates, lipids and nucleic acids. Understanding the role of water will help shed light on the mechanism of cellular function. In the case of proteins, the polar nature of water forces the hydrophobic regions to come together to form a tightly packed core, which provides a driving force for protein folding. Additionally, water

molecules form a network of hydrogen bonds with themselves and the protein, maintaining protein stability. Characterization of the hydration of proteins is essential for understanding protein folding, structure and function. In order to achieve this, techniques such as x-ray crystallography and NMR spectroscopy have been used (*60, 61*). Another approach towards obtaining a global picture is to use molecular dynamic (MD) simulations and neutron scattering experiments. Both small angle scattering (SAS) of x-rays and neutrons in H_2O and D_2O have been used to understand the perturbation of water on the surface of lysozyme and its difference from the bulk solvent (*62*). It was observed that the first hydration shell (~3Å thick) is 15% denser than bulk water. In order to gain insight into the structural properties of the first hydration shell, molecular dynamic simulations were also performed (*63*). Results obtained suggested that the geometry of the water molecules contributed to 75% of the density of the first hydration shell, while other factors such as topographical and electrostatic properties of the protein surface may be responsible for the remaining 25% density of the hydration shell. Thus, these results were similar to those obtained by SAS. Another interesting feature on the interact[ption of water with proteins is that about 55% of these water molecules are bound to the backbone atoms and the remaining to the charged side chains. Therefore, the positions of some of these water molecules are conserved and always found in crystal structures at the same position (*64, 65*).

Since water plays a vital role in maintaining the structure and function of proteins, it is imperative to maintain its concentration in the cell. Any changes in environmental conditions such as osmotic stress, high hydrostatic pressures or dehydration could be lethal to the cell. An in-built mechanism in cells to combat such extreme conditions is the production of organic solutes. Some examples of these solutes are trimethylamine N-oxide (TMAO) and glycine betaine. These compounds are proposed to help in stabilization of the native state of proteins by their preferential exclusion at the protein surface, allowing hydration (*66-68*). Due to these properties, organic

solutes have been used for both *in vitro* and *in vivo* experiments for determining the role of water in ligand binding to proteins (*69, 70*). Addition of these solutes results in a displacement of some water molecules, consequently leading to a perturbation of solvent structure and unfolding of proteins. The basic idea behind using osmolytes for *in vitro* experiments is to control water activity by using solutes (osmolytes), which themselves do not interact with the protein of interest. Addition of osmolytes causes an increase in osmotic pressure, which eventually leads to dehydration and the squeezing out of water molecules from the active site (*71*). By using a range of osmolyte concentrations, the number of water molecules squeezed out can potentially be quantified. Generally, the effect of the osmolyte on the K_a is monitored. A plot of $\ln(K_a)$ versus osmolality gives an estimate of the number of water molecules involved. An increase in K_a due to osmolyte addition suggests a net release of water molecules. On the other hand, a decrease in K_a reflects an uptake of water molecules (*69, 70*). This approach has been used for a number of proteins. For example, hemoglobin has been found to gain 60 water molecules upon binding to 4 oxygens (*72*). In another example, hexokinase was found to lose about 60 water molecules upon binding to a glucose molecule (*73*). Finally, cytochrome oxidase undergoes a hydration/ dehydration cycle involving 10 water molecules as the protein is reduced and then transfers an electron internally (*74*). Additional examples of this phenomenon also include changes in hydration due to conformational change (*75*), as seen in the case of glucose binding to hexokinase (*73*), aspartate to ATCase (*76*) or DNA binding to repressors (*75*).

Depending on their chemical properties, osmolytes can be categorized into two groups: protecting osmolytes and denaturing osmolytes. Protecting osmolytes raise the free energy of the unfolded state and hence favor the folded protein population (for example, trimethylamine oxide (TMAO). On the other hand, denaturing osmolytes lower the free energy of the unfolded state and thereby favor a higher population of the unfolded state (for example, urea and guanidine chloride) (*77*-

79). An example of this is urea, which interacts with the peptide backbone and also with other urea molecules. The effect of these osmolytes on proteins can be evaluated thermodynamically by measuring the transfer free energies (Δg_{tr}) of backbone models from water to 1M osmolyte solutions. A $\Delta g_{tr}>0$ indicates that osmolytes stabilize the protein and $\Delta g_{tr}<0$ indicates that the particular osmolyte has a denaturing effect on the protein (*77, 80, 81*). *Ab initio* calculations further showed that the Δg_{tr} values of many osmolytes are negatively correlated with their fractional polar surface area (*82*). In other words, as the fractional polar surface area increases, the osmolyte interacts more favorably with the protein (decreasing the g_{tr}). Also, the amount of interaction depends on the surface area of the protein.

In the case of R67 DHFR, the volume of the hour-glass shaped active site pore is 2600 $Å^3$, which includes a total of 168 water molecules (*19*). The water molecules are well ordered and their hydrogen-bonding network forms an array of fused pentagonal rings. A crystal structure of the Q67H mutant with bound $NADP^+$ shows that Water 149 has a conserved position and is displaced upon binding of two NADPH molecules (*83*). This suggests that water may play an important role in ligand binding to R67 DHFR. To investigate this, preliminary experiments were performed using osmolytes such as sucrose and trehalose. It was observed that the binding of the substrate weakened as the concentration of osmolytes was increased (*59*). This strongly suggested that water is important in stabilizing the interaction of DHF with R67 DHFR. Further studies were performed using different osmolytes, which will be discussed in chapter 3.

Role Of Water In Binding Enthalpy

Isothermal titration calorimetry provides valuable information on the enthalpy and entropy changes accompanying a binding process. The net enthalpy change measured by ITC is not only

due to hydrogen bonding or ionic interactions, but also due to changes in solvent-solvent, protein-solvent and protein-ligand interactions. From the changes in enthalpy at different temperatures, a heat capacity change can be calculated based on the relationship:

$$\Delta C_p = \partial \Delta H / \partial T \qquad (2)$$

Therefore, the slope of a plot of ΔH versus temperature gives a value for ΔC_p. If the favorable (more negative) enthalpy is increased with temperature, it is compensated by a decrease in favorable entropy. Thus, the entropy change can also be determined from the heat capacity change as shown by the following equation:

$$\Delta G = \Delta C_p (\Delta T) - T\Delta S \qquad (3)$$

A number of factors contribute to heat capacity and entropy:

1) *Dehydration of a non-polar or polar surface:* Dehydration of a non-polar surface leads to a decrease in heat capacity and an increase in favorable entropy (*84*). On the other hand, dehydration of a polar surface results in an increase in the heat capacity and a corresponding increase in the favorable entropy (*85, 86*). Chervenak and Toone performed binding studies in the presence of H_2O and D_2O and observed different binding enthalpies in light and heavy water. This led them to suggest that 'solvent reorganization' is responsible for 25% to 100% of the enthalpy of binding (*54*). A negative heat capacity change is usually observed for ligand-nucleic acid and ligand-protein binding interactions (*87-90*).

2) *Internal vibrations:* Vibrational tightening can decrease the heat capacity of a system and also decrease the favorable entropy (*86, 91, 92*).

3) *Conformational changes:* A binding reaction that is accompanied by a conformational change also has an effect on the heat capacity, which is also associated with a decrease in the entropy (*91, 93, 94*).

4) ***Electrostatic interactions and protonation changes during binding:*** Long range electrostatic interactions also have a strong influence on heat capacity (*95*). Additionally, protonation changes have also shown to contribute to the observed heat capacities (*94*).

Of these possibilities, the heat capacity change due to dehydration of polar / non-polar surfaces in many systems (*96-98*) may indirectly demonstrate the contribution of water molecules in binding of ligands. The heat capacity change involving the folding of various proteins as well as the transfer of hydrocarbons and amides from water to pure liquid phase has been characterized .by the following equation:

$$\Delta C_p \text{ (cal/mol}^o\text{K)} = C_{apolar} * \Delta A_{NP} + C_{polar} * \Delta A_P \qquad (4)$$

where, ΔA_{NP} and ΔA_P are the solvent accessible non-polar and polar surface areas respectively (*85, 99*).

Various groups have studied this and have generated different coefficients for the heat capacity (*100*). The coefficients reported by Spolar and Record are often used as follows (*85*).

$$C_{apolar} = 0.32 \pm 0.04 \text{ and } C_{polar} \text{ -}0.14 \pm 0.04 \qquad (5)$$

In order to thermodynamically characterize the contribution of solvent-reorganization due to the burial/ exposure of polar/non-polar surface of R67 DHFR, heat capacity studies have been performed on R67 DHFR. In summary, the heat capacity change for binding of DHF to form a ternary complex in the presence of the cofactor and R67 DHFR has been measured. In addition to this, the heat capacity change for binary complex binding of NADPH has been studied. These results will be discussed in chapter 3.

Goal Of The Project: How Do The Ligands DHF And NADPH Bind In The Active Site Of R67 DHFR?

R67 DHFR has a promiscuous active site that allows for binding of both the substrate and cofactor in similar positions. Therefore, the manner in which ligands bind to the enzyme in the ground state and transition state is not completely understood. X-ray crystallography, NMR studies, docking studies and molecular dynamic simulations all indicate that the DHF tail is disordered. In this study, we have addressed ligand binding to the enzyme by two different approaches:

1) Using analogs (truncated at the tail region) of folate we investigated the importance of the glutamic acid region of folate. Also, a thermodynamic characterization of the ligand binding in the ground state and transition state has been achieved using Arrhenius plots. These results are discussed in chapter 2.
2) The role of water molecules in DHF and NADPH binding has been studied using osmolytes. Heat capacity studies have also been performed as a part of this study. The experiments and results obtained have been described in chapter 3.

References

(1) Pattishall, K. H., Acar, J., Burchall, J. J., Goldstein, F. W., and Harvey, R. J. (1977) *J Biol Chem 252*, 2319-23.
(2) White, P. A., and Rawlinson, W. D. (2001) *J Antimicrob Chemother 47*, 495-6.
(3) Amyes, S. G., and Smith, J. T. (1976) *Eur J Biochem 61*, 597-603.
(4) Broad, D. F., and Smith, J. T. (1982) *Eur J Biochem 125*, 617-22.
(5) Bystroff, C., Oatley, S. J., and Kraut, J. (1990) *Biochemistry 29*, 3263-77.
(6) Bolin, J. T., Filman, D. J., Matthews, D. A., Hamlin, R. C., and Kraut, J. (1982) *J Biol Chem 257*, 13650-62.
(7) Matthews, D. A., Alden, R. A., Bolin, J. T., Freer, S. T., Hamlin, R., Xuong, N., Kraut, J., Poe, M., Williams, M., and Hoogsteen, K. (1977) *Science 197*, 452-5.
(8) Howell, E. E. (2005) *ChemBioChem 6*, 590-600.
(9) Agarwal, P. K., Billeter, S. R., Rajagopalan, P. T., Benkovic, S. J., and Hammes-Schiffer, S. (2002) *Proc. Natl. Acad. Sci. U. S. A. 99*, 2794-9.
(10) Benkovic, S. J., and Hammes-Schiffer, S. (2003) *Science 301*, 1196-202.
(11) Falzone, C. J., Wright, P. E., and Benkovic, S. J. (1994) *Biochemistry 33*, 439-42.
(12) Sawaya, M. R., and Kraut, J. (1997) *Biochemistry 36*, 586-603.
(13) Fierke, C. A., Johnson, K. A., and Benkovic, S. J. (1987) *Biochemistry 26*, 4085-92.
(14) Bystroff, C., and Kraut, J. (1991) *Biochemistry 30*, 2227-39.
(15) Nichols, R., Weaver, C. D., Eisenstein, E., Blakley, R. L., Appleman, J., Huang, T. H., Huang, F. Y., and Howell, E. E. (1993) *Biochemistry 32*, 1695-706.
(16) Narayana, N., Matthews, D. A., Howell, E. E., and Nguyen-huu, X. (1995) *Nat Struct Biol 2*, 1018-25.
(17) Reece, L. J., Nichols, R., Ogden, R. C., and Howell, E. E. (1991) *Biochemistry 30*, 10895-904.
(18) Dam, J., Rose, T., Goldberg, M. E., and Blondel, A. (2000) *J Mol Biol 302*, 235-50.
(19) Narayana, N. (2006) *Acta Crystallogr D Biol Crystallogr 62*, 695-706.
(20) Bradrick, T. D., Beechem, J. M., and Howell, E. E. (1996) *Biochemistry 35*, 11414-24.
(21) Morrison, J. F., and Stone, S. R. (1988) *Biochemistry 27*, 5499-506.
(22) Li, D., Levy, L. A., Gabel, S. A., Lebetkin, M. S., DeRose, E. F., Wall, M. J., Howell, E. E., and London, R. E. (2001) *Biochemistry 40*, 4242-52.
(23) Brocchieri, L., and Karlin, S. (1994) *Proc Natl Acad Sci U S A 91*, 9297-301.
(24) Andres, J., Moliner, V., Safont, B. S., Domingo, L. R., Picher, M. T., and Krechl, J. (1996) *Bioorganic Chem. 24*, 10-18.
(25) Pitcher, W. H., 3rd, DeRose, E. F., Mueller, G. A., Howell, E. E., and London, R. E. (2003) *Biochemistry 42*, 11150-60.
(26) Howell, E. E., Shukla, U., Hicks, S. N., Smiley, R. D., Kuhn, L. A., and Zavodszky, M. I. (2001) *J. Comput. Aided Mol. Des. 15*, 1035-52.
(27) Bradrick, T. D., Shattuck, C., Strader, M. B., Wicker, C., Eisenstein, E., and Howell, E. E. (1996) *J Biol Chem 271*, 28031-7.
(28) Kuntz, I. D., Blaney, J. M., Oatley, S. J., Langridge, R., and Ferrin, T. E. (1982) *J Mol Biol 161*, 269-88.
(29) Shoichet, B. K., and Kuntz, I. D. (1993) *Protein Eng 6*, 723-32.
(30) Schnecke, V., and Kuhn, L. A. (1999) *Proc Int Conf Intell Syst Mol Biol*, 242-51.
(31) Raymer, M. L., Sanschagrin, P. C., Punch, W. F., Venkataraman, S., Goodman, E. D., and Kuhn, L. A. (1997) *J Mol Biol 265*, 445-64.
(32) Brito, R. M., Reddick, R., Bennett, G. N., Rudolph, F. B., and Rosevear, P. R. (1990) *Biochemistry 29*, 9825-31.

(33) Castillo, R., Andres, J., and Moliner, V. (1999) *J. Am. Chem. Soc. 121*, 12140-12147.
(34) Park, H., Zhuang, P., Nichols, R., and Howell, E. E. (1997) *J Biol Chem 272*, 2252-8.
(35) Deng, H., Callender, R., and Howell, E. (2001) *J Biol Chem 276*, 48956-60.
(36) Park, H., Bradrick, T. D., and Howell, E. E. (1997) *Protein Eng. Des. Sel. 10*, 1415-24.
(37) Krahn, J., Jackson M., DeRose, E.F., Howell, E.E., and London, R.E. (Accepted) *Biochemistry*.
(38) Strader, M. B., Smiley, R. D., Stinnett, L. G., VerBerkmoes, N. C., and Howell, E. E. (2001) *Biochemistry 40*, 11344-52.
(39) Strader, M. B., Chopra, S., Jackson, M., Smiley, R. D., Stinnett, L., Wu, J., and Howell, E. E. (2004) *Biochemistry 43*, 7403-12.
(40) Hicks, S. N., Smiley, R. D., Hamilton, J. B., and Howell, E. E. (2003) *Biochemistry 42*, 10569-78.
(41) Hicks, S. N., Smiley, R. D., Stinnett, L. G., Minor, K. H., and Howell, E. E. (2004) *J. Biol. Chem. 279*, 46995-7002.
(42) Calderone, C. T., and Williams, D. H. (2001) *J. Am. Chem. Soc. 123*, 6262-7.
(43) Williams, D. H., Stephens, E., and Zhou, M. (2003) *Chem. Commun. (Camb.)*, 1973-6.
(44) Williams, D. H., Stephens, E., and Zhou, M. (2003) *J. Mol. Biol. 329*, 389-99.
(45) Ivery, M. T., and Gready, J. E. (1995) *Biochemistry 34*, 3724-33.
(46) Tartof, K., and Hobbs, C. (1987) *BRL Focus 9* 12.
(47) Smiley, R. D., Stinnett, L. G., Saxton, A. M., and Howell, E. E. (2002) *Biochemistry 41*, 15664-75.
(48) Stinnett, L. G., Smiley, R. D., Hicks, S. N., and Howell, E. E. (2004) *J. Biol. Chem. 279*, 47003-9.
(49) Wells, J. A. (1990) *Biochemistry 29*, 8509-17.
(50) Carter, P. J., Winter, G., Wilkinson, A. J., and Fersht, A. R. (1984) *Cell 38*, 835-40.
(51) Mildvan, A. S. (2004) *Biochemistry 43*, 14517-20.
(52) Mildvan, A. S., Weber, D. J., and Kuliopulos, A. (1992) *Arch Biochem Biophys 294*, 327-40.
(53) Jackson, M., Chopra, S., Smiley, R. D., Maynord, P. O., Rosowsky, A., London, R. E., Levy, L., Kalman, T. I., and Howell, E. E. (2005) *Biochemistry 44*, 12420-33.
(54) Chervenak, M. C. T., Eric J. (1994) *Journal of the American Chemical Society 116*, 10533-9.
(55) Jelesarov, I., and Bosshard, H. R. (1994) *Biochemistry 33*, 13321-8.
(56) Poe, M. (1977) *J Biol Chem 252*, 3724-8.
(57) Maharaj, G., Selinsky, B. S., Appleman, J. R., Perlman, M., London, R. E., and Blakley, R. L. (1990) *Biochemistry 29*, 4554-60.
(58) Kallen, R. G., and Jencks, W. P. (1966) *J Biol Chem 241*, 5845-50.
(59) Chopra, S., Lynch, R., Kim, S. H., Jackson, M., and Howell, E. E. (2006) *Biochemistry 45*, 6596-605.
(60) Venu, K., Svensson, L. A., and Halle, B. (1999) *Biophys J 77*, 1074-85.
(61) Badger, J. (1993) *Biophys J 65*, 1656-9.
(62) Svergun, D. I., Richard, S., Koch, M. H., Sayers, Z., Kuprin, S., and Zaccai, G. (1998) *Proc Natl Acad Sci U S A 95*, 2267-72.
(63) Merzel, F., and Smith, J. C. (2002) *Proc Natl Acad Sci U S A 99*, 5378-83.
(64) Loris, R., Langhorst, U., De Vos, S., Decanniere, K., Bouckaert, J., Maes, D., Transue, T. R., and Steyaert, J. (1999) *Proteins 36*, 117-34.
(65) Ogata, K., and Wodak, S. J. (2002) *Protein Eng 15*, 697-705.
(66) Athawale, M. V., Dordick, J. S., and Garde, S. (2005) *Biophys J 89*, 858-66.
(67) Bennion, B. J., DeMarco, M. L., and Daggett, V. (2004) *Biochemistry 43*, 12955-63.
(68) Cayley, S., and Record, M. T., Jr. (2003) *Biochemistry 42*, 12596-609.

(69) Robinson, C. R., and Sligar, S. G. (1995) *Methods Enzymol 259*, 395-427.
(70) Parsegian, V. A., Rand, R. P., and Rau, D. C. (1995) *Methods Enzymol 259*, 43-94.
(71) Rand, R. P. (2004) *Philos Trans R Soc Lond B Biol Sci 359*, 1277-84; discussion 1284-5.
(72) Colombo, M. F., and Bonilla-Rodriguez, G. O. (1996) *J Biol Chem 271*, 4895-9.
(73) Reid, C., and Rand, R. P. (1997) *Biophys J 72*, 1022-30.
(74) Kornblatt, J. A., and Hoa, G. H. (1990) *Biochemistry 29*, 9370-6.
(75) Fried, M. G., Stickle, D. F., Smirnakis, K. V., Adams, C., MacDonald, D., and Lu, P. (2002) *J Biol Chem 277*, 50676-82.
(76) LiCata, V. J., and Allewell, N. M. (1997) *Biochemistry 36*, 10161-7.
(77) Auton, M., and Bolen, D. W. (2005) *Proc Natl Acad Sci U S A 102*, 15065-8.
(78) Bolen, D. W. (2001) *Methods Mol Biol 168*, 17-36.
(79) Bolen, D. W., and Baskakov, I. V. (2001) *J Mol Biol 310*, 955-63.
(80) Auton, M., and Bolen, D. W. (2004) *Biochemistry 43*, 1329-42.
(81) Liu, Y., and Bolen, D. W. (1995) *Biochemistry 34*, 12884-91.
(82) Street, T. O., Bolen, D. W., and Rose, G. D. (2006) *Proc Natl Acad Sci U S A 103*, 13997-4002.
(83) Divya, N., Grifith, E., and Narayana, N. (2007) *Protein Sci 16*, 1063-8.
(84) Ha, J. H., Spolar, R. S., and Record, M. T., Jr. (1989) *J Mol Biol 209*, 801-16.
(85) Spolar, R. S., and Record, M. T., Jr. (1994) *Science 263*, 777-84.
(86) Jen-Jacobson, L., Engler, L. E., and Jacobson, L. A. (2000) *Structure 8*, 1015-23.
(87) Haq, I., Ladbury, J. E., Chowdhry, B. Z., Jenkins, T. C., and Chaires, J. B. (1997) *J Mol Biol 271*, 244-57.
(88) Mazur, S., Tanious, F. A., Ding, D., Kumar, A., Boykin, D. W., Simpson, I. J., Neidle, S., and Wilson, W. D. (2000) *J Mol Biol 300*, 321-37.
(89) Chaires, J. B. (1998) *Curr Opin Struct Biol 8*, 314-20.
(90) Haq, I., Jenkins, T. C., Chowdhry, B. Z., Ren, J., and Chaires, J. B. (2000) *Methods Enzymol 323*, 373-405.
(91) Ladbury, J. E., Wright, J. G., Sturtevant, J. M., and Sigler, P. B. (1994) *J Mol Biol 238*, 669-81.
(92) Sturtevant, J. M. (1977) *Proc Natl Acad Sci U S A 74*, 2236-40.
(93) Ozen, C., Norris, A. L., Land, M. L., Tjioe, E., and Serpersu, E. H. (2007) *Biochemistry*.
(94) Kozlov, A. G., and Lohman, T. M. (2000) *Proteins Suppl 4*, 8-22.
(95) Gallagher, K., and Sharp, K. (1998) *Biophys J 75*, 769-76.
(96) Holdgate, G. A., Tunnicliffe, A., Ward, W. H., Weston, S. A., Rosenbrock, G., Barth, P. T., Taylor, I. W., Pauptit, R. A., and Timms, D. (1997) *Biochemistry 36*, 9663-73.
(97) Wright, E., Vincent, J., and Fernandez, E. J. (2007) *Biochemistry 46*, 862-70.
(98) Cooper, R. L., and Lee, S. A. (2004) *J Biomol Struct Dyn 22*, 375-80.
(99) Spolar, R. S., Livingstone, J. R., and Record, M. T., Jr. (1992) *Biochemistry 31*, 3947-55.
(100) McPherson, A., et al,. (1986) *J. Crystal Growth 76*, 547-553.

Part II: Effects of Temperature on R67 Dihydrofolate Reductase Catalysis

This section is a slightly modified version of a manuscript published in Biochemistry 2006 May 30; 45(*1*): 6596-605 by Shaileja Chopra, Rachel Lynch, Su-Hwa Kim, Michael Jackson and Elizabeth E. Howell

This author contributed the following to this manuscript: (1) some protein expression and purification, (2) protein extinction coefficients, (3) reduction of pteroic acid to dihydropteroic acid (DHP) (4) steady-state kinetic data with DHP, (5) ITC data with DHF and DHP (5) pK_a data for DHP (6) viscosity measurements (7) assistance with writing the manuscript. This research was supported by NSF grant MCB-9808302 (to Elizabeth E. Howell).

Abstract

R67 dihydrofolate reductase (DHFR) is a novel homotetrameric protein that possesses 222 symmetry and a single, voluminous active site pore. This symmetry poses numerous limitations on catalysis, for example, two dihydrofolate (DHF) molecules or two NADPH molecules, or one substrate plus one cofactor can bind. Only the latter combination leads to catalysis. To garner additional information on how this enzyme facilitates transition state formation, the temperature dependence of binding and catalysis was monitored. The binding of NADPH and DHF is enthalpy driven. Recent primary isotope effect studies indicate hydride transfer is the rate-determining step. Accordingly, the activation energy associated with transition state formation is 6.9 kcal/mol ($\Delta H^{\ddagger}_{25}$ = 6.3 kcal/mol). A large entropic component is also found associated with catalysis, $T\Delta S^{\ddagger}_{25}$ = –11.3 kcal/mol. Binding of a poor substrate, dihydropteroate, shows weaker affinity than for dihydrofolate ($\Delta\Delta G$ = 1.9 kcal/mol) and a large loss in the binding enthalpy value ($\Delta\Delta H$ = 6.4 kcal/mol). The k_{cat} value for dihydropteroate reduction is decreased 1600 fold compared to DHF usage. This effect appears to derive mostly from the $\Delta\Delta H$ difference in

binding, demonstrating that the glutamate tail is important for catalysis. This result is surprising as the para-aminobenzoyl-glutamate tail of DHF has been previously shown to be disordered by both NMR and crystallography studies. Viscosity studies were also performed and confirmed that the hydride transfer rate is not sensitive to sucrose addition. Surprisingly, binding of DHF, by both K_m and K_d determination, was found to be sensitive to added viscogens, suggesting a role for water in DHF binding.

Introduction

Dihydrofolate reductase (EC 1.5.1.3) catalyzes the reduction of dihydrofolate (DHF) to tetrahydrofolate (THF) using NADPH as a cofactor. Two different protein scaffolds that catalyze the DHFR reaction have been identified. The first corresponds to chromosomal *E. coli* DHFR, which is the target of the antibacterial drug, trimethoprim (TMP). The second DHFR is encoded by an R-plasmid, which provides resistance to TMP. R67 DHFR is unrelated genetically and structurally to chromosomal DHFR. Chromosomal *E. coli* DHFR has been described as a well-evolved enzyme with an efficiency of 0.15 (*2*), while R67 DHFR has been suggested to be a model for a "primitive" enzyme that has not yet been optimized by evolution (*3, 4*).

The proposal that R67 DHFR is a primitive enzyme arises from the constraints imposed by its structure coupled with its use of two substrates (dihydrofolate and NADPH). As shown in figure 1, R67 DHFR is a homotetramer with a single active site pore that is solvent-accessible, except perhaps at the hourglass center when ligands are bound. The overall structure possesses 222 symmetry (*3*). The obligatory symmetry of the active site results in overlapping binding sites for

Figure 1: Structures of R67 DHFR, Dihydrofolate and Diydropteroate. A) Ribbon structure of R67 DHFR (protein data bank file 1VIE) (*3*). The enzyme is a dimer of dimers; the monomer-monomer interfaces occur on the sides of the structure (sea green + blue or chartreuse + red), while the dimer-dimer interfaces occur on the top and bottom of the structure (sea green + red or chartreuse + blue). The active site pore corresponds to the "doughnut hole" in the center. B) Structures of DHF and DHP with atom labels from N5 to N8.

A

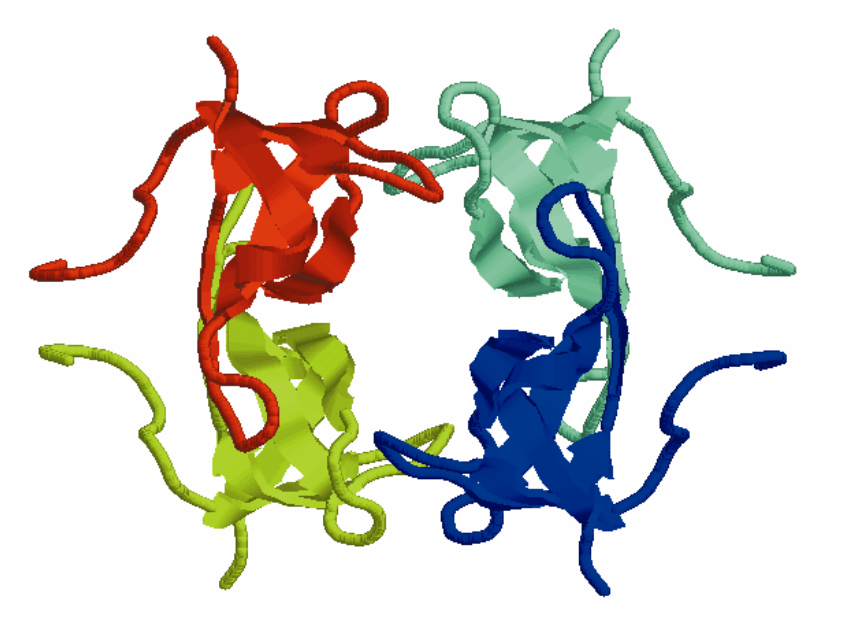

B

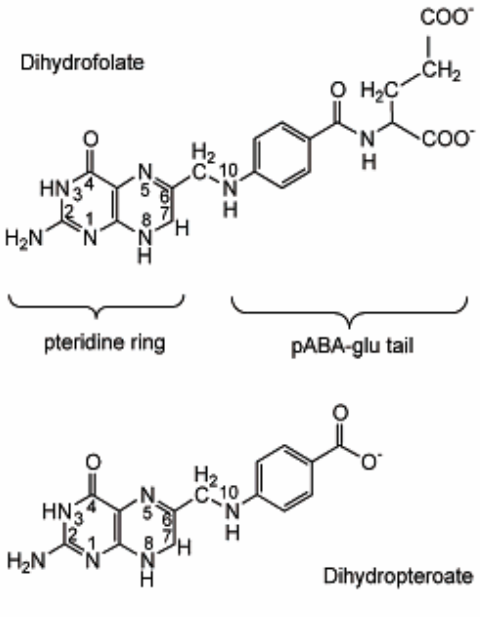

DHF and NADPH. This can be seen experimentally as R67 DHFR binds a total of two ligands; either two NADPH molecules or two folate/DHF molecules or one NADPH plus one folate/DHF molecule (*5*). The first two complexes are dead-end complexes, while the third is the productive catalytic complex (figure 1). The ability to discriminate between the homoligand and heteroligand complexes mostly appears to arise from stacking between the ligands, as well as some contribution from the enzyme (*6, 7*). It has been found experimentally that the greater the enthalpy change associated with formation of the productive ternary complex, the greater the catalytic efficiency (*8*). Other groups have correlated enthalpic effects with structural tightness (*9-11*). Another consequence arising from this particular constellation of structural features is that introduction of a mutation in the gene results in four mutations per active site. These mutations typically have large cumulative effects (*8, 12*) and make it unlikely that R67 DHFR uses a general acid in its active site to facilitate catalysis (as addition of one general acid per gene will result in four general acids per active site pore). Rather, pre-protonated DHF from solution is used as substrate (*13*). Finally, the rate-determining step of R67 DHFR is chemistry as NADPD isotope effects using a H62C mutant of R67 DHFR find ^{D}V (= k_{cat} using NADPH / k_{cat} using NADPD) at pH 5.0 equals 3.6 ± 0.45 and at pH 7.0, ^{D}V = 3.3 ± 0.33 (*13*). These results indicate hydride transfer is rate determining from pH 5–7.

While the 222 symmetry restricts the catalytic strategy of R67 DHFR, there are some advantages associated with this symmetry. The first positive feature is expenditure of less energy and DNA in encoding the genetic information. A second advantage pertains to the consequences of symmetry breaking whereby different properties and packing relationships arise (*14, 15*). For example, the initial binding of NADPH to R67 DHFR utilizes the symmetry of the protein by allowing binding to 1 of 4 symmetry related sites. Once bound, NADPH creates a local asymmetric environment in the active site pore, which results in negative cooperativity

disfavoring binding of a second NADPH molecule or positive cooperativity favoring binding of DHF. Both these cooperativity patterns strongly favor channeling of the binding pathway towards the productive ternary complex, NADPH•DHF. A third benefit of symmetry is the potential for multivalent binding (*16*). Here, once a site is occupied, the proximity of other symmetry related sites can enhance binding by reduction of the associated entropy and/or by decreasing the dissociation rate (*17, 18*). This type of effect appears likely to occur in R67 DHFR (*19, 20*).

A study of the transition state used by R67 DHFR will help further deconvolute its catalytic strategy. From interligand NOEs using NMR, the bound $NADP^+$•folate complex is most consistent with use of an *endo* transition state, where the nicotinamide ring of cofactor overlaps that of the N5 containing pteridine ring of substrate (*6, 21*). The *endo* transition state has been proposed to be 2 kcal/mol more stable than the *exo* transition state used by chromosomal *E. coli* DHFR (*22, 23*). To garner more information concerning the transition state used by R67 DHFR, the temperature dependence of its reaction was studied.

Materials And Methods

Protein Purification R67 DHFR was expressed in *E. coli* SK383 cells in TB media containing 200μg/ml ampicillin and 20μg/ml trimethoprim as previously described (*24*). Briefly, ammonium sulfate precipitation and ion-exchange column chromatography were used to purify the protein to homogeneity. Purified samples were dialyzed against distilled, deionized H_2O and then lyophilized. Protein concentrations were determined with a biuret assay (*25*).

Fluorescence Quenching Binding of NADPH to 2.0 μM R67 DHFR was monitored in MTA buffer at various temperatures using tryptophan fluorescence as per Zhuang et al. (*26*). MTA is a polybuffer containing 50 mM MES, 100 mM Tris and 50 mM acetic acid at pH 7.0, which maintains a constant ionic strength from pH 4.5-9.5 (*27*). Data were fit to:

$$Fl = F_o - 0.5\ F_o\ [P_{tot} + K_d + L_{tot} - [(P_{tot} + K_d + L_{tot})^2 - 4\ P_{tot}\ L_{tot})^{1/2}] \quad (1)$$

where Fl is the observed fluorescence, L_{tot} is the total ligand concentration, and P_{tot}, K_d and F_o are variables describing the number of enzyme binding sites, dissociation constant and fluorescence yield per unit concentration of enzyme, respectively (*28*).

Steady State Kinetics Steady state kinetic data were obtained using either a Perkin-Elmer λ3a or a λ35 spectrophotometer interfaced with an IBM PS2 as previously described (*29*). Briefly, assays were performed at 30°C in MTA polybuffer, by the addition of substrate (DHF) and cofactor (NADPH), followed by the addition of enzyme to initiate the reaction. To obtain k_{cat} and K_m values, the concentration of NADPH was held constant at a subsaturating level while the concentration of DHF was varied. This process was repeated using four additional subsaturating concentrations of NADPH. The data were fit globally to the nonlinear bisubstrate Michaelis Menton equation utilizing SAS (statistical analysis software; (*7, 30*)). The NLINEK macro for use in SAS is available at: http://www.agriculture.utk.edu/ansci/faculty/saxton_software.html.

The temperature dependence of the steady state kinetic behavior of R67 DHFR was studied from 20-50°C. The pH meter was standardized at each temperature and MTA buffer titrated to pH 7.0. Within error, the extinction coefficient of the reaction did not change as temperature was varied (data not shown).

For solutions containing viscogens, the steady state data were initially monitored as described above. When it became apparent that the main variation occurred in the K_m for DHF, data were then collected using saturating NADPH concentrations.

Reduction of the alternate substrate, dihydropteroic acid (DHP), was also studied. Pteroic acid was purchased from Schircks Laboratories and reduced to DHP according to Prabhu et al. (*31*). NMR analysis confirmed formation of the reduced species and the simultaneous disappearance of the oxidized compound. The molar extinction coefficient used to assess reduction of DHP was monitored and found to be the same as for DHF reduction, which is 12,300 $M^{-1}cm^{-1}$ (*32*). Since this is a poor substrate, higher enzyme concentrations were used and Michaelis-Menton conditions did not apply. Data were fit to equation 2:

$$v = \frac{k_{cat} * ([E_{tot}] + [S_{tot}] + K_d) - \{([E_{tot}] + [S_{tot}] + K_d)^2 - 4[E_{tot}][S_{tot}]\}^{1/2}}{2} \qquad (2)$$

where $[E_{tot}]$, $[S_{tot}]$, K_d, v and k_{cat} are the total enzyme and substrate concentrations, the substrate binding constant, the initial velocity and the catalytic rate constant, respectively (*33*).

Determination of Substrate pK_a values The pK_a value for the N5 atom in DHF was determined as per Maharaj et al. (*34*). Essentially, the absorbance of a DHF solution (<30μM) was monitored within 30 seconds at 228 nm. A range of pH values were obtained using 0.2M sodium phosphate buffer or various concentrations of HCl (<0.25M). To minimize any precipitation of DHF near its isoelectric point, DHF was dissolved first, followed by addition of buffer or HCl. The data were fit to an equation describing a standard ionization curve (*35*). An identical approach was used to determine the N5 pK_a of dihydropteroic acid.

Viscosity Measurements Kinematic viscosity (η/ρ in mm^2/s) was monitored using a Cannon-Fenske viscometer equilibrated at 30°C in a Precision Temp-Trol mineral oil bath. Kinematic viscosity was converted to viscosity (η) by multiplying by the density of the solution (ρ in gms/ml). Sucrose ($\leq$1.75M) was added to increase η to $\leq$10.5 cP. Relative viscosities (η/η_o) were calculated using MTA buffer as the reference. Trehalose ($\leq$1.6M), also a disaccharide, was additionally used as a viscogen to determine whether sucrose had a specific or non-specific effect.

Isothermal Titration Calorimetry Affinities, stoichiometries as well as ΔH values were determined for binding studies using isothermal titration calorimetry (ITC) as previously described (*5*). Measurements were performed on a VP-ITC microcalorimeter from MicroCal interfaced to a Gateway PC for data acquisition and analysis. Origin® v.5 scientific software was used to analyze the data. The design and use of this instrument have been previously described (*36*). R67 DHFR concentrations typically ranged between 90-150 μM in MTA buffer (pH 8). Experiments were performed at least in duplicate. For titrations with sucrose present, MTH buffer plus sucrose was used in the reference cell.

Results

What is the Temperature Dependence of NADPH Binding to R67 DHFR? To determine the temperature dependence of the K_d for NADPH, a fluorescence quenching approach was employed. Titration of NADPH into R67 DHFR was performed from 10-35°C and the data fit to obtain a K_d value (table 1). As the temperature rose, so did the K_d (figure2). The data were then analyzed using the van't Hoff equation:

$$\ln K_a = (-\Delta H / RT) + \Delta S / R \qquad (3)$$

Table 1: Temperature dependence for NADPH binding. Data describing the K_d values obtained upon titration of NADPH into R67 DHFR to form enzyme•2NADPH complex at different temperatures.

Temperature (^{o}Celsius)	Temperature (^{o}Kelvin)	1/T (Kelvin^{-1})*10^{-3}	K_d (μM)
10	283	3.53	1.29 ± 0.1
15	288	3.47	1.31 ± 0.2
20	293	3.41	2.22 ± 0.2
20	293	3.41	1.85 ± 0.2
25	298	3.36	2.80 ± 0.2
30	303	3.30	3.34 ± 0.3
35	308	3.25	4.30 ± 0.3
40	313	3.20	4.87 ± 0.9

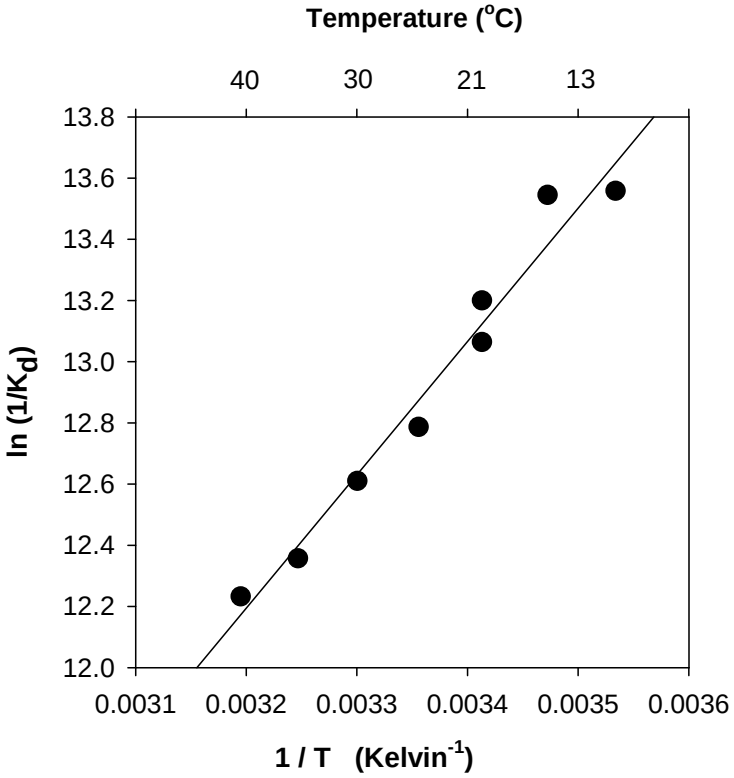

Figure 2: A van't Hoff plot describing the temperature dependence of NADPH binding to R67 DHFR. Binding of NADPH was monitored by fluorescence quenching, which only describes titration of a single NADPH molecule. Errors associated with the K_{d1} values are smaller than the symbol size. Best-fit values are given in the text as well as Table 7.

where the association constant, K_a, equals $1/K_d$, ΔH is the enthalpy change, ΔS is the entropy, R is the gas constant and T is the temperature in degrees Kelvin (table 1). The slope of these plots equals $-\Delta H/R$, and ΔH is calculated to be -8.6 ± 0.6 kcal/mol.

What is the Temperature Dependence of R67 DHFR Catalysis? The steady state kinetic behavior of R67 DHFR was also studied and found to be dependent on temperature from 20 to 50°C. Effects on both k_{cat} and K_m values were observed. The data were then analyzed using the Arrhenius equation:

$$k = Ae^{-Ea/RT} \quad (4)$$

where k is the rate, A is the pre-exponential factor and E_a is the activation energy (*37*). Figure 3 plots the reciprocal temperature versus ln k_{cat} as well as ln $k_{cat}/K_{m\ (DHF)}$. The plots are linear, consistent with a single rate-determining step being monitored. The slope for this plot corresponds to E_a / R where E_a is the activation energy for the reaction. For the k_{cat} plot, E_a is calculated to be 6.90 ± 0.6 kcal/mol. From the equation $\Delta H^{\ddagger} = E_a - RT$, $\Delta H^{\ddagger}_{25}$ for R67 DHFR can be calculated as 6.3 kcal/mol and from $\Delta G^{\ddagger} = -RT \ln (k_{cat} \bullet h / k_B \bullet T)$, $\Delta G^{\ddagger}_{25}$ can be calculated as 17.6 kcal/mol (where h is Planck's constant and k_B is the Boltzmann constant) (*38, 39*). $T\Delta S^{\ddagger}_{25}$ can then be computed as –11.3 kcal/mol from $\Delta G^{\ddagger} = \Delta H^{\ddagger} - T\Delta S^{\ddagger}$ (table 2). Alternate fits were also employed and provided similar values. To minimize error propagation, the raw data were also fit directly to rate $Ae^{(-E_a/RT)}$. For this nonlinear fit, $E_a = 7.1 \pm 0.7$ kcal/mol and $\Delta H^{\ddagger}_{25} = 6.5 \pm 0.7$ kcal/mol.

The temperature dependence of dihydropteroate (DHP) reduction was additionally studied. DHP is a fragment of DHF where a para-amino-benzoate tail replaces the p-amino-benzoyl-glutamate (pABA-glu) tail of DHF (see figure 1B). A negative charge remains on the tail, albeit in a different position. DHP reduction is much slower than DHF reduction, with a k_{cat} value of 4.9 x

$10^{-4} \pm 1.7 \times 10^{-5}$ s^{-1} and a $K_{m\ (DHP)}$ value of 23 ± 2.4 μM at 25 °C. These changes reflect an ~10 fold increase in K_m and an ~1600 fold decrease in k_{cat} with respect to DHF reduction. The temperature dependence of DHP reduction is also shown in figure 3. The corresponding activation energy is 14.3 ± 1.4 kcal/mol. $\Delta H^{\ddagger}_{25}$ can then be calculated as 13.7 kcal/mol with a $\Delta G^{\ddagger}_{25}$ of 22 kcal/mol and a $T\Delta S^{\ddagger}_{25}$ of -8.3 kcal/mol. The various thermodynamic values for DHP binding and catalysis are given in table 3.

The $H^{\ddagger}$, $\Delta G^{\ddagger}$ and $T\Delta S^{\ddagger}$ values for DHF and DHP reduction were also obtained using the Eyring equation:

$$k = (\kappa k_B T)/h * e^{-\Delta G^{\ddagger} / RT} \qquad (5)$$

where κ is the transmission coefficient (with a value of 1); k_B is the Boltzmann constant ($1.38 \cdot 10^{-23}$ JK^{-1} $molecule^{-1}$); h is the Planck's constant ($6.624 \cdot 10^{-34}$ Js $molecule^{-1}$) and R is the gas constant (8.314 JK^{-1} mol^{-1}). The slope of the plot of 1/T vs ln kh/k_BT equals $\Delta H^{\ddagger}/R$ and the y-intercept equals $\Delta S^{\ddagger}/R$. from which, the values of $\Delta H^{\ddagger}$ (6.3 ± 0.6 kcal/mol) and $T\Delta S^{\ddagger}$ (-11.8 ± 0.6 kcal/mol) were obtained at 25°C. The Eyring plot was also used for DHP reduction and $\Delta H^{\ddagger}$ was found to be 13.7 ± 1.4 kcal/mol and $T\Delta S^{\ddagger}_{25}$ = 8.2 ±1.4 kcal/mol (figure 4).

Table 2: Temperature dependence for DHF reduction. Data describing the K_m and k_{cat} values obtained for DHF binding (using steady state kinetics) at different temperatures. van't Hoff, Arrhenius and Eyring plots were used to obtain values for ΔH and ΔS as shown in figure 3 and 4.

Temperature (^{o}Kelvin)	K_m (μM)	k_{cat} (s^{-1})	k_{cat}/K_m ($M^{-1}s^{-1}$) * 10^4
293	1.78 ± 0.2	0.54 ± 0.01	30.6
298	2.37 ± 0.3	0.77 ± 0.02	32.7
303	3.08 ± 0.3	0.88 ± 0.03	28.5
308	5.24 ± 0.3	0.98 ± 0.03	17.0
313	7.31 ± 0.5	1.29 ± 0.04	17.6
318	11.3 ± 0.6	1.37 ± 0.03	12.1
323	15.5 ± 1.4	1.81 ± 0.07	11.7

Table 3: Temperature dependence for DHP reduction. Data describing the K_m and k_{cat} values obtained for DHP binding (using steady state kinetics) at different temperatures. van't Hoff, Arrhenius and Eyring plots were used to obtain values for ΔH and ΔS as shown in figure 3 and 4.

Temperature (^{o}Kelvin)	K_m (μM)	k_{cat} (s^{-1}) * 10^{-4}	k_{cat}/K_m ($M^{-1}s^{-1}$)* 10^{-6}
298	19.7 ± 2.0	4.86 ± 0.2	24.6
	27.0 ± 2.4	5.91 ± 0.2	21.9
	21.5 ± 2.3	3.54 ± 0.1	16.5
300	27.7 ± 5.3	6.59 ± 0.4	23.8
303	31.0 ± 4.9	8.20 ± 0.4	26.5
	31.1 ± 2.1	9.23 ± 0.2	29.5
308	38.0 ± 1.9	9.26 ± 0.2	24.4
	35.1 ± 7.7	11.1 ± 0.9	31.8
	44.0 ± 2.6	9.89 ± 0.2	22.8
311	40.2 ± 1.4	14.7 ± 0.2	36.7
313	37.5 ± 1.3	16.1 ± 0.2	42.8

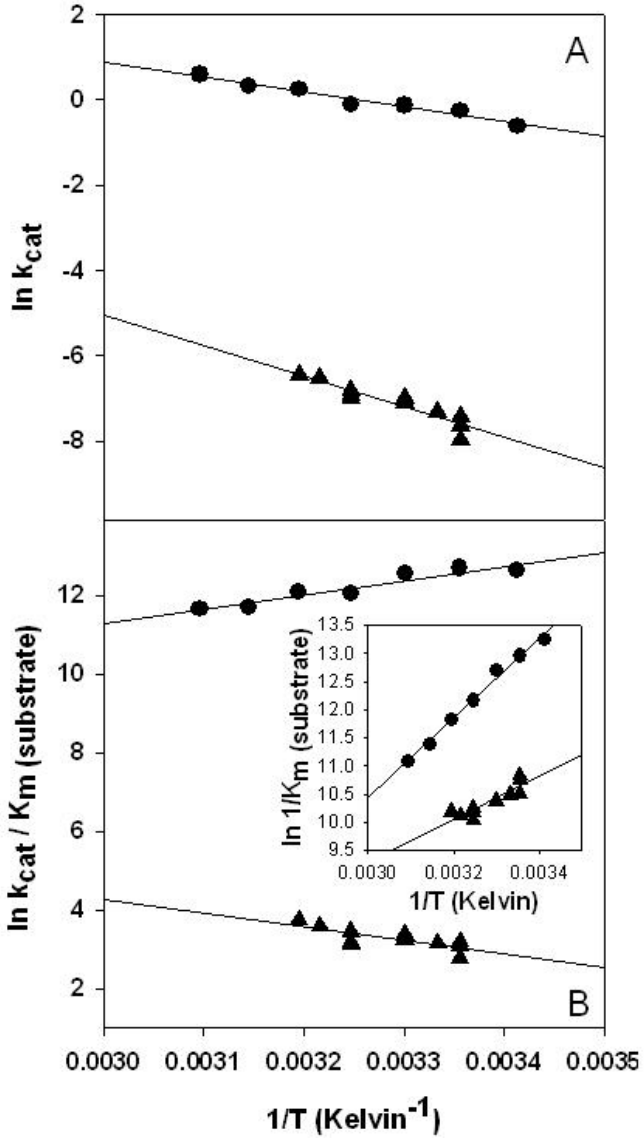

Figure 3: Arrhenius plots describing R67 DHFR catalysis. Steady state kinetic analysis was performed as described in the Materials and Methods section. Reduction of DHF and DHP were both studied and are described by ● and ▲ points, respectively. Errors associated with the various parameters are smaller than the symbol size. Panel A describes the ln k_{cat} values while panel B describes ln $k_{cat}/K_{m\ (substrate)}$ data. The inset plots the variance of ln $1/K_{m\ (substrate)}$ with inverse temperature.

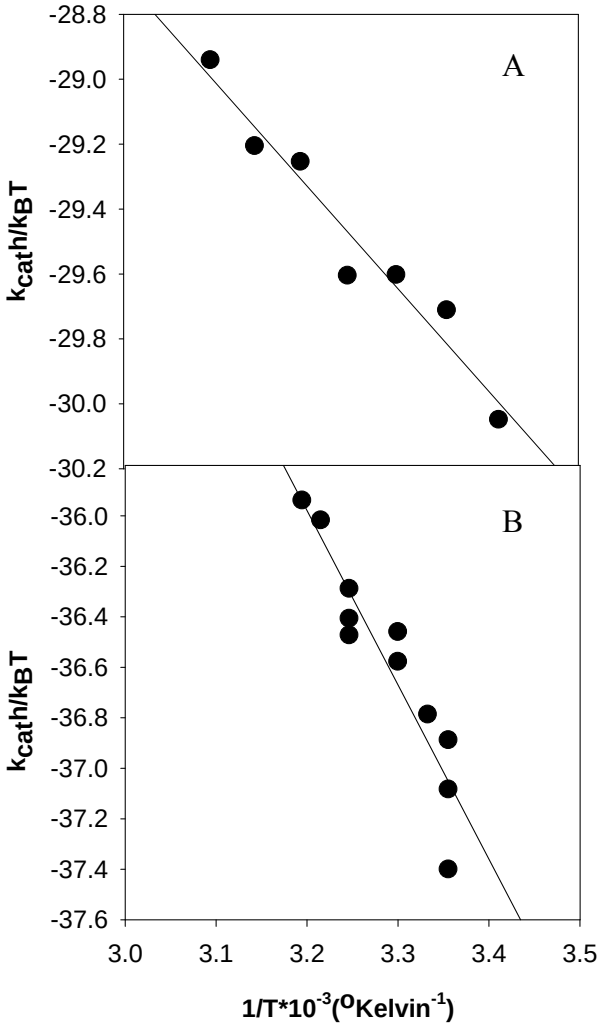

Figure 4: Eyring plots describing R67 DHFR catalysis. An Eyring plot (1/T vs ln(kh/k_BT) was also used to evaluate $\Delta H^{\ddagger}$ and $\Delta S^{\ddagger}$ values, as the slope of this plot equals $\Delta H^{\ddagger}/R$ and the *y*-intercept equals $\Delta S^{\ddagger}/R$. A) For DHF reduction, $\Delta H^{\ddagger} = 6.3 \pm 0.6$ kcal/mol and $T\Delta S^{\ddagger}_{25} = -11.8 \pm 0.6$ kcal/mol. B) For DHP reduction, $\Delta H^{\ddagger}$ was found to be 13.7 ± 1.4 kcal/mol and $T\Delta S^{\ddagger}_{25}$ was determined to be 8.2 ±1.4 kcal/mol using an Eyring plot.

Temperature Dependence of the N5 pK_a in DHF Since R67 DHFR reduces pre-protonated DHF (*13*), a trivial reason for k_{cat} to increase with temperature would be that the N5 pK_a increases with temperature. The structure of DHF is given in figure 1 along with atom labels. While previous studies of organic cyclic compounds predict that the N5 pK_a should decrease with increasing temperature (*40*), the N5 titration in DHF was directly monitored from 10 to 20°C. A typical titration curve is shown in figure 5A. Above 20°C, DHF is not sufficiently stable in acidic solutions to continue the titrations (*34*), however the general trend of a decreased pK_a associated with the N5 atom can be observed with increasing temperature. Specifically, at 10°C, the N5 pK_a is 2.86 ± 0.01, while at 15°C, the pK_a is 2.74 ± 0.03 and at 20°C, the pK_a is 2.69 ± 0.02. Thus the increased k_{cat} associated with R67 DHFR at elevated temperatures does not arise from an increase in the concentration of free, protonated DHF. These values compare with an N5 pK_a equal to 2.59, previously obtained at 20°C (*34*). The effect of temperature on the pK_a of DHP was also estimated (*34*). A value of 2.54 ± 0.03 is obtained at 20°C, indicating no to minimal change in this pK_a compared to DHF.

Table 4: Effect of temperature on the pK_a of the N5 group of DHF. Data describing the pK_a values of the N5 position of DHF at 10°C, 15°C and 20°C. The pK_as obtained were converted to ln K_a and are shown in figure 5B.

Temperature (°Kelvin)	1/T (Kelvin^{-1})*10^{-2}	pK_a
283	3.534	2.86 ± 0.01
288	3.472	2.74 ± 0.03
293	3.413	2.69 ± 0.02

Figure 5: Determination of the N5 pK_a value for dihydrofolate at different temperatures A) Absorbance at 228 nm was monitored as a function of pH at 20°C. From this, the pK_a was determined to be 2.69 ± 0.02 as shown in table 4. B) van't Hoff plot describing protonation of the N5 atom in DHF. The pK_as obtained at different temperatures were converted to K_a. The inverse temperature dependence of ln K_a was plotted and the slope used to calculate a ΔH value of 6.5 ± 1.0 kcal/mol.

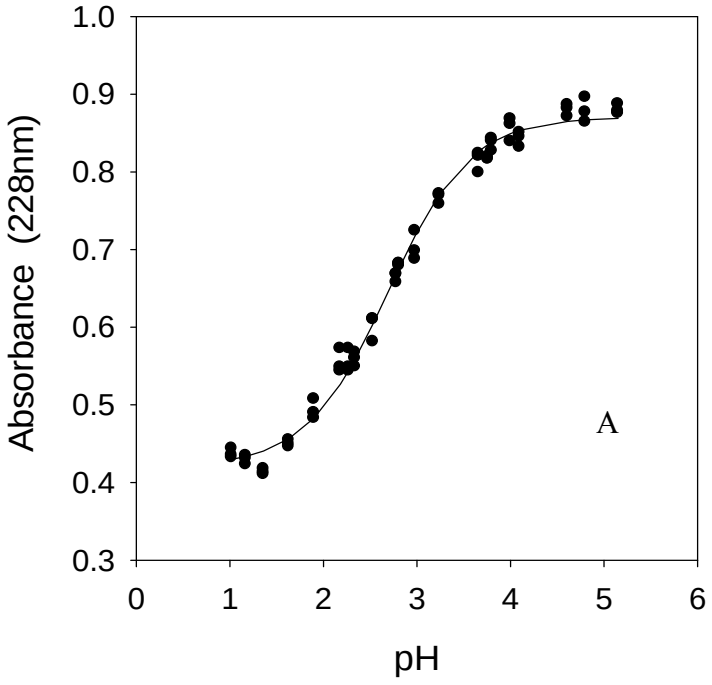
1.0
0.9
0.8
0.7
0.6
0.5
0.4
0.3
Absorbance (228nm)
A
0
1
2
3
4
5
6
pH

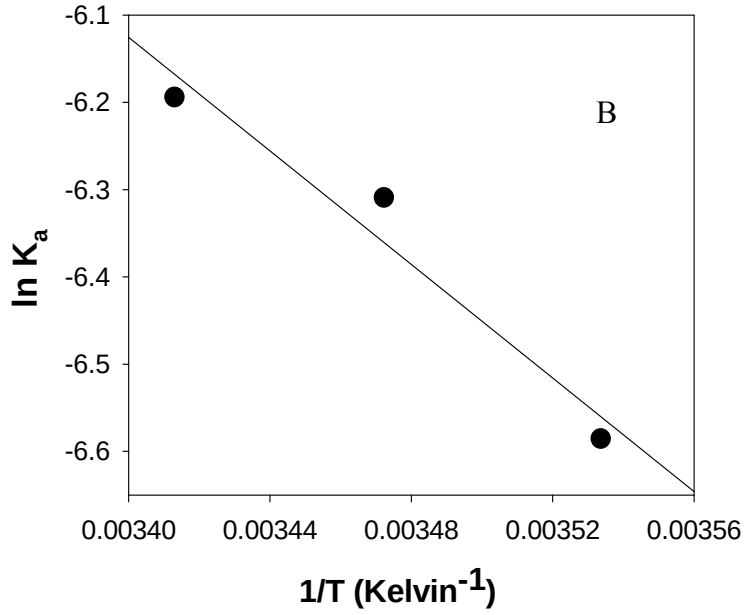
-6.1
-6.2
-6.3
-6.4
-6.5
-6.6
ln K_a
B
0.00340
0.00344
0.00348
0.00352
0.00356
1/T (Kelvin^{-1})

Are There Any Viscosity Effects on k_{cat}/K_m? A common approach to show that the rate of the enzyme under study is not limited by either binding or release of ligands involves monitoring the steady-state rate in solutions of varying viscosities. If ligand binding or release is the rate-determining step, increasing the microscopic viscosity will decrease k_{cat}/K_m in a linear fashion (*41, 42*). Even though an H62C mutant of R67 DHFR shows a NADPD isotope effect ($^DV = k_{cat}$ using NADPH / k_{cat} using NADPD at pH 7.0 = 3.3 ± 0.33 (*13*)), we monitored catalysis in increasing concentrations of sucrose. No effect on k_{cat} was observed. Surprisingly, clear effects on $k_{cat}/K_{m\ (DHF)}$ were seen as well as a small effect on $k_{cat}/K_{m\ (NADPH)}$ (~2 fold at the highest viscosity). The results are plotted in figure 6. Viscogens can have a variety of effects including perturbation of solvent structure. Since the viscogenic effect is predominately observed on $k_{cat}/K_{m\ (DHF)}$, a possibility is that the viscogen affects the water structure, which selectively affects DHF binding.

To investigate whether sucrose acts specifically or whether it acts non-specifically as a viscogen, trehalose was also used to alter the solution viscosity. At comparable relative viscosities (η/η_o), similar kinetic effects were observed using either trehalose or sucrose (see figure 6, table 5), consistent with viscosity being the primary variable.

Table 5: Effect of viscosity on K_m and k_{cat}/K_m of DHF Steady state kinetic experiments were performed in the presence of different concentrations of sucrose and trehalose and the k_{cat} and $K_{m(DHF)}$ was determined at saturating concentrations of NADPH. A plot of the ratio of $k_{cat}/K_{m(DHF)}$ versus ratio of viscosity (relative to MTH) is shown in figure 6. A plot of ratio of k_{cat} versus ratio viscosity is shown in the same figure.

Viscogen	Viscosity at 30°C	Ratio Viscosity	$K_{m\,(DHF)}$ (μM)	k_{cat} (s^{-1})	Ratio k_{cat}	Ratio $k_{cat}/K_{m(DHF)}$ ($M^{-1}s^{-1}$)
Water	0.89	1.02	-	-	-	-
MTH	1.01	1	3.85 ± 0.5	0.90 ± 0.03	1	1
0.8 sucrose	2.34	2.62	5.93 ± 1.2	0.76 ± 0.05	0.85	1.8
1 sucrose	2.80	3.14	12.9 ± 0.8	0.92 ± 0.02	1.02	3.26
1.25 sucrose	4.05	4.53	17.8 ± 3.1	0.88 ± 0.05	0.98	4.71
1.5 sucrose	6.04	6.76	21.5 ± 1.7	0.92 ± 0.03	1.03	5.45
1.6 sucrose	9.34	10.5	28.6 ± 4.1	0.81 ± 0.04	0.91	8.19
1.75 sucrose	10.5	11.8	32.0 ± 3.7	0.82 ± 0.03	0.91	9.14
MTH	0.89	1	3.62 ± 0.2	0.71 ± 0.01	1	1.20
Trehalose (1M)	3.18	3.56	8.90 ± 0.6	0.84 ± 0.03	0.84	2.48
Trehalose (1.4M)	6.42	7.19	13.3 ± 1.1	0.57 ± 0.02	1.24	4.57

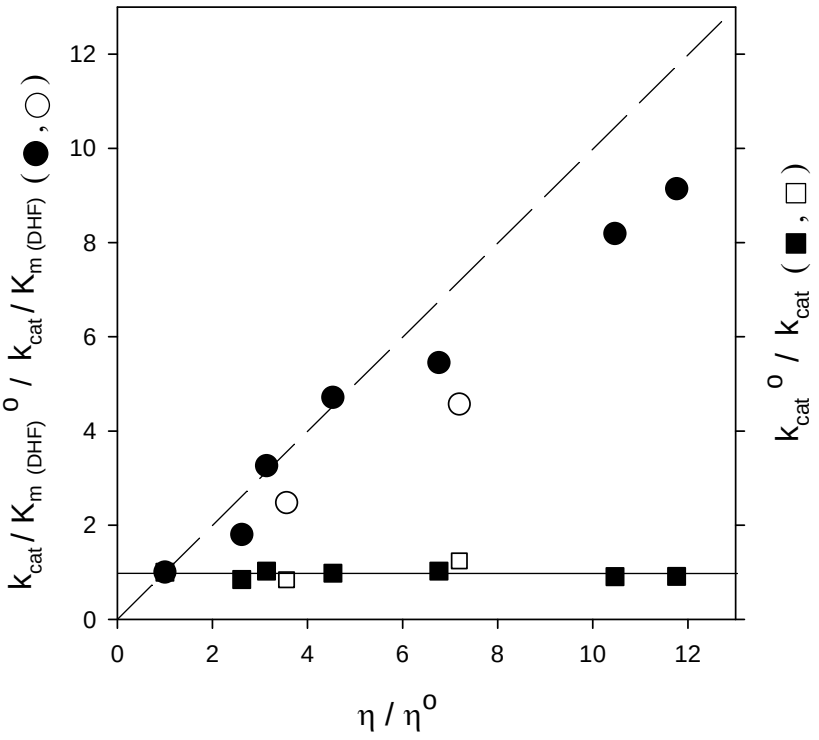

Figure 6: A plot of relative viscosity versus relative k_{cat} and $k_{cat}/K_{m\ (DHF)}$ values. Relative viscosities (η/η_o) were calculated using MTA buffer as the reference (η_o). Relative k_{cat} (squares) and $k_{cat}/K_{m\ (DHF)}$ (circles) values use steady state kinetic values in MTH buffer as the reference. Data using sucrose or trehalose as the viscogen are represented by the filled (●,■) and open (○,□) data points, respectively. A theoretical dashed line is shown with a slope of 1, consistent with diffusion being the rate limiting process for k_{cat}/K_m. The solid line displays a slope of 0, the expected trend if diffusion did not have any effect on catalysis.

To monitor the effect of viscosity on $K_{d\,(DHF)}$ directly, binding of DHF to R67 DHFR•$NADP^+$ was studied in increasing concentrations of sucrose using isothermal titration calorimetry (figure 7, table 6). An approximately 4-fold increase in K_d was observed in buffer containing 1.25 M sucrose ($\eta/\eta_o = 5.1$). A clear effect on K_d is observed (including data obtained at 28 and 30°C, not shown), however as the η/η_o ratio rises, the difference between the K_m and K_d values increases (from two to three fold). Values are not reported using even higher sucrose concentrations as the observed binding stoichiometry was affected. This may have resulted from any effects of higher mixing rates on protein stability or perhaps secondary effects on $NADP^+$ binding.

Use of Dihydropteroate as an Alternate Substrate: The temperature dependence of dihydropteroate (DHP) reduction was additionally studied. DHP is a fragment of DHF where a para-amino benzoate tail replaces the p-aminobenzoylglutamate (pABA-glu) tail of DHF (see figure 1). This fragment diminishes the negative charge to –1 and places the charge at a different position on the tail. DHP reduction is much slower than DHF reduction, with a k_{cat} value of (0.49 ± 0.17)* 10^{-4} s^{-1} and a $K_{m\,(DHP)}$ value of 23 ± 2.4 μM at 25°C. These changes reflect an ~10-fold increase in K_m and ~1600-fold decrease in k_{cat} with respect to DHF reduction. The temperature dependence of DHP reduction is also shown in figure 3. The corresponding activation energy is 14.3 ± 1.4 kcal/mol. $\Delta H^{\ddagger}_{25}$ can then be calculated as 13.7 ± 1.4 kcal/mol with a $\Delta G^{\ddagger}_{25}$ of 22 ± 0.1 kcal/mol and a $T\Delta S^{\ddagger}_{25}$ of –8.3 ± 1.4 kcal/mol. The various thermodynamic values comparing DHF versus DHP binding and catalysis are given in Table 7. To determine whether the reduction in catalytic rate could arise partly from a decrease in the N5 pK_a of DHP, a spectrophotometric titration was performed as described above or DHF (*34*). The N5 pK_a for DHP is 2.54 ± 0.03 at 20°C indicating no to minimal change in this pK_a compared to DHF.

Table 6: Formation of the ternary R67 DHFR•$NADP^+$•DHF complex as monitored by isothermal titration calorimetry.

Condition	K_d (μM)	ΔH (kcal/mol)	Stoichiometry
MTH buffer	1.6 ± 0.1	-13.3 ± 0.8	0.85 ± 0.01
MTH buffer + 0.75M sucrose (η/η_o = 2.0)	3.7 ± 0.2	-12.8 ± 1.0	1.1 ± 0.1
MTH buffer + 1.25M sucrose (η/η_o = 5.1)	6.0 ± 0.4	-11.3 ± 1.3	1.0 ± 0.1

DHF was titrated into a 1:3.5 (to 1:4) mixture of R67 DHFR•$NADP^+$ at a pH of 8.0 and 25°C as previously described (*3, 5*). The protein concentration ranged from 89-130 μM.

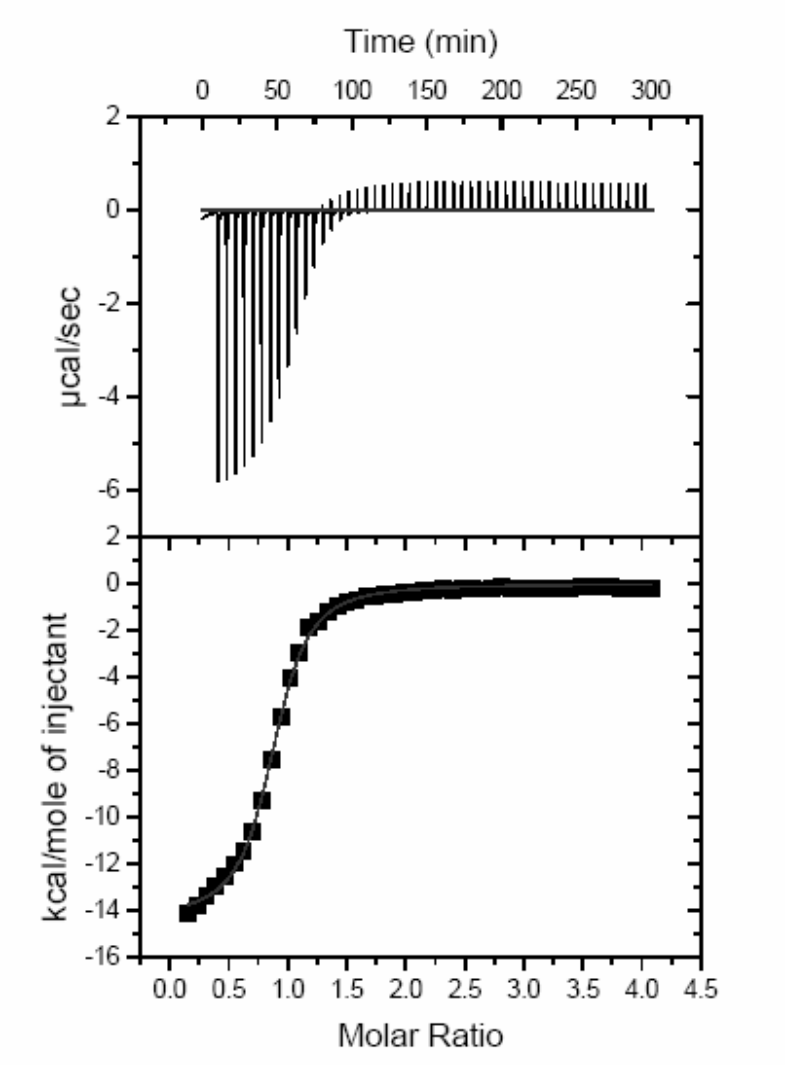

Figure 7: Titration of DHF into R67 DHFR•NADP$^+$ in 0.75 M sucrose as monitored by isothermal titration calorimetry at 25^{o}C. The top panel shows the series of peaks generated from the heat liberated upon binding of dihydrofolate. As the protein approaches saturation, less of each subsequent addition is bound, so the peaks decrease in intensity. The protein concentration was 110µM tetramer. The bottom panel shows the heat liberated per mole of titrant vs. the dihydrofolate: protein molar ratio. The smooth line shows the fit of the data to a single interacting sites model. Best-fit values are given in Table 6 of the text.

Table 7: Thermodynamic values describing binding and reduction of DHF and DHP by R67 DHFR

Complex	Value	ΔG (kcal/mol)	ΔH (kcal/mol)	TΔS (kcal/mol)
E•NADPH[a]	$K_{d\ (NADPH)}$ = 2.8 μM	-7.5	-8.6	-1.1
E•NADPH•DHF[b]	$K_{m\ (DHF)}$ = 2.4 μM	-7.7	-14.1	-6.4
[E•NADPH•DHF]$^{\neq}$	k_{cat} = 0.77 s^{-1}	17.6	6.3	-11.3
E•NADPH•DHP[c,]	$K_{m\ (DHP)}$ = 23 μM	-6.3	-7.5	-1.2
Relative to DHF binding		ΔΔG = 1.4	ΔΔH = 6.6	Δ(TΔS) = 5.2
[E•NADPH•DHP]$^{\neq}$	k_{cat} = 4.9 x10^{-4} s^{-1}	22.0	13.7	-8.3
Relative to DHF reduction		ΔΔG = 4.4	ΔΔH = 7.4	Δ(TΔS) = 3.0

[a] For comparison, ITC values describing binding of NADPH at 28°C, pH 8 are: K_d = 2.5 μM, ΔG = -7.7 kcal/mol, ΔH = -8.6 kcal/mol, TΔS = -0.9 kcal/mol (*5*).

[b] For comparison, ITC values describing binding of DHF to R67 DHFR•$NADP^+$ at 25°C, pH 8 are: K_d = 1.6 μM, ΔG = -7.9 kcal/mol, ΔH = -13.3 kcal/mol, TΔS = -5.4 kcal/mol (Table 6). ITC experiments are performed at pH 8 rather than pH 7 to minimize any contribution to the enthalpy change from the pH-dependent tetramer to 2 dimers dissociation.

[c] For comparison, ITC values describing binding of DHP to R67 DHFR•NADPH at 25°C, pH 8 are: K_d = 18.3 ± 0.5 μM, ΔG = -6.0 kcal/mol, ΔG = -6.5 ± 0.1 kcal/mol, ΔH = -9.5 ± 0.2 kcal/mol TΔS = -3.0 ± 0.2 kcal/mol (*43*).

Discussion

Role of Water No effects on k_{cat} were observed in our viscosity studies, consistent with hydride transfer being the rate-determining step. However an effect was observed on the K_m for DHF using both sucrose and trehalose. To determine if the K_d for DHF was also affected, ITC studies were also performed. At low viscosities, $K_{d\ (DHF)}$ did increase with increasing viscosity and $K_{m(DHF)}$ approximated $K_{d\ (DHF)}$ (within a factor of 2). However as the relative viscosity increased to 5.1, a greater divergence was noted between K_d and K_m (~3 fold), suggesting that the DHF K_m may contain some kinetic terms at higher viscosities.

If water is involved in a binding interaction, perturbation of water content should alter binding. For example, closer contact distances typically exclude water. In binding of ferredoxin to ferredoxin: $NADP^+$ reductase, Jelesarov and Bosshard (*44*) found increasing concentrations of glycerol resulted in tighter binding. They interpreted this behavior as arising from dehydration of the protein-protein interface, which led to tighter binding as water was released. For R67 DHFR, the opposite behavior has been observed, i.e. weaker binding in increasing sucrose concentrations, suggesting water stabilizes DHF binding. This observation is consistent with previous NMR and crystallography studies which have found the pABA-glu tail of DHF/folate is disordered when bound (*3, 6*). Also, docking studies predicted the pABA-glu tail could interact with either symmetry related K32 residue in one half of the pore (*21, 45*). Finally, addition of two asymmetric K32M mutations on opposite sides of the pore can have two topologies, i.e. they can occur on the same dimer-dimer interface or they can exist diagonally on both dimer-dimer interfaces (see figure 1 in (*19*)). These two asymmetric K32M double mutant topologies have been constructed and found to have similar effects on steady state kinetic values. If a preferred topology existed for the pABA-glu tail - K32 interaction, then the asymmetric mutants would

have shown different behavior (*19*). These various studies, combined with the present viscosity studies, support a role for water in binding of DHF. We have previously proposed solvent separated ion pairs (*46-50*) may exist between the glu tail of DHF and K32 residues in R67 DHFR (*19, 43*). Solvent separated ion pairs would also diminish the desolvation penalty involved in binding (*51*). Water stabilized binding has also been seen in an antibody - lysozyme interaction (*52*) as well as ligand binding to adenosine deaminase (*53*).

Comparison of Enthalpies Derived from Temperature Dependent Kinetic Studies and ITC

Previously, a strong preference for initial binding of NADPH to R67 DHFR, followed by binding of DHF, has been proposed based on the relative K_d values as well as the behavior of site directed mutants (*5, 19*). This preferred binding mechanism will be used here as well. The enthalpy change associated with binding NADPH was found to be –8.6 ± 0.6 kcal/mol using a van't Hoff approach (figure 8A). This value compares well with an ΔH of –8.6 ± 0.2 kcal/mol previously monitored by ITC at 28°C (*5*), indicating the two approaches converge to similar answers (figure 8B).

The enthalpy change associated with formation of the R67 DHFR•NADPH•DHF complex from R67 DHFR•NADPH can be estimated by monitoring the temperature dependence of $1/K_{m\ (DHF)}$. The value obtained is -14.1 ± 0.6 kcal/mol. Figure 8A compares well with an ITC derived ΔH value of -13.3 ± 0.9 kcal/mol describing binding of DHF to R67 DHFR•$NADP^+$ (25°C, table 6). While the latter is a product-substrate complex, the convergence of the ΔH values (from ITC and Arrhenius plots) suggests it is a good mimic of the productive ternary complex.

Figure 8: A Gibbs free energy diagram describing R67 DHFR catalysis at 25°C. A) The ΔG values for DHF reduction were obtained from the observed $K_{d\ (NADPH)}$, $K_{d\ (DHF)}$ and k_{cat} values and are shown in black. The enthalpic contributions were calculated as described in the text. Since $K_{m\ (DHF)}$ could possibly contain kinetic terms, the K_d for DHF binding to R67 DHFR•$NADP^+$ was used to mimic productive ternary complex formation. Use of the poor substrate, DHP, is shown in gray. B) The bottom panel shows a bar graph depicting the differences between DHF and DHP binding and reduction describing ΔΔG, ΔΔH and Δ(TΔS) terms. The binding differences were calculated using ITC data for formation of R67 DHFR•$NADP^+$•DHF and R67 DHFR•NADPH•DHP at 25 and 13°C respectively (*43*).

A

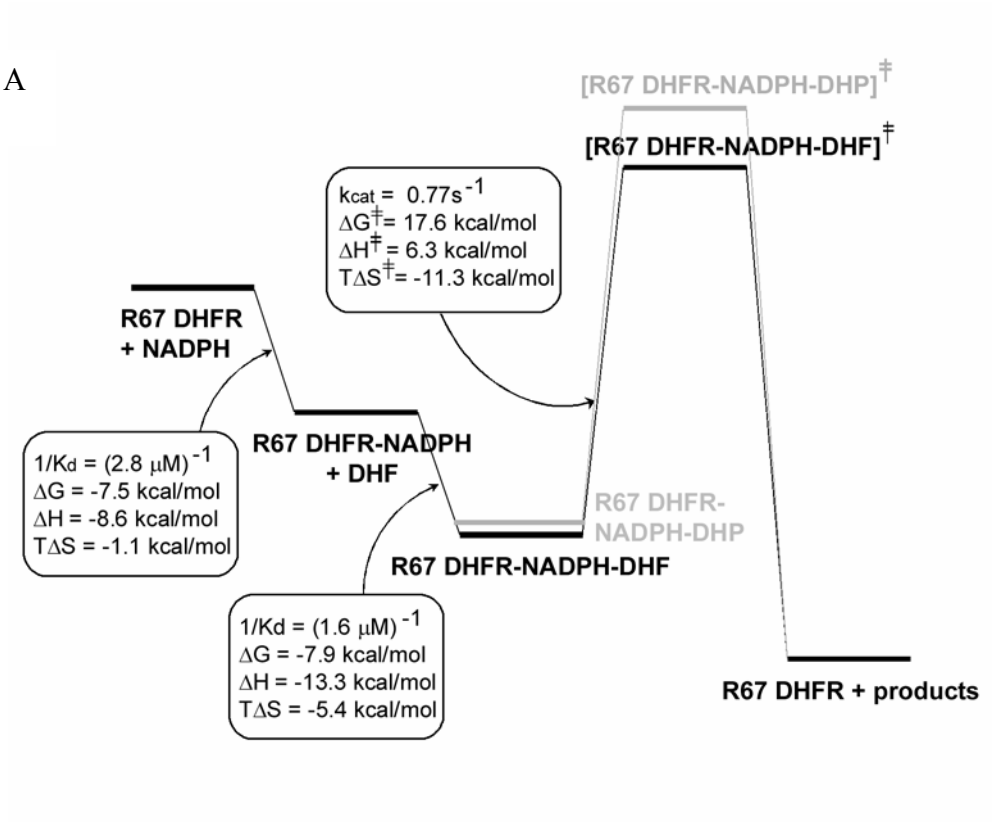
[R67 DHFR-NADPH-DHP]‡
[R67 DHFR-NADPH-DHF]‡
kcat = 0.77s-1
ΔG‡= 17.6 kcal/mol
ΔH‡= 6.3 kcal/mol
TΔS‡= -11.3 kcal/mol
R67 DHFR
+ NADPH
1/Kd = (2.8 μM)-1
ΔG = -7.5 kcal/mol
ΔH = -8.6 kcal/mol
TΔS = -1.1 kcal/mol
R67 DHFR-NADPH
+ DHF
R67 DHFR-
NADPH-DHP
R67 DHFR-NADPH-DHF
1/Kd = (1.6 μM)-1
ΔG = -7.9 kcal/mol
ΔH = -13.3 kcal/mol
TΔS = -5.4 kcal/mol
R67 DHFR + products

B

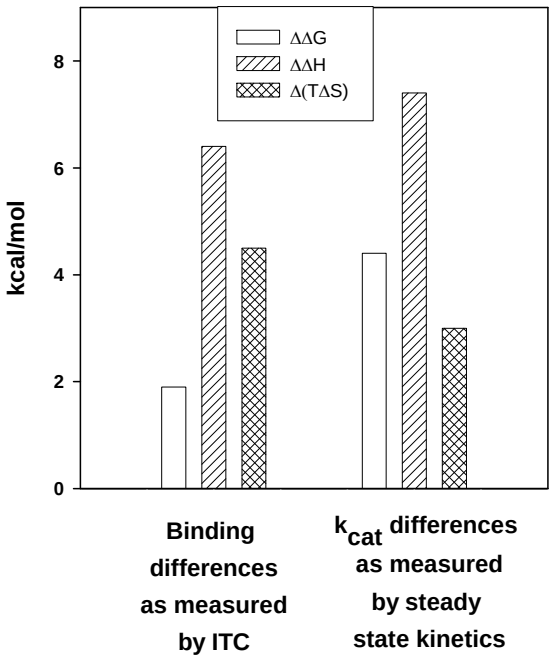
ΔΔG
ΔΔH
Δ(TΔS)
kcal/mol
0
2
4
6
8
Binding differences as measured by ITC
kcat differences as measured by steady state kinetics

The ΔH value for the formation of R67 DHFR•2NADPH complex has also been determined using the heat capacity (ΔC_p) for binding of NADPH to R67 DHFR (from chapter 3). A ΔC_p value of –178 cal/^{o}K mol is obtained and from this the ΔH and ΔS and be determined using the following equations (*44*):

$$\Delta H = \Delta H^* + \Delta C_p [(T-T^*_h) \quad (6)$$

$$\Delta S = \Delta S^* + \Delta C_p \ln(T/ T^*_s)] \quad (7)$$

Where ΔH^* is the enthalpy change at T^*_h and ΔS^* the enthalpy change at T^*_s

From the plot of ΔH versus temperature for formation of the R67 DHFR•2NADPH complex, a ΔC_p of –0.178 kcal/^{o}K mol has been calculated. Also, the ΔH^* value at 303^{o}K (T^*_h) is –9.25 kcal/mol. Applying these values to equation (6), the ΔH at 25^{o}C (298^{o}K) was determined to be -8.1± 0.2 kcal/mol. Similarly using equation (7), ΔS at 298^{o}K was calculated to be -9.79 cal/mol. The corresponding value of TΔS at this temperature is –2.9 ± 0.2 kcal/mol. Additionally, ΔG was calculated to be –5.2 ± 0.2 kcal/mol using the relationship,

$$\Delta G = \Delta H – T\Delta S \quad (8)$$

Since ΔC_p is small, the ΔG, ΔH and TΔS values obtained are not different from the values determined using the van't Hoff equation. Similarly, using a ΔC_p value of –0.199 kcal/^{o}K mol for formation of the ternary R67 DHFR•$NADP^+$•DHF complex (chapter 3), the corresponding values of ΔG, ΔH and TΔS were calculated to be -8.3 ± 0.4 kcal/mol, -10.9 ± 0.2 kcal/mol and –2.7 ± 0.3 kcal/mol respectively.

Construction of a Gibbs Free Energy Diagram Combining the above ΔG and ΔH values as well as values obtained from the Arrhenius plot describing k_{cat} allows construction of a Gibbs free

energy diagram at 25°C. The resulting plot is shown in figure 8B. Formation of the binary and ternary complexes is clearly enthalpy driven, while formation of the transition state contains a large entropic contribution. Jencks has suggested large entropic components can be associated with enzyme catalysis, particularly those describing bisubstrate reactions (*54, 55*). However, previous studies have found wide distributions of enthalpy and entropy terms can be associated with k_{cat}. As examples of bisubstrate reactions: 1) for peptide bond formation in the ribosome, $\Delta G^{\ddagger}$ = 16.5 kcal/mol, $\Delta H^{\ddagger}$ = 17.2 kcal/mol and $T\Delta S^{\ddagger}$ = 0.7 kcal/mol (*56*); 2) for truncated ATP sulfurylase from *Penicillium chrysogenum,* a $\Delta G^{\ddagger}$ value of 17.4 kcal/mol was calculated as well as a $\Delta H^{\ddagger}$ value of 16.3 kcal/mol with a $T\Delta S^{\ddagger}$ value of -1.1 kcal/mol (at 30°C and where the rate determining step describes catalysis of the ternary substrate complex to the ternary product complex coupled with Mg-pyrophosphate release) (*57*); 3) for thymidylate synthetase, a $\Delta G^{\ddagger}$ value of 10.6 kcal/mol describing the hydride transfer rate was determined with a $\Delta H^{\ddagger}$ of 3.4 and a corresponding $T\Delta S^{\ddagger}$ of -7.2 kcal/mol (*58*); and 4) for the catalytic antibody 29G12 catalyzing a 1,3-dipolar cycloaddition reaction, a $\Delta G^{\ddagger}$ value of 17.7 kcal/mol with a $\Delta H^{\ddagger}$ of 7.1 and a $T\Delta S^{\ddagger}$ of -10.6 kcal/mol were observed (*59*).

As noted above, our Arrhenius data describing R67 DHFR catalysis indicate that $\Delta G^{\ddagger}$ is dominated by the entropy term. Typically, positive $\Delta S^{\ddagger}$ values are associated with reorganization of solvent (*60-62*) while studies with ordered water molecules in active sites suggest entropic values can be negative, but coupled with an approximately equal ΔH contribution ((*63, 64*) and references therein). Negative $\Delta S^{\ddagger}$ terms typically describe loss of translational and rotational motion in the transition state (*65*). Since crystal structure and NMR data indicate minimal motion

of R67 DHFR upon ligand binding (*3, 66*), changes in ligand orientation are more likely to describe the large, negative entropic term in R67 DHFR. Additionally when substrates form more charged transition states (as is likely in DHFR with DHF protonated at N5), $\Delta S^{\ddagger}$ is usually negative. Thus many factors could be involved in this large, negative $\Delta S^{\ddagger}$ term.

Typical hydride transfer reactions have enthalpies of activation near 8-15 kcal/mol (*67*). However activation energies of 11.9, 5.5 and 3.7 kcal/mol have been calculated for chromosomal DHFRs from *Thermotoga maritima* (*68*), *Bacillus stearothermophilus* (*69*) and *E. coli* (*70*). The *E. coli* chromosomal DHFR value was obtained at pH 9.0 where hydride transfer rate is rate determining (*71*). At pH 9, $\Delta G^{\ddagger}_{25}$, $\Delta H^{\ddagger}_{25}$ and $T\Delta S^{\ddagger}_{25}$ values are 16.0, 3.1, and -12.9 kcal/mol respectively. These values are near those observed for R67 DHFR, indicating the same general range for these reactions. This convergence could either indicate similar chemistry or alternatively, coincidence as chromosomal and R67 DHFRs have entirely different structures, active sites and transition states (*4, 6, 22, 23*).

Finally, use of DHP as an alternate substrate leads to only 10 fold weaker binding with respect to DHF. However since the glutamic acid moiety of the pABA-glu tail appears to provide most of the enthalpic signal associated with DHF binding (*43*), substitution of glutamate by a carboxylate group weakens the enthalpic contribution. Thus a $\Delta\Delta H$ value of ~6.5 kcal/mol can be calculated when ITC values or the slopes in the Arrhenius plots describing $1/K_m$ for DHF vs. DHP binding are compared. This value appears to correlate with the decrease in k_{cat}, where a $\Delta\Delta H$ of 7.6 kcal/mol is observed (compared to DHF reduction), strongly implicating the pABA-glu tail in correctly docking DHF in the active site pore pursuant to catalysis. A comparison of the $\Delta\Delta G$ values shows a smaller difference (4.4 kcal/mol), indicating partial entropic compensation of the

effects that alter ΔΔH. These results all suggest increases in the range of motion associated with bound DHP could interfere with catalysis.

Does Protonation Play a Role? Another possible interpretation of the thermodynamic values for R67 DHFR arises if protonation and hydride transfer are concerted events. To address this issue, the question of how DHF is protonated in the R67 DHFR active site needs consideration first. In one scenario, the predominant species, neutral DHF would bind and then be protonated. Alternatively, R67 DHFR could preferentially bind protonated DHF (HDHF). However, this species is at an extremely low concentration at pH 7. Since the N5 $pK_a = 2.60$ (extrapolated to 25°C), the ratio of DHF to HDHF can be calculated as 2.5×10^4 at pH 7. If protonated DHF is the actual substrate, then the observed K_m is an apparent value. A K_m of 96 pM for protonated DHF can be calculated by dividing the apparent K_m by the HDHF concentration (*72*). If productive binding of substrate in R67 DHFR indeed utilizes the protonated species, the observed DHF K_m would be expected to decrease as the concentration of HDHF increases (i.e. decreasing pH). However in our H62C mutant, the reverse is observed as the $K_{m\ (DHF)}$ rises going from pH 7 to 5 (*13*). While other ionizations could be occurring that affect K_m, the simplest interpretation suggests this mutant binds neutral DHF, followed by protonation.

To estimate whether the thermodynamic values associated with protonation of DHF at N5 are at all near the catalytic thermodynamic parameters, a plot of inverse temperature vs. ln K_a of the ionization constant was constructed (*73*). While this plot only contains 3 data points (figure 5), it allows estimation of ΔH value for N5 protonation of 6.5 ± 1.0 kcal/mol.

While the local environment could alter the thermodynamic values associated with protonation of free versus enzyme bound DHF (*73, 74*), a comparison of the DHF protonation values with the

values associated with k_{cat} suggests the enthalpy change associated with substrate protonation could play a role in transition state formation if protonation and hydride transfer are concerted events. However the entropic term for DHF protonation is positive, so this term would fight against the observed negative value observed during catalysis, leaving the question of whether protonation and hydride transfer are concerted unresolved. Solvent isotope effects could allow further analysis of this possibility.

Conclusion

In our present studies as well as our ITC binding studies (*5*), R67 DHFR uses enthalpic interactions to form its NADPH•DHF complex. However, because R67 DHFR uses a "one site fits both approach" whereby both ligands are accommodated by a generalized binding surface, this binding is not optimal (*12, 21*). Thus it seems likely that some adjustment of the complex position and/or orientation is necessary to reach the transition state, which could be reflected by the $T\Delta S^{\ddagger}$ value of –11.3 kcal/mol. In general, both the 222 symmetry and large active site exposed to solvent support non-optimal binding or a loose ground state. In addition, previous steady state studies in the presence of increasing salt concentrations found that k_{cat} increased (*75*). This surprising observation suggested that a salt sensitive interaction needed to be broken to reach the transition state, again consistent with a large entropic contribution associated with transition state formation.

Appendix

Protocol For Reduction Of Pteroic Acid To Dihydropteroic Acid (DHP)

Pteroic acid was purchased from Schircks and reduced to 7,8-dihydropteroic acid (DHP) according to Prabhu et al. (*31*). About 8 mg of pteroic acid was first dissolved in 5 ml of 0.1N NaOH. Reduction was then carried out by addition of 300 mg of sodium hydrosulfite (in the presence of 5mM β-mercaptoethanol (~20ml). The solution was stirred and incubated at room temperature for 30 minutes. The resulting precipitate was dirty white in color (in contrast to the bright yellow color of pteroic acid). The precipitate was separated by centrifugation and washed 2 to 3 times with 0.005N HCl to remove any traces of reducing agents. The reduction step can be repeated 2 more times to reduce any remaining pteroic acid in the supernatant. The 100µl aliquots of the precipitate were taken and stored at –80^{o}C.

The formation of DHP was confirmed by obtaining a ^{1}H NMR spectrum of DHP in DMSO. Comparison with the ^{1}H NMR spectrum of pteroic acid in DMSO also indicated that the 7,8 positions of pteroic acid were indeed reduced to obtain dihydropteroic acid (DHP). Very little amount of pteroic acid was also detected as an impurity in DHP. However, integration of the peaks indicated the purity of DHB to be greater than 90%.

The extinction coefficient of DHP was 22000 $M^{-1}cm^{-1}$ at 278 nm (*76*). Also, the molar extinction coefficient used to assess reduction of DHP was monitored and found to be the same as for DHF reduction, which is 12 300 L M-1 cm-1 (*32*).

Additionally, the absorbance spectrum of DHP in 0.1N NaOH at room temperature remained unchanged for 4 to 5 hours. This indicates that DHP is reasonably stable for at least 5 hours.

Figure 9: Structure of Dihydropteroic acid (DHP) and its ^{1}H NMR spectrum obtained in DMSO. A) Structure of dihydropteroic acid with chemical shifts for different functional groups. B) ^{1}H NMR spectrum of DHP obtained in DMSO.

A

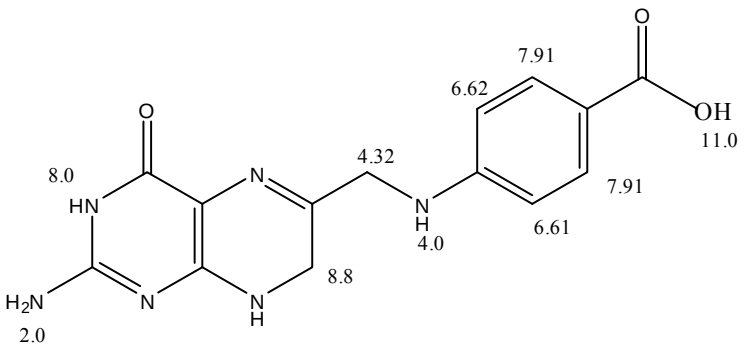
O
7.91
6.62
OH
11.0
4.32
8.0
HN
N
N
H
7.91
6.61
4.0
8.8
H_2N
N
N
H
2.0

B

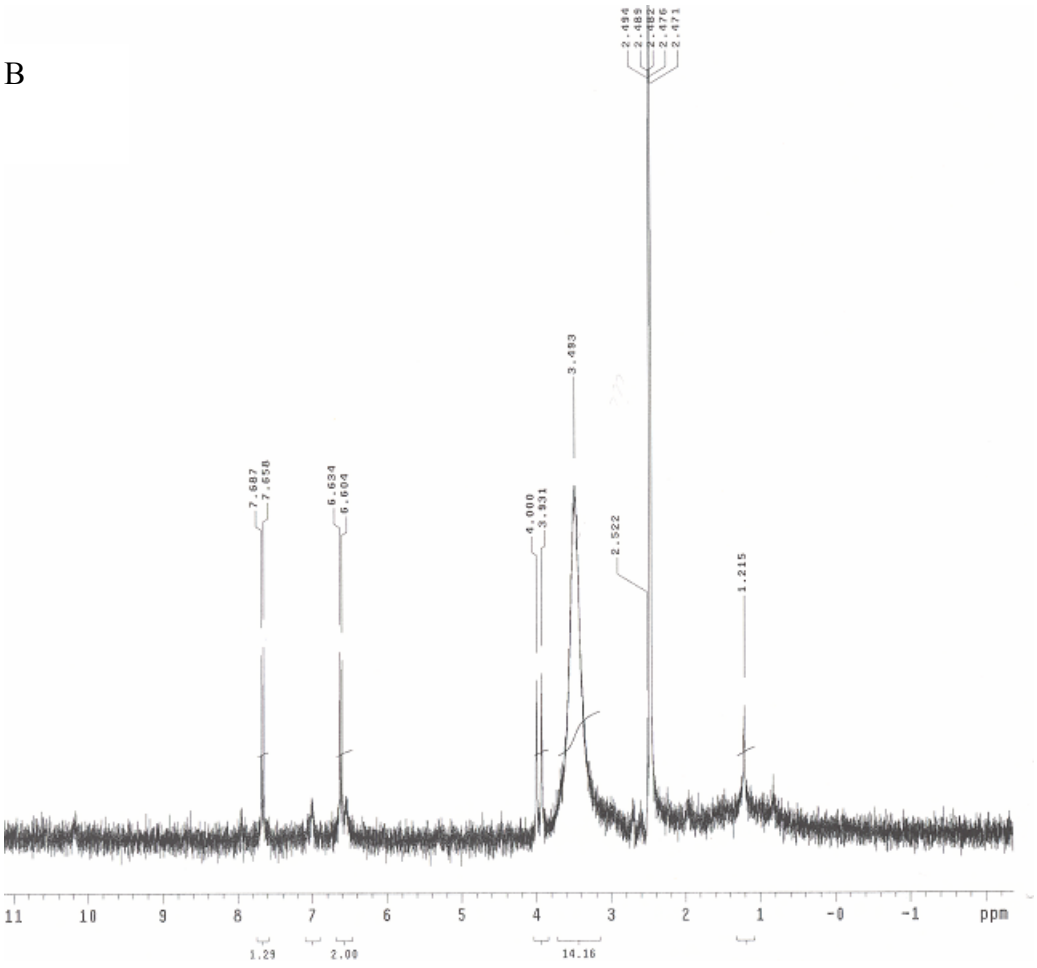
2.494
2.489
2.482
2.476
2.471
7.687
7.658
6.634
6.604
4.000
3.931
3.493
2.522
1.215
11
10
9
8
7
6
5
4
3
2
1
-0
-1
ppm
1.29
2.00
14.16

Protocol for pK_a Determination of DHF/ DHP (based on method by Maharaj et al.) (*34*)

1. Prepare 0.2M sodium phosphate buffer. Aliquot about 10 to 15 mls in different tubes and adjust to different pH values ranging from pH 2.0 to 5.0.
2. Combine DHF pellets from about 2 appendorf tubes and wash 3 times with cold 0.001N HCl to remove any traces of β-mercaptoethanol.
3. Resuspend the washed DHF pellet in 20mM Tris-EDTA buffer (pH 8.0). Add a small amount of dilute NaOH to dissolve the DHF, till the solution appears clear. Store the DHF solution on ice to minimize the degradation of DHF.
4. Determine the concentration of the stock DHF solution (extinction coefficient of DHF at 228 nm = 28,000 $M^{-1}cm^{-1}$) (*77*). From this calculate the volume of DHF required to obtain 3ml of a 30μM solution.
5. For pK_a measurements the absorbance of 30μM DHF is measured (at 228 nm) at different pH values:
    - Absorbance readings in the pH range of 1.0 to 2.0 are carried out in 0.25N HCl, while absorbance measurements at pH values above 2.0 are performed in sodium phosphate buffer.
    - For measurements in HCl, determine the amount of water and 0.25N HCl to add to reach the desired pH. Zero the spec using water as a blank. To 1.5ml of water, add the appropriate amount of DHF and mix. Then add the appropriate volume of 0.25N HCl to obtain a final volume of 3.0 and the desired pH. Immediately take 3 readings of the absorbance. Then measure the pH of the solution. The pH meter should be calibrated in the particular pH range and the temperature at which the experiment is being performed.
    - For measurements in sodium phosphate buffer, first zero the spectrophotometer using 1.5ml of H_2O and 1.5ml of sodium phosphate buffer. For DHF absorbance

measurements, add 1.5 ml H_2O to the cuvette followed by DHF to get a concentration of 30μM and mix. Then add 1.5ml of sodium phosphate buffer (at a particular pH) and mix. Transfer the DHF + water + sodium phosphate mixture in a 15ml falcon tube and place it in a water bath at the desired temperature. Then measure the pH of the solution.

6. Use Sigma plot to determine the pK_a of DHF (from the plot of absorbance versus pH) to determine the pK_a of the N5 position of DHF.

References

1. Agarwal, P. K., Billeter, S. R., Rajagopalan, P. T., Benkovic, S. J., and Hammes-Schiffer, S. (2002) *Proc. Natl. Acad. Sci. U. S. A. 99*, 2794-9.
2. Fierke, C. A., Kuchta, R. D., Johnson, K. A., and Benkovic, S. J. (1987) *Cold Spring Harbor Symp. Quant. Biol. 52*, 631-638.
3. Narayana, N., Matthews, D. A., Howell, E. E., and Nguyen-huu, X. (1995) *Nat. Struct. Biol. 2*, 1018-1025.
4. Howell, E. E. (2005) *ChemBioChem 6*, 590-600.
5. Bradrick, T. D., Beechem, J. M., and Howell, E. E. (1996) *Biochemistry 35*, 11414-24.
6. Li, D., Levy, L. A., Gabel, S. A., Lebetkin, M. S., DeRose, E. F., Wall, M. J., Howell, E. E., and London, R. E. (2001) *Biochemistry 40*, 4242-52.
7. Smiley, R. D., Stinnett, L. G., Saxton, A. M., and Howell, E. E. (2002) *Biochemistry 41*, 15664-75.
8. Strader, M. B., Chopra, S., Jackson, M., Smiley, R. D., Stinnett, L., Wu, J., and Howell, E. E. (2004) *Biochemistry 43*, 7403-12.
9. Calderone, C. T., and Williams, D. H. (2001) *J. Am. Chem. Soc. 123*, 6262-7.
10. Williams, D. H., Stephens, E., and Zhou, M. (2003) *Chem. Commun. (Camb.)*, 1973-6.
11. Williams, D. H., Stephens, E., and Zhou, M. (2003) *J. Mol. Biol. 329*, 389-99.
12. Strader, M. B., Smiley, R. D., Stinnett, L. G., VerBerkmoes, N. C., and Howell, E. E. (2001) *Biochemistry 40*, 11344-52.
13. Park, H., Zhuang, P., Nichols, R., and Howell, E. E. (1997) *J. Biol. Chem. 272*, 2252-8.
14. Marijuan, P. C. (1996) *BioSystems 38*, 163-71.
15. Blundell, T. L., and Srinivasan, N. (1996) *Proc. Natl. Acad. Sci. U. S. A. 93*, 14243-8.
16. Goodsell, D. S., and Olson, A. J. (2000) *Annu. Rev. Biophys. Biomol. Struct. 29*, 105-53.
17. Kitov, P. I., and Bundle, D. R. (2003) *J. Am. Chem. Soc. 125*, 16271-84.
18. Kortt, A. A., Dolezal, O., Power, B. E., and Hudson, P. J. (2001) *Biomol. Eng. 18*, 95-108.
19. Hicks, S. N., Smiley, R. D., Stinnett, L. G., Minor, K. H., and Howell, E. E. (2004) *J. Biol. Chem. 279*, 46995-7002.
20. Stinnett, L. G., Smiley, R. D., Hicks, S. N., and Howell, E. E. (2004) *J. Biol. Chem. 279*, 47003-9.
21. Howell, E. E., Shukla, U., Hicks, S. N., Smiley, R. D., Kuhn, L. A., and Zavodszky, M. I. (2001) *J. Comput. Aided Mol. Des. 15*, 1035-52.
22. Andres, J., Moliner, V., Safont, B. S., Domingo, L. R., Picher, M. T., and Krechl, J. (1996) *Bioorganic Chem. 24*, 10-18.
23. Castillo, R., Andres, J., and Moliner, V. (1999) *J. Am. Chem. Soc. 121*, 12140-12147.
24. Reece, L. J., Nichols, R., Ogden, R. C., and Howell, E. E. (1991) *Biochemistry 30*, 10895-904.
25. Gornall, A. G., Bardawill, C. J., and David, M. M. (1949) *J. Biol. Chem. 177*, 751-766.
26. Zhuang, P., Yin, M., Holland, J. C., Peterson, C. B., and Howell, E. E. (1993) *J. Biol. Chem. 268*, 22672-9.
27. Ellis, K. J., and Morrison, J. F. (1982) *Methods Enzymol. 87*, 405-26.
28. Dunn, S. M., Lanigan, T. M., and Howell, E. E. (1990) *Biochemistry 29*, 8569-76.
29. Howell, E. E., Warren, M. S., Booth, C. L., Villafranca, J. E., and Kraut, J. (1987) *Biochemistry 26*, 8591-8.
30. Smiley, R. D., Saxton, A. M., Jackson, M. J., Hicks, S. N., Stinnett, L. G., and Howell, E. E. (2004) *Anal. Biochem. 334*, 204-6.

31. Prabhu, V., Lui, H., and King, J. (1997) *Phytochemistry 45*, 23-27.
32. Baccanari, D., Phillips, A., Smith, S., Sinski, D., and Burchall, J. (1975) *Biochemistry 14*, 5267-73.
33. Segel, I. H. (1975) *Enzyme Kinetics: Behavior and Analysis of Rapid Equilibrium and Steady-State Enzyme Systems*, John Wiley and Sons, New York.
34. Maharaj, G., Selinsky, B. S., Appleman, J. R., Perlman, M., London, R. E., and Blakley, R. L. (1990) *Biochemistry 29*, 4554-60.
35. Fersht, A. (1985) *Enyzme Structure and Mechanism*, W.H. Freeman and Company, New York.
36. Wiseman, T., Williston, S., Brandts, J. F., and Lin, L. N. (1989) *Anal. Biochem. 179*, 131-137.
37. Laidler, K. J., and Peterman, B. F. (1979) *Methods Enzymol. 63*, 234-57.
38. Wolfenden, R. (1999) *Bioorg. Med. Chem. 7*, 647-52.
39. Bienvenue, D. L., Mathew, R. S., Ringe, D., and Holz, R. C. (2002) *J. Biol. Inorg. Chem. 7*, 129-35.
40. Perrin, D., Dempsey, B., and Serjeant, E. (1981) *pKa Prediction for Organic Acids and Bases*, Chapman and Hall, London.
41. Snider, M. J., Gaunitz, S., Ridgway, C., Short, S. A., and Wolfenden, R. (2000) *Biochemistry 39*, 9746-53.
42. Sampson, N. S., and Knowles, J. R. (1992) *Biochemistry 31*, 8488-94.
43. Jackson, M., Chopra, S., Smiley, R. D., Maynord, P. O., Rosowsky, A., London, R. E., Levy, L., Kalman, T. I., and Howell, E. E. (2005) *Biochemistry 44*, 12420-33.
44. Jelesarov, I., and Bosshard, H. R. (1994) *Biochemistry 33*, 13321-8.
45. Alonso, H., Gillies, M. B., Cummins, P. L., Bliznyuk, A. A., and Gready, J. E. (2005) *J. Comput. Aided Mol. Des. 19*, 165-87.
46. Roca, M., Marti, S., Andres, J., Moliner, V., Tunon, I., Bertran, J., and Williams, I. H. (2003) *J. Am. Chem. Soc. 125*, 7726-37.
47. Umezurike, G. M. (1987) *Biochem. J. 241*, 455-62.
48. Bagnol, L., Horner, J. H., and Newcomb, M. (2003) *Org. Lett. 5*, 5055-8.
49. Dougherty, R. C., and Howard, L. N. (2003) *Biophys. Chem. 105*, 269-78.
50. Harder, S., Feil, F., and Repo, T. (2002) *Chemistry 8*, 1991-9.
51. Chong, L. T., Dempster, S. E., Hendsch, Z. S., Lee, L. P., and Tidor, B. (1998) *Protein Sci. 7*, 206-10.
52. Bhat, T. N., Bentley, G. A., Boulot, G., Greene, M. I., Tello, D., Dall'Acqua, W., Souchon, H., Schwarz, F. P., Mariuzza, R. A., and Poljak, R. J. (1994) *Proc. Natl. Acad. Sci. U. S. A. 91*, 1089-93.
53. Dzingeleski, G. D., and Wolfenden, R. (1993) *Biochemistry 32*, 9143-7.
54. Page, M. I., and Jencks, W. P. (1971) *Proc. Natl. Acad. Sci. U. S. A. 68*, 1678-83.
55. Jencks, W. P. (1975) *Adv. Enzymol. Relat. Areas Mol. Biol. 43*, 219-410.
56. Sievers, A., Beringer, M., Rodnina, M. V., and Wolfenden, R. (2004) *Proc. Natl. Acad. Sci. U. S. A. 101*, 7897-901.
57. Hanna, E., Ng, K. F., MacRae, I. J., Bley, C. J., Fisher, A. J., and Segel, I. H. (2004) *J. Biol. Chem. 279*, 4415-24.
58. Agrawal, N., Hong, B., Mihai, C., and Kohen, A. (2004) *Biochemistry 43*, 1998-2006.
59. Toker, J. D., Tremblay, M. R., Yli-Kauhaluoma, J., Wentworth, A. D., Zhou, B., Wentworth, P., Jr., and Janda, K. D. (2005) *J. Org. Chem. 70*, 7810-5.
60. Houck, W. J., and Pollack, R. M. (2003) *J. Am. Chem. Soc. 125*, 10206-12.
61. Jen-Jacobson, L., Engler, L. E., and Jacobson, L. A. (2000) *Structure Fold. Des. 8*, 1015-23.
62. Jelesarov, I., and Bosshard, H. R. (1999) *J. Mol. Recognit. 12*, 3-18.

63. Phillips, R. S. (2002) *J. Mole. Catalysis B: Enzymatic 19-20*, 103-107.
64. Holdgate, G. A., Tunnicliffe, A., Ward, W. H., Weston, S. A., Rosenbrock, G., Barth, P. T., Taylor, I. W., Pauptit, R. A., and Timms, D. (1997) *Biochemistry 36*, 9663-73.
65. Anslyn, E. V., and Dougherty, D. A. (2006) *Modern Physical Organic Chemistry*, University Science Books, Sausalito, CA.
66. Pitcher, W. H., 3rd, DeRose, E. F., Mueller, G. A., Howell, E. E., and London, R. E. (2003) *Biochemistry 42*, 11150-60.
67. Kohen, A., and Klinman, J. P. (1998) *Acc. Chem. Res. 31* 397-404.
68. Maglia, G., and Allemann, R. K. (2003) *J. Am. Chem. Soc. 125*, 13372-3.
69. Kim, H. S., Damo, S. M., Lee, S. Y., Wemmer, D., and Klinman, J. P. (2005) *Biochemistry 44*, 11428-39.
70. Sikorski, R. S., Wang, L., Markham, K. A., Rajagopalan, P. T., Benkovic, S. J., and Kohen, A. (2004) *J. Am. Chem. Soc. 126*, 4778-9.
71. Fierke, C. A., Johnson, K. A., and Benkovic, S. J. (1987) *Biochemistry 26*, 4085-92.
72. Schmitzer, A. R., Lepine, F., and Pelletier, J. N. (2004) *Protein Eng. Des. Sel. 17*, 809-19.
73. Bhattacharya, S., and Lecomte, J. T. (1997) *Biophys. J. 73*, 3241-56.
74. Sarmini, K., and Kenndler, E. (1999) *J. Biochem. Biophys. Methods 38*, 123-37.
75. Hicks, S. N., Smiley, R. D., Hamilton, J. B., and Howell, E. E. (2003) *Biochemistry 42*, 10569-78.
76. Shiota, T., Disraely, M. N., and McCann, M. P. (1964) *J Biol Chem 239*, 2259-66.
77. Blakley, R. L. (1960) *Nature 188*, 231-232.

Part III: A Balancing Act: Net Uptake of Water During Dihydrofolate Binding And Net Release of Water Upon NADPH Binding in R67 Dihydrofolate Reductase

This section is a slightly modified version of a manuscript accepted in the Journal of Biological Chemistry by Shaileja Chopra, Russ Dooling, Caroline Horner and Elizabeth E. Howell.

This author contributed the following to this manuscript: (1) Protein expression and purification, (2) protein extinction coefficients, (3) steady-state kinetic data with osmolytes, (4) ITC data with osmolytes, (5) osmolality measurements, (6) pH titration and fluorescence measurements, (7) some viscosity measurements and (8) assistance with writing the manuscript. This research was supported by NSF grant MCB-0445728 (to Elizabeth E. Howell).

Abstract

R67 Dihydrofolate reductase (DHFR) catalyzes the NADPH dependent reduction of dihydrofolate (DHF) to tetrahydrofolate (THF). The enzyme is a homotetramer with 222 symmetry and a single active site pore that is 24 Å long and 18 Å wide. The two ligands enter the pore from opposite ends. One molecule of DHF and NADPH bind to form a productive ternary complex. X-ray crystallography results find the cofactor NADPH binds to the active site in a fixed conformation and the pteridine ring of DHF adopts a fixed position, while the para-amino benzoyl-glutamate tail is disordered. In this study, the role of water in DHF and NADPH binding has been investigated by subjecting the protein to osmotic pressure. For this, varying concentrations of osmolytes were employed. The ligand binding properties of R67 DHFR were studied using steady state kinetics and isothermal titration calorimetry (ITC). An increase in osmotic pressure resulted in a decrease in the K_d for NADPH and an increase in the K_d and/or K_m of DHF. Also the k_{cat} of the reaction was unaffected. Quantifying the number of water molecules showed that there is a net release of 38 water molecules upon NADPH binding, while the net number of water molecules taken up by DHF binding varied. Thermodynamic characterization of ligand binding at different temperatures was also explored. A heat capacity change of –178

cal/mol^{o}K was estimated for formation of the enzyme•NADPH complex, while a heat capacity change of -199 cal/mol^{o}K was determined for the formation of the enzyme•NADP^{+}•DHF complex. The involvement of water was also probed by *in vivo* experiments using resistance to the antibacterial drug trimethoprim, as a selection for R67 DHFR. Increasing concentrations of sorbitol in the media resulted in a decrease in the catalytic efficiency of mutant R67 DHFRs and decreased ability of the clone to grow in sorbitol containing media. These results are consistent with *in vitro* experiments, suggesting that water is involved in ligand binding in R67 DHFR.

Introduction

Dihydrofolate reductase (DHFR) reduces dihydrofolate to tetrahydrofolate using NADPH as a cofactor. The reaction product, tetrahydrofolate, is essential for the synthesis of thymidylate, purine nucleosides, methionine and other metabolic intermediates. R67 DHFR is a type II plasmid encoded enzyme that catalyses the same reaction. However, this enzyme is genetically and structurally different from chromosomal DHFR. Unlike the chromosomal enzyme, R67 is a homotetramer with a single active site pore (figure 1A). Therefore, a mutation in the gene results in 4 mutations in the pore. The chromosomally encoded enzyme is inhibited by low concentrations (1nm) of trimethoprim (TMP). However, R67 DHFR is not affected by TMP and remains fully active. Chromosomal DHFR is also strongly inhibited by methotrexate, while R67 DHFR is only weakly inhibited (*1, 2*). Therefore, even though both enzymes catalyze the same reaction, their ligand binding and catalytic properties are significantly different.

Narayana et al. have crystallized R67 DHFR and observe that the enzyme exhibits 222-symmetry (*3*). The electron density was fit to two asymmetrically bound molecules of folate, the first with Fol1 bound with its *si* face exposed towards the center of the pore. The other orientation has Fol2

Figure 1: Structure of tetrameric R67 DHFR (1VIE) A) Frontal view of the active site. The four monomers are represented in green, pink, ochre and violet. The dimer-dimer interface occurs on the top (green and violet) and bottom (pink and ochre) of the structure. B) Side view of the active site obtained by rotation of the top structure by 90^{o} along the y-axis. The inside surface of the pore (obtained by slicing through the active site) is represented by a Connolly surface. The key residues K32 (orange), Q67 (blue), I68 (light yellow) and Y69 (green) are shown. Also shown are the two ligands in the ternary complex crystal structure (*4*): $NADP^{+}$ (left) and DHF (right). The positions of $NADP^{+}$ and the pteridine ring of DHF are fixed (colored by the code of atoms, carbon in green, nitrogen in blue, oxygen in red, hydrogen in white and phosphorous in magenta). However, the position of the pABA-glutamate tail is disordered (one potential conformer represented in yellow). The dotted circle indicates the potential rotation of the pABA glutamate tail to form intermittent contacts with K32 residues on either side of the pore.

A

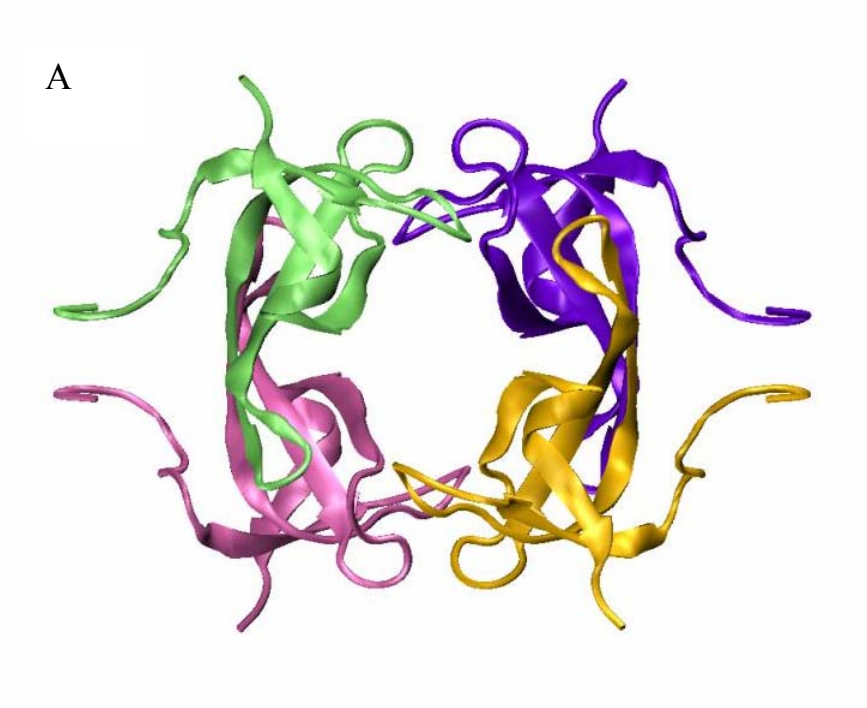

B

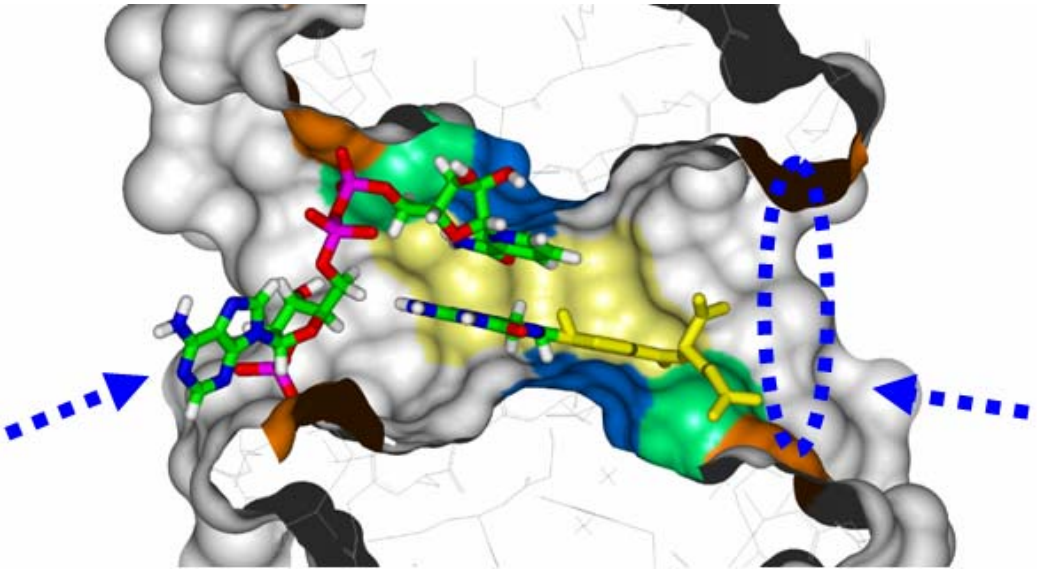

bound with its *si* face facing the protein surface. Fol1 describes a productive orientation as it agrees with the stereochemistry of the hydride transfer reaction.

Using ITC, Bradrick et al. found that three types of complexes can be formed with R67 DHFR: either 2 NADPH molecules, or 2 DHF molecules, or one molecule of NADPH and DHF (*5*). The DHF•NADPH complex is the productive pair that binds to the enzyme with each ligand occupying one half of the pore (*6*) (figure 1B). The reactants meet at the middle of the pore where the reaction occurs.

The volume of the active site pore has been determined to be 2398 $Å^3$ using CASTp (*7, 8*). Also, a recent crystal structure of R67 DHFR shows that water molecules in the pore are well ordered and form a network of hydrogen bonds with an array of fixed pentagonal rings (*9*). This suggests that water may play an important role in ligand binding to R67 DHFR.

Binding of ligands (DHF and NADPH) to R67 DHFR has been studied by various techniques. For DHF binding, crystal structures have been solved using R67 DHFR•2folate (binary) complex (*3*) and DHFR •$NADP^+$•DHF (ternary) complex (*4*). In both structures, electron density was observed for the pteridine ring. However, no electron density was observed for the pABA-glutamate tail, consistent with disorder. Studies were also performed by Li et al. using transferred NOE (Nuclear Overhauser Effect) experiments with bound $NADP^+$ and folate (*10*). Positive NOEs of the pABA-glutamate tail for both the binary and ternary complexes also indicated tail disorder. Additionally, docking of DHF or folate (an analog of DHF) resulted in a series of structures with varying tail positions (*6*). Results from docking as well as x-ray crystallography studies show that the glutamate tail of DHF interacts with symmetry related K32 residues present at the edge of the pore (*3, 4, 9*).

To determine how NADPH binds to R67 DHFR, NOE studies were carried out by Britto et al. and they demonstrated that the cofactor binds in an extended conformation (*11*). Also, the ribonicotinamide bond of cofactor adopts a *syn* conformation, while the glycosidic bond of the adenosine moiety adopts an *anti* conformation. Interligand NOE (ILOE) experiments with bound $NADP^+$ and folate showed that both ligands bind in an extended conformation in the active site pore (*12*). In addition, stacking between the pteridine (of folate) and nicotinamide (of $NADP^+$) rings is observed. These interligand interactions appear to play a crucial role in facilitating the formation of the ternary complex. Also, NMR and docking results predict that R67 uses an *endo* transition state complex in its catalytic mechanism. Therefore, in this enzyme, interligand cooperativity is likely important in transition state formation.

Also, from the R67 DHFR•DHF•$NADP^+$ structure (*4*), the N3 and O4 atoms of DHF form hydrogen bonds with the backbone atoms of I68. Also, hydrogen bonds are formed between the carboxamide group of NADPH and the backbone NH and O atoms of a symmetry related I68 residue.

The simplest approach to determine whether or not water contributes significantly to the energetics of a reaction is to vary the concentration or activity of water and measure how that influences the reaction. This approach is known as osmotic stress. The basic idea behind these experiments is to control water activity by addition of neutral solutes (osmolytes), which themselves do not interact with the protein of interest. Addition of osmolytes causes an increase in osmotic pressure, which eventually leads to dehydration and the squeezing out of water molecules from the active site (*13*). This approach has been used for a number of enzymes. For example, hexokinase was found to release about 60 water molecules upon binding to glucose (*14*). Also, cytochrome oxidase undergoes a hydration/ dehydration cycle involving 10 water

molecules as the protein is reduced and then transfers an electron internally (*15*). Preliminary studies with R67 DHFR demonstrated that addition of an osmolyte such as sucrose weakens the binding of DHF, suggesting that water is important in stabilizing the interaction of DHF with the enzyme (*16*). In the present study we have investigated the role of water in ligand binding to R67 DHFR using osmolytes.

Materials and Methods

Protein purification *Escherichia coli* SK383 cells containing the plasmid encoding R67 DHFR were grown in Terrific broth (TB) (*17*) at 37^{o}C in the presence of 200ug/ml ampicillin (AMP) and 20ug/ml trimethoprim (TMP). The cells were grown until the late stationary phase, after which the cells were lysed. Purification was achieved by a series of steps including ammonium sulfate precipitation, molecular sieving (using G-75 sephadex column), and anion exchange chromatography (using DEAE Fractogel, Hi-Q and mono-Q chromatography columns). The purity of the samples was checked using SDS-PAGE analysis and activity assays. The pure protein was extensively dialyzed against deionized water and stored by lyophillization at –80^{o}C. Finally, the Biuret assay was used to determine protein concentration (*18*).

Viscosity measurements A Cannon-Fenske viscometer equilibrated at 30^{o}C in a Precision Temp-Trol mineral oil bath was used to determine the kinematic viscosity (η/ρ in mm^2/s). The viscosity (η) was then calculated by multiplying the kinematic viscosity by the density of the solution (ρ in g/ml). The relative viscosity was obtained from the ratio of viscosity of the sample with that of MTA buffer (control).

Dielectric constant The dielectric constant (D) was calculated based on the equation,

$$D = D_o + C(\delta) \quad (1)$$

where, D_o is the dielectric constant of water, C is the molarity of the osmolyte and δ is the dielectric increment. The values of the dielectric increments were obtained from (*19*).

Steady state kinetics Steady state kinetic data were obtained using a Perkin-Elmer λ35 spectrophotometer interfaced with an IBM PC as described before (*20*). Kinetic assays were performed in MTA polybuffer (containing 50mM 100mM MES, Tris, 50 mM acetic acid and 10mM β-mercaptoethanol) at pH7.0, 30°C. The advantage of using this buffer is that it maintains a constant ionic strength from pH 4.5 to 9.5 (*21*). Kinetic parameters such as $K_{m\ (DHF)}$, $K_{m\ (NADPH)}$ and k_{cat} were determined by varying the concentration of one ligand, while maintaining the concentration of the other ligand constant. This was performed at five different sub saturating ligand concentrations. Extinction coefficients of 7750 $M^{-1}cm^{-1}$ at 340nm for DHF (*22*), 6220 $M^{-1}cm^{-1}$ at 340nm for NADPH (*23*) and 12,300 $M^{-1}cm^{-1}$ at 340nm for the reaction were used (*24*). Statistical analysis software (SAS) was then employed to fit the data using the non-linear bisusbtrate Michelis Menten equation (*25, 26*), (see http://animalscience.ag.utk.edu/faculty/saxton/software.htm).

pH dependence of tetramer to dimer equilibrium in presence of osmolytes The equlibrium between the tetramer (T) and two protonated dimers ($2DH_n$) of R67 DHFR can be represented by the following equation:

$$T + 2nH^+ \underset{}{\overset{\mathbf{K_{overall}}}{\rightleftharpoons}} 2\ DH_n \qquad (2)$$

where $K_{overall}$ equals K_a^{2n} / K_d. This model comes from Nichols et al. (*27*), where dissociation of the tetramer into two dimers was found to be linked to the protonation of symmetry related H62 residues located at the dimer-dimer interfaces.

Since W38 also occurs at these interfaces, tryptophan fluorescence can be used to monitor this equilibrium. In order to probe the pH dependence equilibrium between the tetramer and the 2 protonated dimers in the absence and presence of osmolytes (cosolutes), tryptophan fluorescence was monitored using a Perkin Elmer LS-50B luminescence spectrometer. Wild type R67 DHFR (1.3 μM) in MTH buffer pH 8.0 and/or buffer containing osmolytes was titrated with 2N HCl (containing osmolytes) and the pH of the sample was measured. The emission spectra for tryptophan fluorescence (excitation at 295 nm) were also recorded from 300 to 450 nm for each pH titration. The intensity averaged emission wavelength (λ) was then calculated using the equation:

$$\lambda = \Sigma(I_i \lambda_i)/ \Sigma(I_i) \quad (3)$$

where I is the intensity and λ is the wavelength (*28*).

The data obtained were fit to the following equation, which describes the linkage between the tetramer and the two protonated dimers (*27*):

$$Flu_{obs} = \{(Flu_{di} - Flu_{tet})[[H]^{2n}/(4K_{overall} P_{tot})][-1 + (1+8K_{overall} P_{tot} /[H]^{2n})^{1/2}]\} + Flu_{di} \quad (4)$$

where Flu_{obs} is the observed fluorescence; Flu_{di} and Flu_{tet} are the calculated limits for dimer and tetramer fluorescence at low and high pH, respectively; P_{tot} is the total protein concentration in terms of dimer (*29*) and $K_{overall} = ([tetramer][H]^{2n})/([dimer]H_{2n}^{2})$ in units of M, M^2 or M^3 for n = 1, 1.5 or 2, respectively. Sigma Plot was used to fit the data for 2n=3.

For comparison of the pH profiles in different osmolytes, the data were normalized by fitting to the equation:

$$F_{app} = (Y_{obs} - Y_{pH8})/(Y_{pH5} - Y_{pH8}) \quad (5)$$

where F_{app} is the fractional value between 0 and 1 and Y_{obs}, $Y_{pH8,}$ and Y_{pH5} are the optical values associated with the observed pH and the pH limits of 8 and 5 respectively.

Osmotic pressure measurements The osmotic pressure exerted by various cosolutes was measured using a Wescor vapor pressure osmometer. The osmolality obtained was then converted to water activity using the equation:

$$\ln a_{H2O} = - O_s \cdot \overline{V} \qquad (6)$$

where a_{H2O} is the water activity (*30*), O_s is the osmolality in osmol kg^{-1} and $\overline{V}$ is the molal volume of water (55.56 M).

Analysis of ligand binding in the presence of osmolytes The binding of DHF to the NADPH•R67 DHFR complex in the presence of cosolutes/ osmolytes can be represented as:

$$DHF + NADPH\bullet R67\ DHFR \rightleftharpoons DHF\bullet\ NADPH\bullet R67\ DHFR + \nu_{H2O}\ H_2O + \nu s\ S \qquad (7)$$

where ν_{H2O} and νs are the stoichiometric coefficients of water and the cosolute respectively. This can also be described using the Wyman linkage equation (*31*)

$$\frac{\partial \ln K_a}{\partial \ln a_{H2O}} = \nu_{H2O} + \nu_S \left(\frac{\partial \ln a_s}{\partial \ln a_{H2O}} \right) \qquad (8)$$

where K_a is the association constant for DHF binding and a_s is the activity of the cosolute.

Isothermal Titration calorimetry (ITC) ITC experiments were performed to determine the binding affinity (K_a), stoichiometry (n) and enthalpy of binding (ΔH) for the formation of enzyme•2NADPH and enzyme•$NADP^+$•DHF complexes. A Microcal VP isothermal titration calorimeter was employed connected to a Gateway PC (*32*). Protein concentrations in the range of 60-150μM were used and titrations were carried out in MTA buffer (or MTA buffer containing osmolyte) at pH 7.0 at 30°C. Data were collected using VPITC software and were analyzed using

the Origin 5.0 software. For tirations involving osmolytes, buffer containing osmolyte was used in the reference cell. A c-value (=$[P_{total}]/K_d$) of 3 to 127 was observed for all binding experiments, which is within the suggested range of 1 to 1000 (*32*).

Heat capacity experiments were also performed using isothermal titration calorimetry. The enthalpy change was determined at different temperatures (T) ranging from 278-303^{o}K. The relationship between heat capacity change (ΔC_p) and enthalpy change (ΔH) can be described as:

$$\Delta C_p = \frac{\partial \Delta H}{\partial T} \qquad (11)$$

Determination of total, polar and non-polar surface areas Solvent accessible surface areas were calculated using the access surf command in the NMR refine module in InsightII (Accelrys). A probe radius of 1.4 ± 0.1 Å for a water molecule was used to access the change in solvent accessible areas for the following structures: Apo R67 DHFR (*4*) and binary $NADP^+$•R67 DHFR complex (which was obtained by removal of DHF from the ternary complex of DHF• $NADP^+$•R67 DHFR (*4*)). The change in solvent accessible surface area (ΔASA) for the formation of each complex was calculated using the relationship:

$$\Delta ASA = ASA_{E\bullet NADP+} - (ASA_E + ASA_{NADP+}) \qquad (12)$$

A correlation between heat capacity and the solvent exposure of non-polar and polar areas of the protein has been determined by various groups (*33-35*). Using protein folding or ligand binding events, a general relationship is as follows:

$$\Delta C_p = C_{apolar}\,\Delta ASA_{apolar} + C_{polar}\,\Delta ASA_{polar} \qquad (13)$$

where C_{apolar} and C_{polar} are the coefficients for the apolar and polar contributions respectively.

Propagation of errors was calculated using the method described in the following link: www.colby.edu/chemistry/PChem/scripts/error.html.

***Escherichia coli* growth in the presence of sorbitol** The *E.coli* DH5α strain was first transformed with a pUC8 plasmid containing the R67 DHFR gene. The cells containing wild type and/ or mutant R67 DHFR genes were then tested for their ability to show TMP resistance by growing on M9 minimal media (*36*) containing 0.02% casamino acids and 20μg TMP/ml. Further screening was done by adding increasing concentrations of sorbitol to the media. The water activity of the plates containing sorbitol was measured using an Aqualab meter (Decagon devices).

Results

Effect of osmolytes on the oligomeric structure of R67 DHFR In order to study the role of water in ligand binding to R67 DHFR, varying concentrations of different osmolytes were employed. Also, the catalytic activity of R67 DHFR depends on the tetrameric nature of the enzyme (*37*). Therefore, prior to performing ligand-binding studies in the presence of osmolytes, we tested if addition of osmolytes had any effect on the tetramer-dimer equilibrium of R67 DHFR. Hence, pH titration experiments were performed in the presence of different osmolytes.

At low pH, the histidine 62 residues of R67 DHFR get protonated and the tetramer dissociates into two protonated dimers, which is described by $K_{overall}$ (*27*), where

$$T + 2nH^{+} \underset{}{\overset{K_{overall}}{\rightleftharpoons}} 2DH_n \qquad (14)$$

and n is the number of protons (H). The W38 residues present at the dimer-dimer interface show changes in fluorescence during the titration from tetramer (hydrophobic) to dimer (solvent exposed environment). Therefore, to calculate the $K_{overall}$, the fluorescence emission spectrum of

R67 DHFR is measured at each pH during the titration. The experiment was performed in MTA buffer containing different osmolytes such as 10% ethylene glycol, 12.5% DMSO or 15% PEG400 and the $K_{overall}$ compared to that observed in MTA buffer. It was observed that the titrations in the presence of each osmolyte overlapped (figure 2). This suggested that osmolyte addition did not perturb the tetramer structure of R67 DHFR. $K_{overall}$ values varied 3 fold (table 1) also indicating osmolytes have minimal effects on the oligomeric state of R67 DHFR.

Correlation between ligand binding and osmolyte properties The effect of various osmolytes on the binding and catalysis of R67 DHFR was measured using both steady state kinetics as well as isothermal titration calorimetry. Various osmolytes such as glycerol, ethylene glycol, trimethylamine N-oxide (TMAO), dimethylsulfoxide (DMSO), glycine betaine, and sucrose were employed, the structures of which are shown in figure 3. We observed that addition of osmolytes affected the K_m and K_d values associated with DHF and/or NADPH binding, but had little (<1.5 fold) or no effect on the k_{cat} of the reaction. This suggested that introduction of osmolytes affected ligand binding, but had not catalysis.

The next step was to determine which property of the osmolyte was affecting binding of the ligand. Solutes used as osmolytes are chemically distinct and could affect proteins differently depending on their properties. For example, betaine and sucrose change the dielectric constant of the medium in different directions. Similarly, polyethylene glycols (PEG) are neutral, but can cause a volume exclusion effect depending on their size (*38*). The use of different osmolytes with R67 DHFR will allow us to determine if these properties affect DHF and/or NADPH binding.

Table 1: $K_{overall}$ values for the $T + 2nH^{+} \rightleftharpoons 2DH_n$ equilibrium in the presence of osmolytes monitored by fluorescence.

Osmolyte	$K_{overall}$ ($=K_a^{2n} / K_d$) for 2n = 3 in units of M^2
MTA buffer	1.42e-13 ± 4.54e-15
10% Ethylene glycol	1.08e-13 ± 3.54e-15
12.5% DMSO	8.99e-14 ± 2.78e-15
20% PEG 400	2.78e-13 ± 6.34e-14

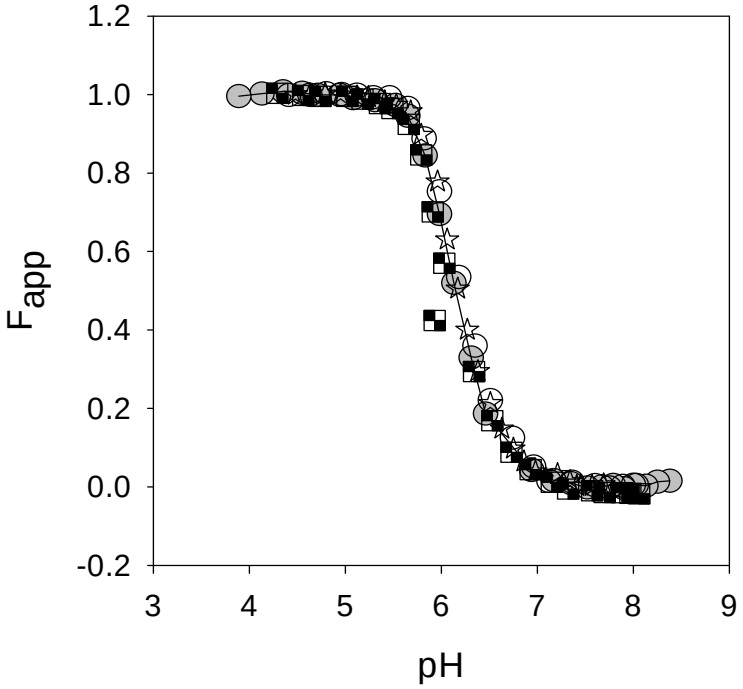

Figure 2: pH titration curves describing the tetramer-dimer equilibrium in the presence of osmolytes. Fluorescence spectroscopy was used to monitor the environment of W38 residues. At pH 8, these residues are buried at the dimer-dimer interfaces. As the pH is decreased, W38 residues become exposed upon titration of nearby H62 residues. Data are presented for MTH buffer (●), buffer containing 10% ethylene glycol (☆), buffer containing 12.5% DMSO (○) and buffer containing 20% PEG400 (◪)

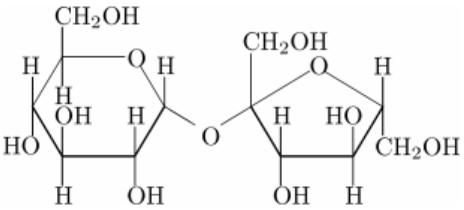

Sucrose

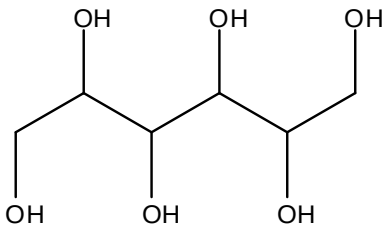

Sorbitol

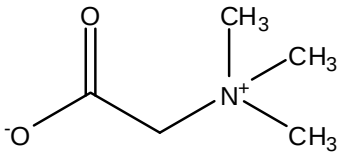

Betaine

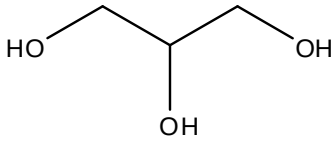

Glycerol

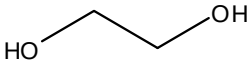

Ethylene Glycol

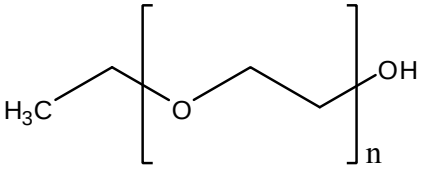

Polyethylene Glycol
(PEG)

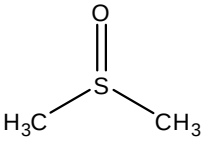

Dimethylsulfoxide
(DMSO)

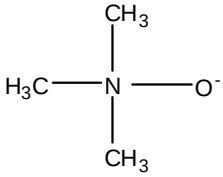

Trimethylamine oxide
(TMAO)

Figure 3: Structures of Sucrose, Sorbitol, Betaine, Glycerol, Ethylene glycol, Polyethylene glycol, Dimethyl sulfoxide and Trimethylamine oxide.

The relationship between ln K_a (for binding of first molecule of NADPH to R67 DHFR) and *osmolality* was first analyzed. Isothermal titration calorimetry (ITC) was performed in this determination. For this, NADPH was titrated into R67 DHFR at pH 7.0 and 30^{o}C and the K_a of binding was determined after fitting the raw isotherm to a sequential sites model. The potential number of water molecules was then determined using the relationship:

$$\ln(K_a)/O_s = \Delta n_w/-V, \quad (15)$$

where Δn_w is the number of water molecules, V is the molal volume of water (0.018 M) and O_s is the osmolality given in units of osmol Kg^{-1}

Overlapping data were obtained with a plot of ln (K_{a1}) versus osmolality. From this plot, the value of Δn_w was determined to be –38 ± 6 consistent with binding of NADPH to R67 DHFR being accompanied by a release of water from the active site (figure 4A, table 2).

Q-total (or total heat) plots were concurrently used to analyze the effect of osmolytes on NADPH binding. These plots show the total heat associated with the binding process. Q-total analyses were performed using sucrose, betaine, DMSO, PEG 400, glycerol and ethylene glycol. A representative plot in the presence of betaine is shown in figure 4B. From the plot, it is clear that increasing osmolyte concentrations shows tighter binding of NADPH. Another observation from the figure is that as the osmolyte concentration increases, more heat is evolved during binding of NADPH to R67 DHFR (ΔH becomes more negative). Similar observations have been made during the interaction of ferredoxin with ferredoxin $NADP^+$ reductase in the presence of glycerol as an osmolyte (*39*). It was suggested that this may be due to 'heat of dilution', which is caused by mixing of osmolytes into water (an exothermic process) (*40-42*). Enthalpy-entropy compensation resulting from the involvement of water can also explain the changes in enthalpy (*43*). A plot of K_{a2} (binding of the second molecule of NADPH) and osmolality

Table 2: Data for effect of osmolality on the association constant (K_{a1}) for binding of the first molecule of NADPH. The data is plotted in figure 4A.

Osmolyte	Osmolality (Osm)	K_{a1} (M) * 10^{-4}
MTA buffer	0.22	10.5 ± 0.9
MTA buffer	0.22	8.9± 0.5
5%Betaine	0.86	18.8 ± 1.2
5%Betaine	0.86	24.9 ± 0.9
10%Betaine	1.45	34.0 ± 0.4
10%Betaine	1.45	39.5 ± 1.6
15%Betaine	1.86	135 ± 23
20%Betaine	2.97	89.4 ± 9.6
20%Betaine	2.97	60.1 ± 2.3
5% DMSO	0.95	20.1 ± 1.2
5% DMSO	0.95	16.9 ± 0.6
5%DMSO	0.88	22.3 ± 0.5
7.5% DMSO	1.18	21.3 ± 1.0
7.5% DMSO	1.18	22.6 ± 1.0
12.5% DMSO	1.92	25.3 ± 0.9
12.5%DMSO	1.91	41.5 ± 3.1
5% Ethylene glycol	0.87	17.9 ± 0.4
5% Ethylene glycol	0.87	20.1 ± 0.7
10% Ethylene glycol	1.73	23.5 ± 0.5
10% Ethylene glycol	1.73	21.9 ± 0.4
15%PEG400	0.95	28.1 ± 0.6
25%PEG400	1.25	30.1 ± 1.2

Figure 4: Binding of NADPH to R67 DHFR in presence of osmolytes A) A plot of ln K_{a1} values vs. osmolality is shown, where K_{a1} describes binding of the first NADPH molecule. The solutions used are: MTH buffer (●), buffer containing glycine betaine (△), DMSO (○), ethylene glycol (☆) or PEG400 (◪). K_a increases as osmolality increases. Also, overlapping data points are observed, and can be fit with a single slope. Therefore, osmolality can be used as a parameter to describe the change in K_a values upon ligand binding. A value –38 ± 6 is obtained for Δn_w using the relationship: d ln K_a / d [Osmolal] = - Δn_w / 55.6. B) A plot of total heat (Q_{total}) vs NADPH concentration in the presence of different concentrations of betaine. Data describing NADPH binding in MTH buffer (○), 5% betaine (□) and 20% betaine (△) are shown.

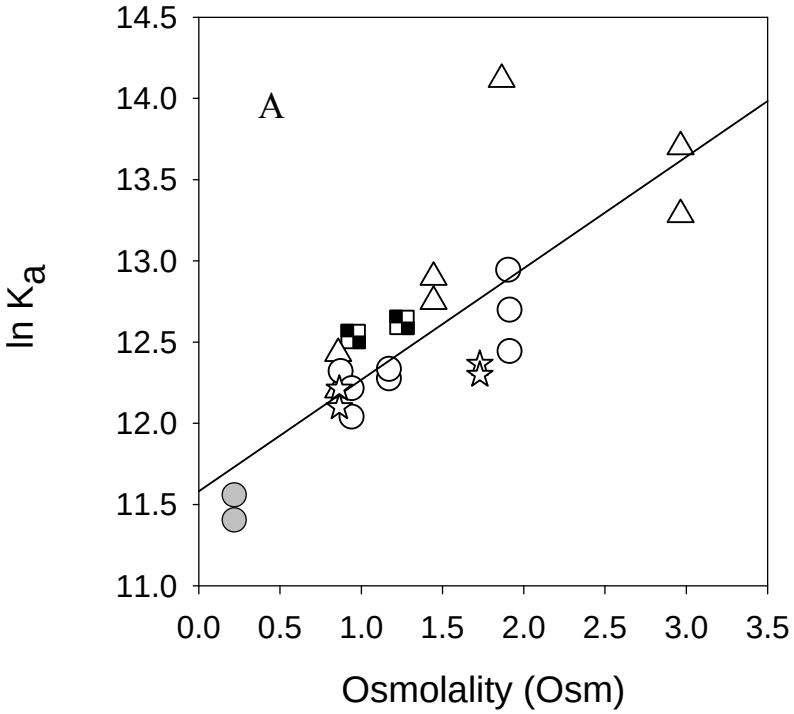
A
ln K_a
Osmolality (Osm)
14.5
14.0
13.5
13.0
12.5
12.0
11.5
11.0
0.0
0.5
1.0
1.5
2.0
2.5
3.0
3.5

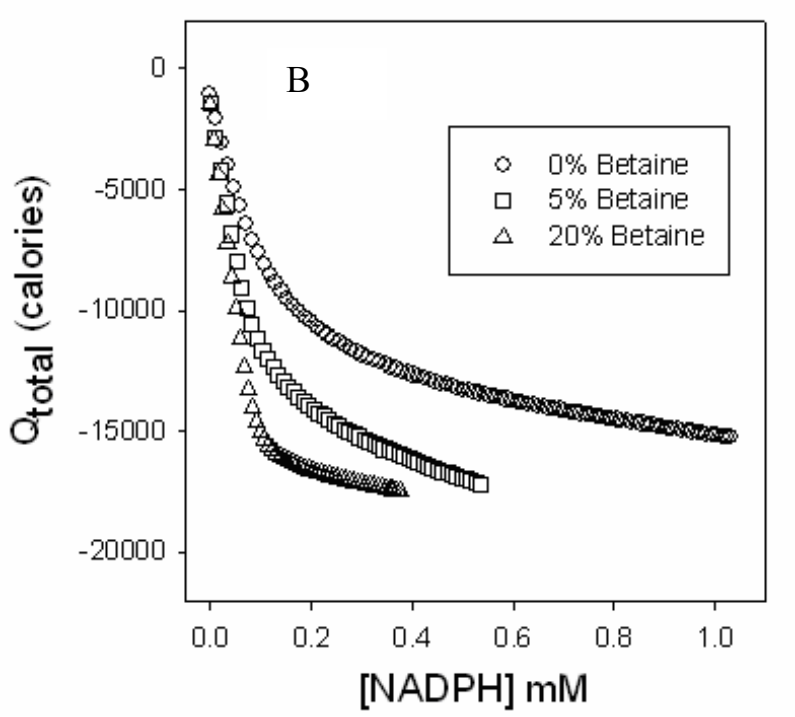
B
Q_{total} (calories)
[NADPH] mM
0% Betaine
5% Betaine
20% Betaine
0
-5000
-10000
-15000
-20000
0.0
0.2
0.4
0.6
0.8
1.0

was also used to determine the net change in water molecules upon NADPH binding. A Δn_w value of –20 ± 8 was obtained. However, there is a larger variation in the K_{a2} as it shows weaker binding (data not shown).

An analysis of the plot of $K_{a1\ (NADPH)}$ vs. viscosity showed that the data did not overlap indicating that viscosity was not the variable that affected DHF binding (figure 5A). Finally, a plot was constructed to see if there was any correlation between the *dielectric constant* and $K_{a\ (NADPH)}$. It was observed that there was a wide-range of slopes using different osmolytes (figure 5B), which led us to conclude that the dielectric constant does not explain effects on NADPH binding.

Therefore, osmolality was the property that was used to explain the observed change in K_a values upon ligand binding. For NADPH binding (in the 1st site), a net release of –38 ± 6 water molecules (between free NADPH and free R67 DHFR and the bound complex) was estimated

Figure 5: Relationship between catalytic efficiency (k_{cat}/K_m) and viscosity and dielectric constant A) Plot of $\ln(k_{cat}/K_{m\ (DHF)})$ vs. viscosity. Viscosity was calculated as described in the Materials and Methods section. Data describe MTH buffer (●), buffer containing glycine betaine (△), DMSO (○), ethylene glycol (☆) or PEG400 (◪). B) Plot of $\ln(k_{cat}/K_{m\ (DHF)})$ vs. dielectric coefficient. Dielectric coefficients were calculated as described in the Materials and Methods section. Data points describe MTH buffer (●), buffer containing sucrose (□), glycine betaine (△) and PEG400 (◪).

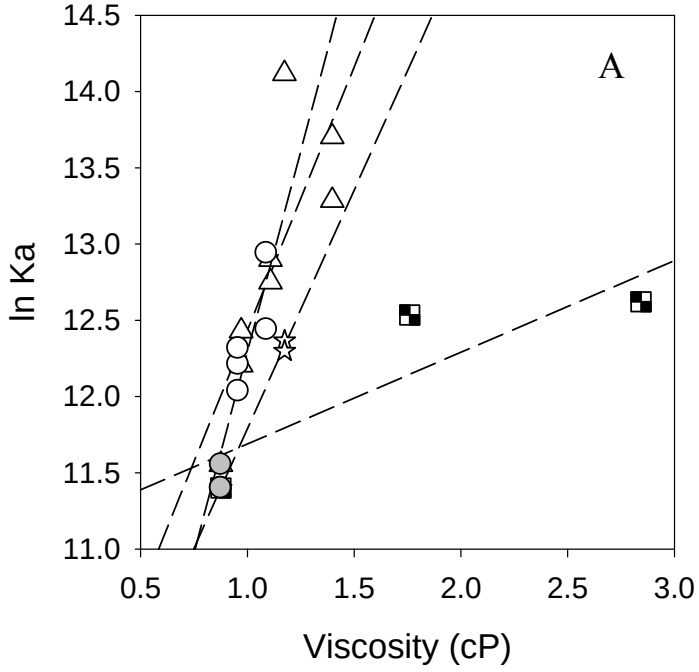
14.5
14.0
13.5
13.0
12.5
12.0
11.5
11.0
ln Ka
A
0.5
1.0
1.5
2.0
2.5
3.0
Viscosity (cP)

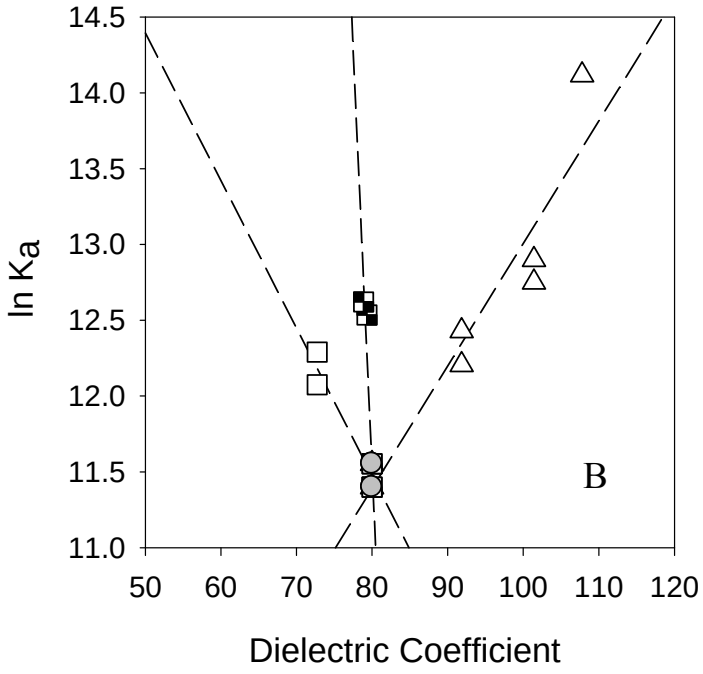
14.5
14.0
13.5
13.0
12.5
12.0
11.5
11.0
ln Ka
B
50
60
70
80
90
100
110
120
Dielectric Coefficient

Role of water in DHF binding The effects of viscosity and dielectric constant on DHF binding was also tested. The data obtained with different osmolytes did not overlap (as Osmotic pressure was also used to test binding of the substrate, DHF to enzyme•NADPH (by kinetics) or enzyme•$NADP^+$ (by ITC). It was observed that as the osmolality increased, $k_{cat}/K_{m\ (DHF)}$ also increased (table 3). However, variable slopes were observed with different osmolytes (figure 6). This resulted in different values for the net change in water upon DHF binding (Δn_w). The Δn_w determined using TMAO, glycerol and ethylene glycol ranged from around 16 to 25 (combined fit gave a slope of 17 ± 2), whereas the Δn_w estimated using sucrose, betaine and DMSO ranged from 40 to 60. Additionally, PEG 400, PEG 3350 and PEG 8000 showed Δn_ws of 78, 145 and 353 respectively as listed in table 4. The origin of variable slopes for DHF binding is not completely understood and can be due to different possibilities, which are considered in the discussion section.

Table 3: Data for the effect of osmolytes on the $K_{m(DHF)}$ and k_{cat} for the binding of DHF to the R67 DHFR•NADPH complex. A plot for this data is shown in figure 6.

Osmolyte	Concentration	Osmolality (Osm)	K_m(μM)	k_{cat} (sec^{-1})
MTH buffer	0%	0.22	4.3 ± 0.3	0.7 ± 0.01
	0%	0.27	5.99 ± 0.2	0.8 ± 0.01
Glycerol	7.5%	1.52	9.02 ± 0.3	0.8 ± 0.01
	15%	2.53	11.4 ± 0.5	0.7 ± 0.01
	20%	3.38	10.0 ± 0.8	0.6 ± 0.01
Ethylene glycol	5%	1.00	7.18 ± 0.4	0.8 ± 0.01
	10%	1.73	10.9 ± 0.9	0.8 ± 0.02
TMAO	12.5%	1.80	11.3 ± 0.5	0.8 ± 0.01
	15%	2.07	11.8 ± 0.8	0.8 ± 0.02
DMSO	2.5%	0.55	5.17 ± 0.3	0.8 ± 0.01
	5%	0.91	9.65 ± 0.6	0.7 ± 0.02
	10%	1.63	13.5 ± 1.4	0.7 ± 0.02
	12.5%	1.92	18.0 ± 1.0	0.8 ± 0.02
Sucrose	0.25M	0.46	6.20 ± 0.5	0.6 ± 0.01
	0.5M	0.78	6.09 ± 0.5	0.6 ± 0.01
	0.75M	1.24	10.9 ± 0.7	0.6 ± 0.01
	1M	1.73	12.0 ± 0.7	0.6 ± 0.01
	1.5M	2.10	14.0 ± 1.1	0.6 ± 0.01
	1.75M	2.06	15.4 ± 0.9	0.5 ± 0.01
Betaine	2.5%	0.37	7.55 ± 0.7	0.5 ± 0.01
	5%	0.86	10.2± 0.5	0.5 ± 0.01
	10%	1.43	15.3 ± 0.6	0.5 ± 0.01
	15%	1.84	22.1 ± 1.3	0.4 ± 0.01
PEG 400	10%	0.61	12.5 ± 1.2	0.7 ± 0.02
	15%	0.85	15.0 ± 1.1	0.8 ± 0.02
	20%	1.40	30.7 ± 2.5	0.7 ± 0.02
	25%	1.63	26.5 ± 1.2	0.7 ± 0.01
	30%	1.74	49.4 ± 3.9	0.6 ± 0.02

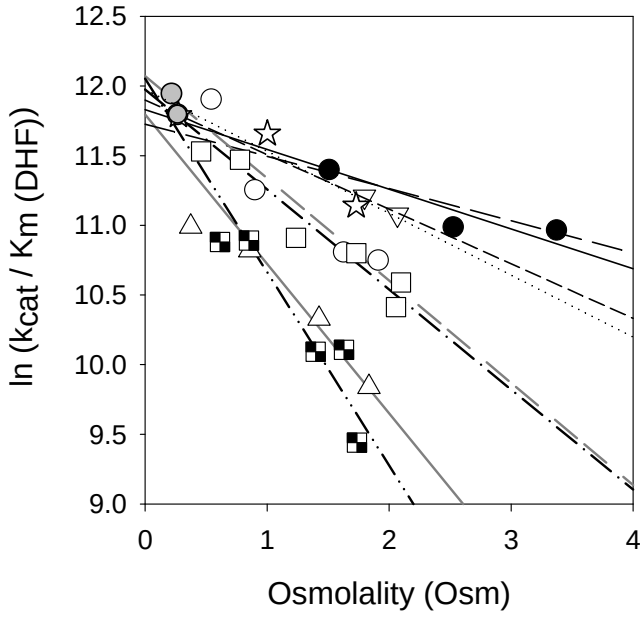

Figure 6: Relationship between ln $k_{cat}/K_{m(DHF)}$ and osmolality. Steady state kinetic data were obtained at saturating concentrations of NADPH in the presence of different osmolytes. Using the Michaelis-Menten equation, k_{cat} and K_m values were extracted. Data for MTH buffer (●), glycerol (●), ethylene glycol (☆), TMAO (▽), sucrose (□), DMSO (○), glycine betaine (△) and PEG400 (◪) are shown. It is observed that as the osmolality increases, binding of DHF to the enzyme•NADPH complex is weakened. In contrast to NADPH binding with a single slope, variable slopes are obtained for DHF binding. The slopes of these plots were converted to Δn_w using the relationship: d ln k_{cat} / $K_{m\ (DHF)}$ / d [Osmolal] = - Δn_w / 55.6. A plot of ln k_{cat} / $K_{m\ (DHF)}$ vs. ln water activity can also be used to determine Δn_w. These values are reported in Table 4.

Table 4: Osmolyte properties and slopes (Δn_w) associated with plots of ln a_{H2O} vs. ln $k_{cat}/K_{m\ (DHF)}$ as determined by steady state kinetics (as shown in figure 6).

Osmolyte	MW (Daltons)	V_{mol} (ml/mol)	Δn_w
Ethylene Glycol	62	54.1 [a]	25 ± 8
Glycerol	92	71.6 [a]	16 ± 3
TMAO	111	73 [b]	22 ± 1
DMSO	78	71 [c]	41 ± 7
Sucrose	342	214.4 [d]	40 ± 4
Glycine betaine	118	75.2 [a]	60 ± 13
PEG400	400	343.6 [a]	78 ± 11
PEG3350	3350	2913 [e]	145 ± 42
PEG8000	8000	6760 [a]	353 ± 38

V_{mol} is the molar volume of the osmolyte determined from literature: [a] from (*38*); [b] from (*44*); [c] from (*45*); [d] from (*46*) and [e] from (*47*).

Isothermal Titration calorimetry to determine K_a for binding of DHF to R67 DHFR•$NADP^+$

Isothermal titration calorimetry studies were also performed to determine the ternary complex K_a describing binding of DHF to enzyme•$NADP^+$ complex in the presence of different osmolytes. For this, DHF was titrated into a mixture of R67 DHFR and $NADP^+$ at pH 7.0 and 30°C and the K_a of binding determined after fitting the raw isotherm to a single sites model (table 5). Using glycine betaine and sucrose, a value of 29 ± 3 was obtained, consistent with an uptake of 29 water molecules during DHF binding (figure 7A). A general observation is that the K_d values (determined from $1/K_a$) are ~2 fold lower than the K_m values in the presence of added osmolytes. This may be because K_m can contain kinetic terms, while K_d represents a true binding constant. Good ITC fits could not be obtained for data at high osmolyte concentrations. This behavior is not completely understood and hence data for high concentrations of osmolytes are not presented.

Q-total (or total heat) plots for DHF binding also confirm a weaker interaction in the presence of different osmolytes. Figure 7B represents a Q-total plot for DHF titration in R67 DHFR•$NADP^+$ complex in the presence of different concentrations of betaine. Titration of folate into R67 DHFR (to form a binary complex with folate) in the presence of osmolytes was also performed. These data were analyzed by a Q-total plot (figure 7C) and showed a similar trend, wherein increasing osmolyte concentrations showed weakened binding of folate. Another observation from the Q-total plots is that as the osmolyte concentration increases, the heat evolved during binding of DHF to R67 DHFR•$NADP^+$ complex (or 2 folates binding to R67 DHFR) becomes less negative. Similar observations have been made during the interaction of HyHEL5 antibody with lysozyme in the presence of glycerol as an osmolyte (*48*).

Overall, these data suggest that NADPH and DHF bind differently to the enzyme with NADPH releasing water molecules upon binding and DHF taking up water molecules.

Table 5: Data for the effect of osmolytes on the binding (K_a) of DHF. A plot for this data is shown in figure 7A.

Osmolyte	Osmolality (Osm)	K_a (M) * 10^{-2}	Stoichiometry (N)
MTH buffer	0.23	23.7 ± 0.4	1.29 ± 0.01
MTH buffer	0.23	28.4 ± 0.8	1.29 ± 0.01
10%Betaine	1.45	14.1 ± 0.5	1.42 ± 0.01
10%Betaine	1.45	15.7 ± 0.3	1.28 ± 0.01
20%Betaine	2.70	6.46 ± 0.1	1.38 ± 0.01
20%Betaine	2.70	8.15 ± 0.2	1.33 ± 0.01
0.75M sucrose	1.30	16.7 ± 0.5	1.27 ± 0.01
0.75Msucrose	1.30	12.5 ± 0.9	1.34 ± 0.01
15%PEG400	0.95	6.79 ± 0.2	1.43± 0.01
25%PEG400	1.25	4.84 ± 0.2	1.36 ± 0.01

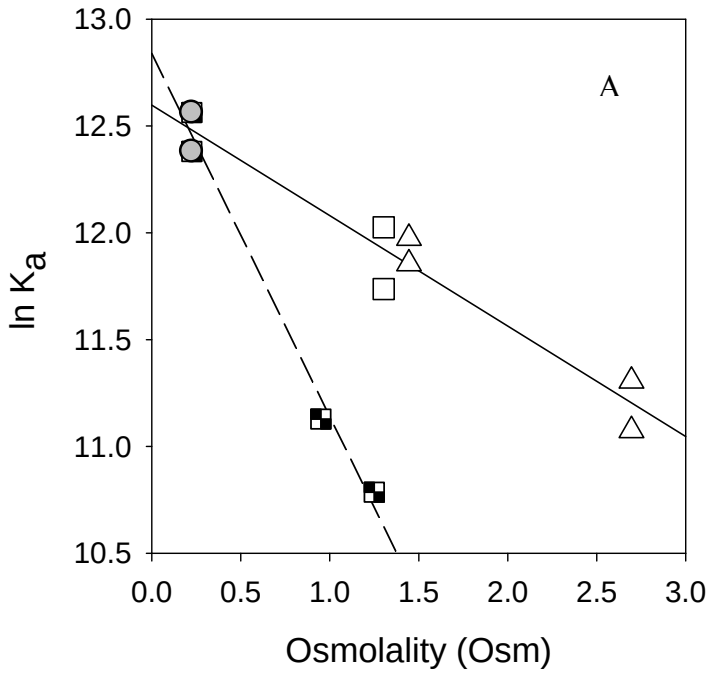

Figure 7: Binding of DHF to R67 DHFR in presence of osmolytes A) The K_a of binding of DHF to the enzyme•$NADP^+$ complex has been plotted as a function of osmolality. A decrease in K_a is observed as osmolality is increased, indicative of weaker binding of DHF. Overlapping data are obtained for MTH buffer (●) containing sucrose (□) and buffer containing glycine betaine (△), and a Δn_w of 29 ± 3 is estimated. When buffer containing PEG400 (◪) is used, a steeper slope is obtained, resulting in a higher value of Δn_w (77 ± 11). B) Plot of total heat (Q_{total}) vs DHF concentration in the presence of different concentrations of betaine. Data describing DHF binding in MTH buffer (○), 10% betaine (□) and 20% betaine (△) are shown in the figure. The Q-total limit decreases as the concentration of betaine increases. C) Q-total plot for the binding of folate to the apo enzyme to form the enzyme•2folate complex. A trend similar to DHF binding is observed, where Q-total decreases as the concentration of betaine increases.

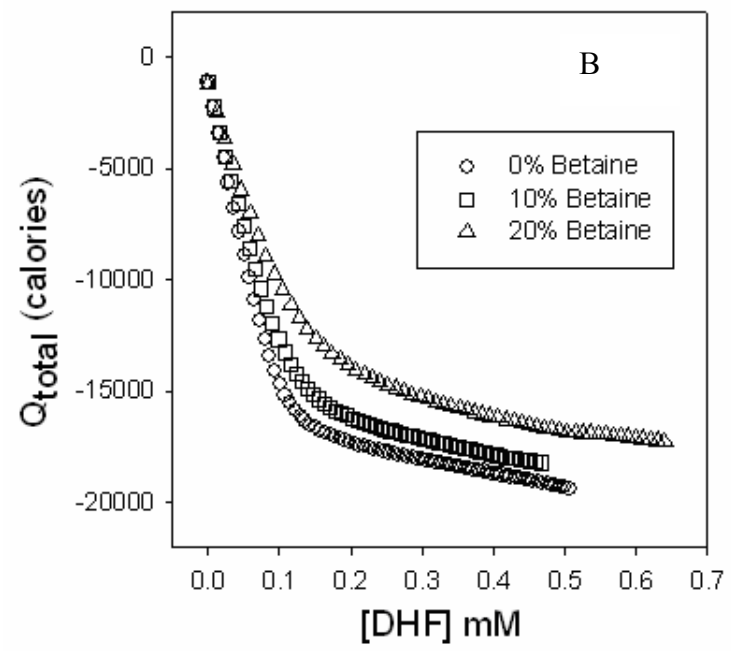

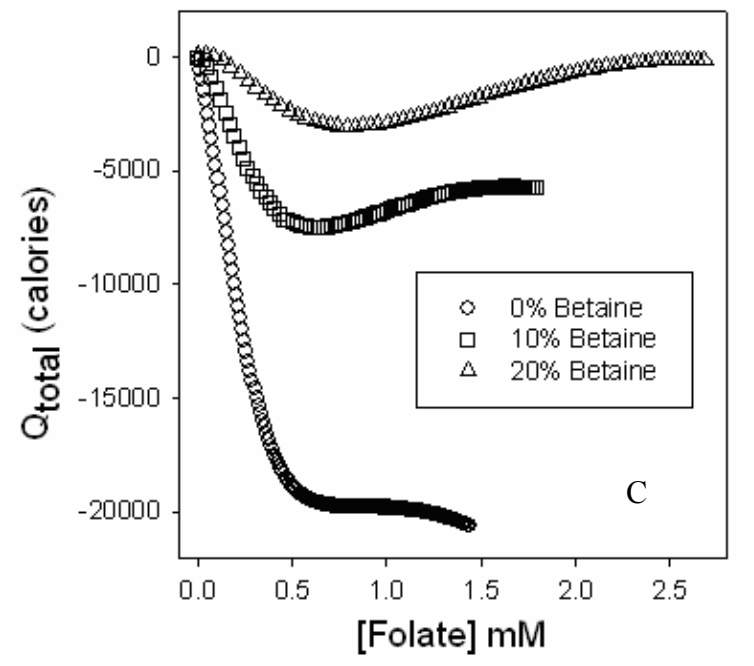

Figure 7: (continued): Binding of DHF to R67 DHFR in the presence of osmolytes.

Effect of osmolytes on R67 DHFR function *in vivo* Extremes in environmental conditions such as high salinity, dehydration or high temperature are deleterious to cell growth. Adaptation to conditions of osmotic stress is important as it protects organisms from fluctuations in water activity and solute content in the environment (*49*). One of the ways that cells survive under these conditions is by intracellular accumulation of solutes, which help prevent water loss and thereby maintain the turgor pressure of cells. These solutes can either be synthesized *de novo* by certain strains or taken up from their environment by specific transport systems. These molecules not only stabilize the native state of various globular proteins, but also favor formation of protein assemblies (*50, 51*). Some of the solutes that aid in osmoprotection of cells are potassium glutamate, proline, trehalose, betaine and ecotine. Which osmolyte is produced depends on the type of bacteria or the medium in which they are grown (*49, 52, 53*). Tolerance to osmolality varies from one bacterial strain to the other. For example, *E. coli* can withstand osmotic pressures in the range of 0.015 Osm ~1.9 Osm in minimal medium (*53-55*).

As described earlier, our *in vitro* experiments indicate that water stabilizes DHF binding. Another approach to test the importance of water is by performing *in vivo* experiments. This was addressed by adding increasing concentrations of sorbitol to M9 minimal media (*56, 57*). The effect of osmolyte concentration was then tested on *E.coli* DH5α, which is transformed with wild type or mutant R67 DHFR clones.

For this experiment, two types of controls were used. The first control involved use of 20μg TMP/ml in M9 minimal media plates. This condition results in inhibition of chromosomal DHFR, but rescue by R67 DHFR. Both wild type and mutant clones of R67 DHFR (transformed in *E.coli*) were tested for their ability to show TMP resistance. A range of growth patterns was observed on media containing mutant clones. In general, wild type and mutant clones with high $k_{cat}/K_{m(DHF)}$

values showed confluent growth with overnight incubation. The clones with lower catalytic efficiency showed a slow growth pattern. For example, the Y69L mutant showed growth after 72 hours of incubation. Also, the K32M mutant has a low catalytic efficiency and low protein expression levels and is also not able to withstand the TMP pressure.

The second set of control plates involved the use of increasing concentrations of sorbitol in M9 minimal medium plates. The purpose of these control plates was to determine the highest osmolality levels at which *E.coli* DH5α cells could survive. It was observed, that confluent growth of the cells occurred up to 1.95 Osm Also, at this high concentration, 48 hours of incubation was required for confluent growth (figure 8).

Once the controls were established, cells containing the wild type and mutant clones were grown in the presence of 20μg TMP/ml and increasing concentrations of sorbitol at 37^{o}C (table 6). The wild type clone can grow up to an osmolality of 1.95 Osmol, beyond which the cells cease to grow. The Q67H mutant has a reasonable catalytic efficiency, but also shows substrate and cofactor inhibition (*58*). This mutant is able to grow in a medium with osmolality as high as 1.81 Osmol. On the other hand, mutants with lower catalytic efficiencies such as I68M and Y69L are able to grow in media with osmolalities of 1.44 and 0.81 Osmol respectively. Therefore, an increase in the osmotic pressure results in a decrease in the cellular water content which affects the ability of substrate to bind to the enzyme, thereby resulting in a decrease in catalytic efficiency. Since the cell growth is related to the catalytic efficiency of the mutants, another level of selection is conferred when intracellular water is decreased. Overall, there exists a correlation between *in vivo* function and *in vitro* water uptake.

Table 6: Number of days required for the growth of *E.coli* DH5α cells on M9 minimal media containing osmolytes. *E.coli* DH5α cells transformed with a pUC8 plasmid containing wild type and/or mutant R67 DHFR genes were tested for their ability to grow in M9 minimal media containing the osmolyte sorbitol and trimethoprim (TMP) at 37°C.

		Wt R67 DHFR	Q67H	I68M	Y69L	K32M	DH5α
k_{cat}/K_m (DHF) ($M^{-1}s^{-1}$)		2.2*e 5	1.4*e 5 (pH 8)	6800	890	<200 & low expression levels	-
Condition	1.44 Osmol	1	1	1	1	1	1
	1.81 Osmol	1	1	1	1	1	1
	1.95 Osmol	2	2	2	2	2	2
	0.31 Osmol + 20µg TMP/ml	1	1	1	3	-	-
	0.81 Osmol + 20µg TMP/ml	1	1	1	4	-	-
	0.81 Osmol + 20µg TMP/ml	1	1	1	-	-	-
	0.81 Osmol + 20µg TMP/ml	1	1	1	-	-	-
	0.92 Osmol + 20µg TMP/ml	1	1	1	-	-	-
	1.01 Osmol + 20µg TMP/ml	1	1	2	-	-	-
	1.44 Osmol + 20µg TMP/ml	1	2	-	-	-	-
	1.81 Osmol + 20µg TMP/ml	1	2	-	-	-	-
	1.95 Osmol + 20µg TMP/ml	2	-	-	-	-	-

Figure 8: Effect of sorbitol on growth of wild type and mutant DHFR clones. Wild type R67 DHFR and its mutants were tested for their ability to grow on M9 minimal media containing 20μg/ml trimethoprim (TMP) and varying concentrations of sorbitol. Each petri plate containing the media is divided into 6 zones. Position 1 shows the region where *E.coli* DH5α cells (lacking a plasmid) are streaked on the plate. Position 2 indicates the region where *E.coli* cells (containing the wild type R67 DHFR gene cloned into pUC8) are streaked. Positions 3, 4, 5 and 6 indicate the regions where the Q67H, I68M and Y69L mutant clones are plated. No growth is observed in position 1, indicating that *E.coli* DH5α cells are susceptible to TMP. Also no growth is observed for the K32M clone in media containing 20μg/ml TMP as well as in the presence of sorbitol. Cells containing the gene for wild type R67 DHFR however, are able to grow in 20μg/ml TMP and can withstand sorbitol concentrations of 0.5M. The Q67H and I68M mutants are also not much affected by concentrations of sorbitol as high as 0.25M. The Y69L mutants can grow on plates containing TMP and 0.25M sorbitol, but cease to grow in 0.5M sorbitol.

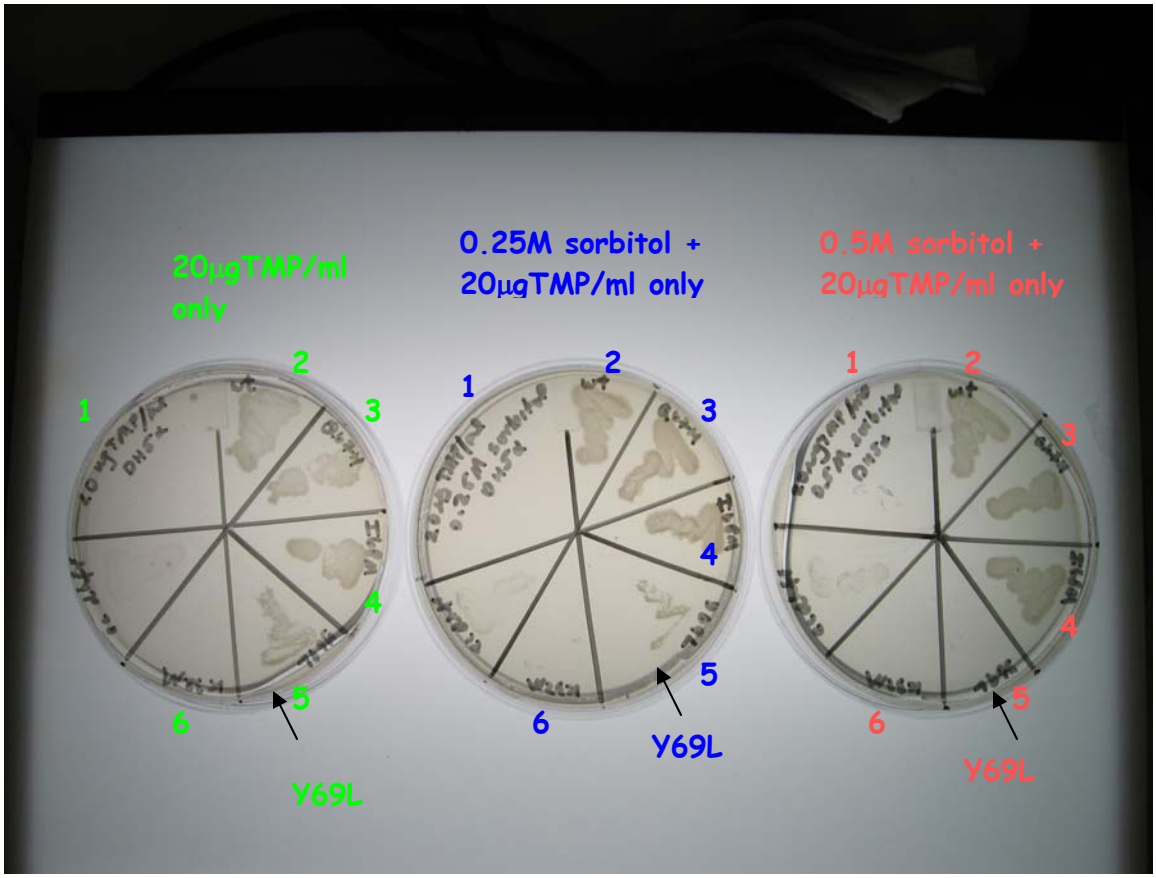
20μgTMP/ml only
0.25M sorbitol + 20μgTMP/ml only
0.5M sorbitol + 20μgTMP/ml only
1
2
3
4
5
6
Y69L
Y69L
Y69L

Role of water in binding enthalpy Isothermal titration calorimetry provides valuable information on the enthalpy and entropy changes accompanying a binding process. The net enthalpy change measured by ITC is not only due to hydrogen bonding or ionic interactions, but also due to changes in protein-solvent, solvent-solvent and protein-ligand interactions (*59*). From the changes in enthalpy (ΔH) at different temperatures (T), a heat capacity change can be calculated, which is based on the relationship:

$$\Delta C_p = \partial \Delta H / \partial T \qquad (16)$$

Therefore, the slope of a plot of ΔH versus temperature gives a value for ΔC_p.

A number of factors contribute to heat capacity values. These include dehydration of a non-polar or polar surface, internal vibrations during a binding reaction, conformational change, electrostatic interactions and protonation changes during binding (*60-63*). A heat capacity change that is caused by dehydration of polar/ non-polar surfaces may indirectly indicate that water is involved in ligand binding. From our results in R67 DHFR, water uptake is associated with DHF binding and release of water occurs upon NADPH binding, so it is of interest to monitor ΔC_p in this enzyme.

In order to thermodynamically characterize ligand binding to R67 DHFR, heat capacity studies have been performed. In brief, the heat capacity change for binding of DHF to form a ternary complex in the presence of the $NADP^+$ and R67 DHFR has been measured (table 7, figure 9A). In addition to this, the heat capacity change for binary complex binding of NADPH has been studied (table 8, figure 9B). The enthalpy of binding of the ligands was determined at temperatures ranging from 278^{o}K to 303^{o}K and the slope of the plot was used to calculate the heat capacity. For NADPH binding, a heat capacity of –178 ± 15cal/ ^{o}K mol was observed and for

Table 7: Data for ΔH, TΔS and ΔG at different temperatures for the formation of enzyme• DHF•$NADP^+$ complex. The value of ΔH is more negative as the temperature increases, while the value of -TΔS is more negative as the temperature increases. However, the ΔG values do not change significantly with temperature.

Temperature (^oK)	ΔH (cal/mol)	-TΔS (cal/mol)	ΔG (cal/mol)
278	-7000 ± 31	780	-7800 ± 65
	-6800 ± 28	960	-7700 ± 57
283	-7900 ± 43	-400	-7500 ± 66
	-7960 ± 42	-390	-7600 ± 65
288	-9300 ± 35	-1700	-7600 ± 44
295	-10000 ± 44	-2900	-7300 ± 30
	-11000 ± 34	-3700	-7300 ± 44
303	-12300 ± 29	-4900	-7400 ± 19
	-11200 ± 38	-3600	-7550 ± 31

Table 8: Data for ΔH, TΔS and ΔG at different temperatures for the formation of enzyme•2NADPH complex. Raw ITC data were fit to sequential binding sites model. Data for only the 1st site are given. The value of ΔH is more negative as the temperature increases, while the value of -TΔS is more negative as the temperature increases. No significant change is observed for the ΔG values as a function of temperature.

Temperature (°K)	ΔH (cal/mol)	-TΔS (cal/mol)	ΔG (cal/mol)
278	-5300 ± 22	1600	-6900 ± 41
	-4500 ± 24	2900	-7300 ± 86
288	-6400 ± 37	1070	-7400 ± 77
	-6300 ± 42	1070	-7400 ± 86
295	-8000 ± 287	-1200	-6800 ± 245
303	-9600 ± 147	-2700	-7000 ± 109
	-8900 ± 88	-2000	-6900 ± 65

Figure 9: Heat capacity plots A) Temperature dependence of ΔH (●), ΔG (□) and -TΔS (△) for DHF binding to the enzyme•2NADP$^+$ complex. From the ΔH plot, a heat capacity of –199 kcal/^{o}K.mol is obtained. B) Temperature dependence of ΔH (●), ΔG (□) and -TΔS (△) for the binding of the first molecule of NADPH to the apo enzyme to form the enzyme•2NADP$^+$ complex.

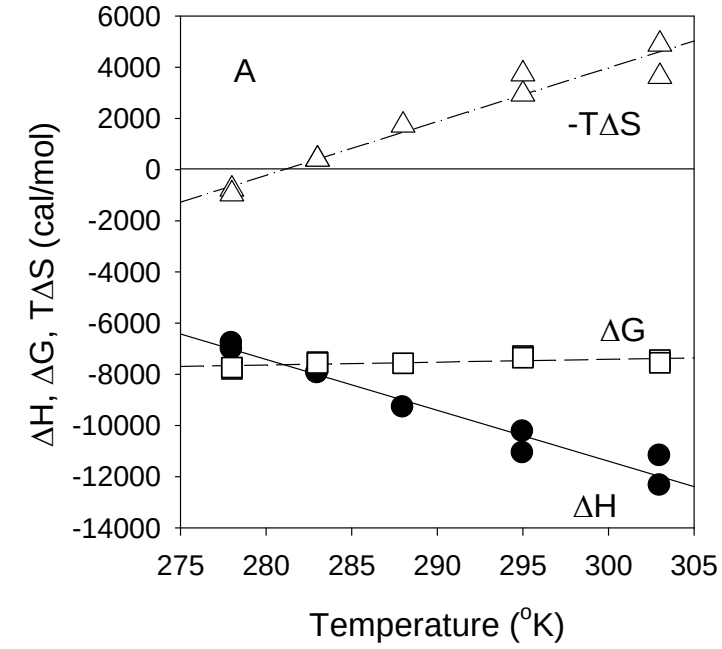
A
-TΔS
ΔG
ΔH
ΔH, ΔG, TΔS (cal/mol)
Temperature (°K)
6000
4000
2000
0
-2000
-4000
-6000
-8000
-10000
-12000
-14000
275
280
285
290
295
300
305

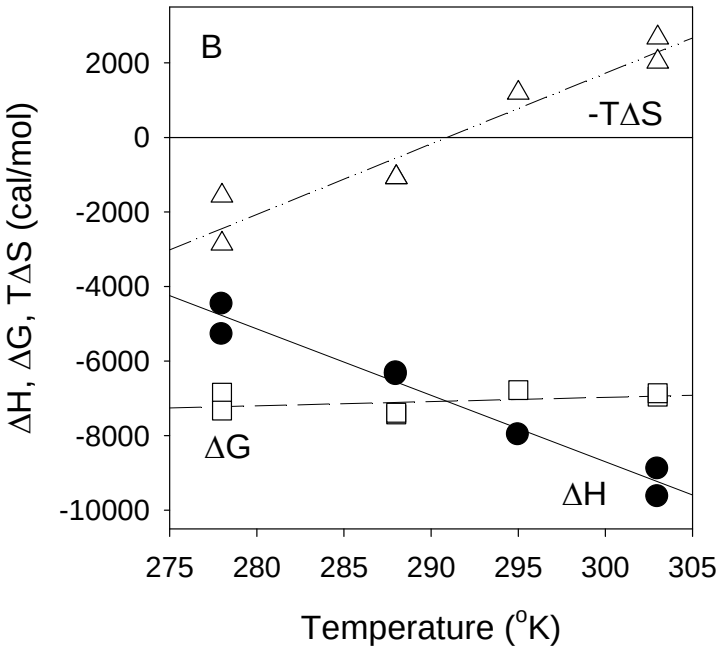
B
-TΔS
ΔG
ΔH
ΔH, ΔG, TΔS (cal/mol)
Temperature (°K)
2000
0
-2000
-4000
-6000
-8000
-10000
275
280
285
290
295
300
305

DHF binding, a heat capacity of -199 ± 16 cal/^{o}K mol was observed. The observed heat capacity change does not involve any contributions from protonation as binding of neither DHF nor NADP(H) involves release or uptake of protons (*64*).

In the case of NADPH, the carboxamide group forms interactions with the backbone NH and O atoms of I68. Also the phosphate groups interact with K32 residue. Similar interactions with N3 and O4 groups of pteridine ring of DHF with the I68 residue are observed. Also the carboxylate group of DHF likely forms ionic interactions with K32. The common modes of interaction of the two ligands may explain the similar values of $\Delta C_{p.}$

Discussion

Water molecules in proteins are present in cavities or molecular interfaces and are also in contact with the protein surface. Of these, solutes are specifically excluded from cavities and interfaces and these aid in determination of the net change in water molecules upon ligand binding (*65-67*). Using a variety of osmolytes possessing different properties, the effects of osmotic pressure on the binding of DHF and NADPH to R67 DHFR was studied. Binding of NADPH involves net release of water, while binding of DHF involves net uptake of water.

Possible factors contributing to different Δn_w observed for DHF binding Analysis of the plot for DHF binding (figure 7) indicated that different osmolytes showed variable slopes, which is in contrast to the single slope obtained for NADPH binding. These variable slopes observed could potentially be the result of the following possibilities:

1) ***Preferential binding of solutes:*** If this scenario has occurred, then the observed change in the number of water molecules taken up may have been overestimated. From equation (8),

Timasheff has proposed that the slope can be generated using different combinations of number for ν_{H2O} and ν_{solute} (assuming that ν_{solute} is a positive value) (*68*). For example, a value of 10 for Δn_w can be generated by $10_{H2O} + 0_{solute}$ or $9_{H2O} + 1_{solute}$ or $5_{H2O} + 5_{solute}$, etc. Conversely, if water molecules were released upon binding, then the number of water molecules may have been underestimated (*68, 69*). From the data presented in table 5, betaine, DMSO and sucrose show higher slopes, suggesting a preferential binding of these osmolytes to the protein. On the other hand, the glycerol, ethylene glycol and TMAO conditions show the lowest slopes, suggesting these osmolytes might be associated with the best estimate of Δn_w.

2) ***Volume exclusion:*** A second possible explanation for variable slopes is crowding or volume exclusion effects, which are due to steric exclusion of solutes from large surfaces (*38, 44, 70, 71*). In the case of R67 DHFR, the maximum radius of the active site pore is 12 Å (*72*). Also, the average radius of gyration of PEG 400 is 8.1 Å (*73*). However, hydration of the PEG causes an increase in the overall radii to 15 Å (depending on the macromolecule studied). Therefore PEGs with larger molecular weights (such as PEG 3350 and PEG 8000) will have a much higher radius of gyration, consequently not allowing the molecule to fit into the active site pore. The high slopes of 78, 145 and 353 observed for PEG400, PEG 3350 and PEG8000 respectively (figure 10 and table 4) seem to suggest volume exclusion or crowding effect. Therefore, these higher molecular weight PEGs cannot be used to estimate the net change in water molecules involved in DHF binding.

3) Overlapping slopes are obtained if water is entrapped in a cavity or a channel (*67*). However, the slopes can vary 2 to 5 fold when a larger surface area is probed because of the difficulty of desolvating large areas (*55, 74*).

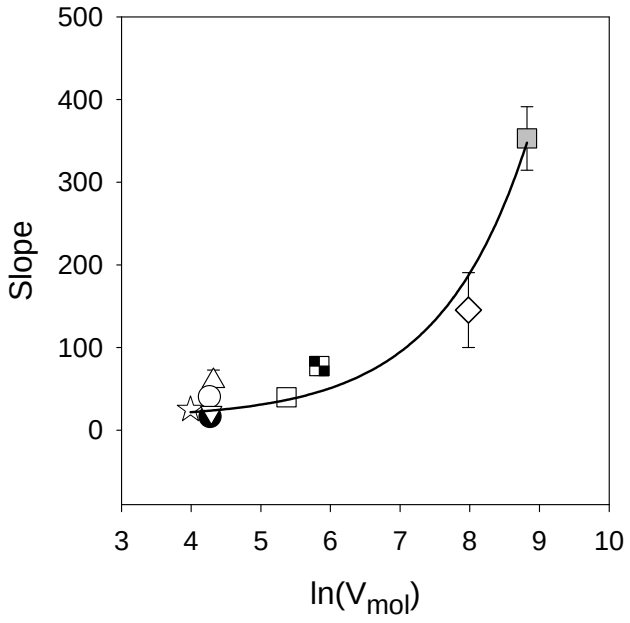

Figure 10: Relationship between molar volume (V_{mol}) and slope of the plot of ln k_{cat} / $K_{m\ (DHF)}$ vs. osmolality The molar volumes for the osmolytes are listed in table X, as are slopes obtained from the plots of ln k_{cat} /$K_{m\ (DHF)}$ vs osmolality. The plot of V_{mol} vs. slope shows data points for the following osmolytes: glycerol (●), ethylene glycol (☆), TMAO (▽), sucrose (□), DMSO (○), glycine betaine (△), PEG400 (◪), PEG3350 (◇) and PEG8000 (▣). From the figure it is evident that the slopes of high molecular weight osmolytes such as PEG 400, PEG3350 and PEG8000 are dependent on V_{mol}, indicating a crowding/ volume exclusion effect.

4) A change in protein conformation upon introduction of osmolytes may also lead to different slopes. However, this seems less likely in the case of R67 DHFR as crystal and NMR structure suggest that the conformation of the protein does not change upon ligand binding (*75, 76*). A recent crystal structure by Krahn et al. shows that there is a small shift in the positions of the Q67 and Y69 residues upon ligand binding (*4*).

Finally, other possible reasons for the different binding behavior of DHF and NADPH in the presence of osmolytes may be due to the properties of the ligands themselves. NADPH prefers binding first and therefore binds to the apo enzyme. In contrast, DHF binds to the enzyme•NADPH complex. Moreover, binding of 2 folate molecules to the apo enzyme also indicate water uptake as shown in figure 7C. This suggests that the binding sequence of the ligands is not responsible for the variation in slopes for DHF binding. Instead, the property of the ligands may be responsible for this.

As can be seen, a number of factors could possibly contribute to variable slopes and their origin is not completely understood.

Protein Hydration and Different Models to Explain the Role of Water in Ligand Binding

Water plays a major role in maintaining protein stability and dynamics. A number of approaches such as thermodynamic analyses and molecular dynamic simulations have been used to study the interplay between water and proteins (*67, 68, 77*). However, understanding of protein stability, folding and protein-ligand interactions at the molecular level of protein hydration is limited due to dearth of suitable techniques. Results obtained form some studies have been summarized briefly as mentioned below:

In order to determine if water molecules present on the surface of a protein are different from that in the bulk solvent, small angle scattering (SAS) of x-rays and neutrons (in H_2O and D_2O) have been performed. Using these techniques on lysozyme as a model protein, Merzel and Smith demonstrated that the first hydration shell (~3Å thick) is 15% denser than bulk water (*78*). These results compared well to results from molecular dynamic simulations, which suggested that the geometry of water molecules around the protein surface contributed to about 75% of the density of the first hydration shell (*79*). Another viewpoint on protein hydration is by Chandler (*80*). According to this model, hydrogen-bonding networks of water near small hydrophobic surfaces result in an increase in the density of water by two (*80*). This results in 'wetting' of the surface. In contrast, larger cavities are 'dewetted' or 'dry' as these cavities cause the hydrogen-bonding network of water to break away.

The solvation of proteins and/ or ligands has also been used to explain the variable slopes obtained for DHF binding to the R67 DHFR•NADP(H) complex. These have been discussed using different models:

Mechanistically, one possible explanation for water uptake may be explained by two phases of water as proposed by Tanaka (*81, 82*). The first phase is an ordered phase and has a lower energy. Ordered water has a tetrahedral configuration in which other molecules do not penetrate, making it less dense (figure 11). The second phase is a more disordered phase and of higher density. This phase describes the bulk phase. In the case of DHF binding, the pABA-glu tail forms intermittent contacts with the K32 residues on either side of the pore (*83, 84*), making the water molecules around it disordered. This may lead to an increase in density of water in the active site as compared to the density of water in the apo enzyme pore, which has highly ordered water

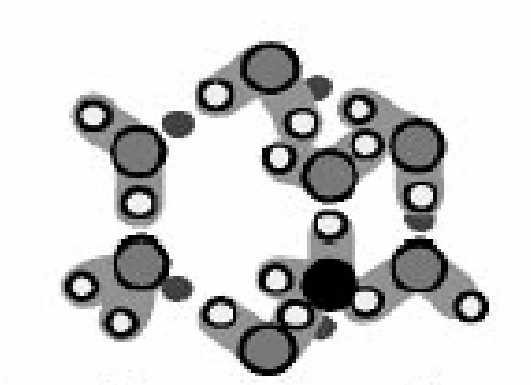

Figure 11: Pentagonal structure of ordered water. Figure taken from Tanaka et al. (*81*). Water molecules have an ordered structure in the less dense phase, while water molecules are disordered in the more dense phase Since the pABA-glutamate tail of DHF is disordered, water may be more dense around this region.

molecules (as shown in a recent crystal structure of the apo enzyme by Narayana) (*9*). As a result, this model may provide a mechanism whereby there is an uptake of water upon DHF binding.

Another model by Sidorova et al. utilizes 'preferential hydration' to explain the interaction of water by protein (*74, 85*). Preferential hydration can be explained as a tendency of proteins to bind water as compared to cosolutes (or osmolytes). Thus, solutes are excluded from protein surfaces (*38, 68, 73*). This exclusion of solutes not only depends on the protein surface, but also depends on the nature of the solutes themselves. According to Sidorova et al., water molecules that are entrapped in cavities, channels or pockets are more associated with the protein surface and would exclude osmolyte. Thus it is relatively straightforward to estimate the net change in number of water molecules (upon ligand binding) on this surface. In contrast to this, water molecules hydrating exposed surfaces are more difficult to remove, resulting in variable effects.

To test this hypothesis, the binding of BamHI binding to specific and non-specific DNA sequences was tested (*85*). When only non-specific DNA sequences were tested, the number of water molecules released upon binding of BamHI was less than that estimated for BamHI binding to specific DNA sequences. In other words, the non-specific DNA-BamHI complex was found to sequester about 120 to 150 more water molecules than the specific complex. Thus the interface between protein and non-specific DNA sequence can accommodate more number of water molecules as compared to that specific DNA-BamHI complex. Additionally, variable slopes were obtained for a plot of binding constant versus osmolality for both specific and non-specific DNA sequences.

When the ratio of specific to non-specific binding constants was measured as a function of osmolality, the net change in water molecules released was determined to be -130 ± 7 water molecules. This number is consistent with results from crystal structure. Using this approach, only a weak dependence on solute nature is observed using 7 different osmolytes. Thus, for estimation of water molecules involved in ligand binding, the type of macromolecular surface also needs to be considered.

The effect of osmolytes on the transition state can also be explained by considering an energy profile diagram (for the case of $[S]<K_m$) (*86*). Since the substrate concentration is much lower than the K_m, the rate of the reaction is determined by the second order rate constant (k_{cat}/K_m), describing $E + S \rightleftharpoons ES^{\ddagger}$. To decrease k_{cat}/K_m, a higher reaction barrier is required. This can be achieved in 2 different ways. The first possibility is that the osmolytes destabilize both the ES and $ES^{\ddagger}$ complexes equally. The ES complex is destabilized since K_m rises upon osmolyte addition. Also, since the k_{cat} does not change in presence of osmolytes, the barrier height for the formation of the transition state must increase by the same amount. This results in the increase of the total height required for the enzyme to reach the transition state (figure 12A). A second possibility is where the enzyme (or substrate) is stabilized by osmolytes in the ground state itself, resulting in a less negative ΔG. Therefore, the barrier height for formation of the transition state is increased (figure 12B).

Molecular dynamic simulations of the ternary complex of R67DHFR•NADPH•DHF suggest that the interaction between the K32 residues and the carboxylate moiety of the glutamate tail of folate may involve both direct and solvent separated ion-pairs (Beahm and Guo, personal communication). From average snapshots along a 2ns trajectory, the tail is mobile and some snapshots show more than one solvent molecule may be mediating the interaction between the K32 residues and the glutamate tail, indicating that possibility more than one hydration

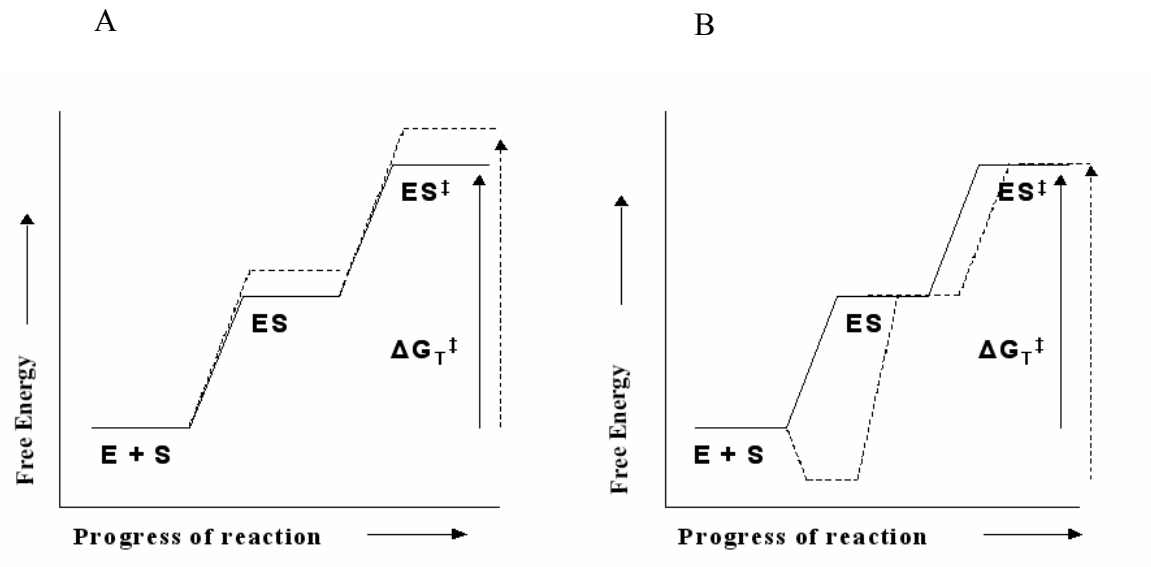

Figure 12: Energy profile diagram describing the effect of osmolytes on the formation of transition state when [S] < K_m. A) Binding of osmolytes results in increase in K_m of the substrate (DHF). This is reflected by an increase in the ΔG required for formation of the ES complex. Since the k_{cat} of the reaction is not affected (and the overall k_{cat}/K_m decreases), the energy required for formation of the transition state $ES^{‡}$ also increases by an equal amount. Therefore, a barrier height from ground state to the transition state increases, which is also reflected by a decrease in catalytic efficiency as concentration of osmolytes in increased. B) Binding of osmolytes causes stabilization of the enzyme, resulting the ΔG of the ground state to be more positive. Therefore more energy is needed to form the ES complex. This would consequently result in an increase in the energy barrier required to reach to transition state ($ES^{‡}$).

shell can be present. Osmolyte studies mostly describe the first hydration shell. As it is unclear how osmolytes can affect additional hydration shells, a greater sensitivity of bound DHF to osmolyte addition may arise. This might be a mechanism whereby destabilization of the ES and $ES^{\ddagger}$ complexes are achieved as depicted in figure 12A.

Another model has been proposed by Dzingeleski and Wolfenden (*87*), according to which solvent molecules interact differently with the protein due to their irregular surfaces. In their study, substrate binding to adenosine deaminase involves an uptake of 9 water molecules. They proposed that the enzyme exists in 2 conformers, one more hydrated than the other. The more hydrated species is the one that binds substrate.

Water + Enzyme $\rightleftharpoons$ Enzyme•9waters + Substrate $\rightleftharpoons$ Enzyme•Substrate•9Waters $\longrightarrow$ Product

This possibility can be represented by figure 12B, where stabilization of the enzyme in the ground state results in a les negative ΔG in the ground state and hence a higher energy barrier to reach the transition state.

Importance of water in the catalytic efficiency *in vivo* Our results from *in vitro* experiments indicate that binding of DHF involves uptake of water. The net change in water molecules taken up varies depending on the osmolyte used. However, the common observation is that there is an uptake of water. *In vivo* experiments using sorbitol demonstrate that water is required for the catalytic efficiency of R67 DHFR. In the cell, R67 DHFR is present in the cytoplasm. The presence of solutes in the cytoplasm may mimic the behavior of osmolytes, causing macromolecular crowding. Additionally, in conditions of osmotic stress, osmolytes may be generated within the cell, leading to further crowding. In this scenario, the binding of NADPH

will be tightened, which may potentially lead to inhibition by 2 NADPH molecules. On the other hand, formation of a binary complex of DHF will be weakened. Therefore, the high solute concentration in the cell may lead to a decreased catalytic efficiency of R67 DHFR, making the enzyme sensitive to the osmolality (*7*).

It is interesting to note that even though a common binding site is available for ligand binding, the mechanism by which the ligands bind is different. Due to the release of water by one ligand and uptake by another, the binding of either ligand is not optimal in the active site pore, which is consistent with low catalytic efficiency of this enzyme.

Burial of Solvent Accessible Surface Various groups have found a correlation between heat capacity and the solvent exposure of non-polar and polar areas of the protein (*33-35*). This information can be obtained by determining the solvent accessible surface areas of the apo enzyme and the ligand bound enzyme. The glutamic acid tail of DHF is disordered when bound to R67 DHFR and hence we are not able to determine the change in solvent accessible surface area for this complex. However, the R67 DHFR•$NADP^+$ complex is available (*12*). Therefore, surface area calculations could be performed for this model. The ΔASA for the formation of the enzyme•$NADP^+$ complex (*4*) (a mimic of the enzyme· NADPH complex) was determined from the following relationship:

$$\Delta ASA = ASA_{E \cdot NADP^+} - (ASA_E + ASA_{NADP+}) \quad (17)$$

where E is the apo enzyme; E•$NADP^+$ is the enzyme•$NADP^+$ complex and $NADP^+$, the ligand only complex. The latter was obtained by removal of $NADP^+$ from the ternary structure.

Using the NMR refine module in Insight II (along with a probe diameter of 1.4 Å for solvent), a change in total solvent accessible surface area of 754 $Å^2$ was calculated. Also using probe radius of 1.3 Å for the solvent, a ΔASA of 657$Å^2$ was calculated. The ΔASA from our experimental data was calculated to be 369 ± 75 $Å^2$ (using the data for release of 38 ± 6 water molecules due to

NADPH binding to the enzyme and assuming the area of water to be 9 ± 1 $Å^2$ (*76*)). This value is lower than the calculated values of 754 $Å^2$ (using probe radius of 1.4 $Å^2$) or 657$Å^2$ (using probe radius of 1.3 $Å^2$). This discrepancy might arise from the different conformations adopted by NADPH; extended when bound and compact when free (*88*). Another possibility is that geometric, cavity or electrostatic effects can cause an ~15% increase in the density of water at a surface as proposed by Merzel and Smith (*79*).

Heat Capacity From the temperature dependence of ΔH, a heat capacity change of –178 cal/^{o}K.mol for binding of NADPH to the apo enzyme has been determined. Additionally, the changes in entropy (ΔS) and Gibbs free energy (ΔG) at different temperatures have been determined. From the plot in figure 8A, it is observed that binding of NADPH to the enzyme is associated with a favorable enthalpy change and a positive (favorable) entropy change until about 281^{o}K. Beyond this temperature, the entropy is unfavorable (more negative) and binding is only enthalpically driven. Also, the change in ΔG is small, which is consistent with enthalpy-entropy compensation (*89, 90*). A small heat capacity change of –199 cal/^{o}K.mol has also been observed for DHF binding to the enzyme•NADPH complex (table 9). As shown in figure 8B, a positive entropic contribution is observed till about 291^{o}K, beyond which the entropy is negative (unfavorable). In addition, the change in ΔG is small. Similar results have been observed for binding of folate to an enzyme•$NADP^+$ complex in the presence of increasing salt concentrations wherein a significant change in ΔH is observed, while not much change is observed in ΔG (*83*). A small change in ΔG as compared to ΔH and TΔS suggests that enthalpy-entropy compensation may be involved in this process. Enthalpy-entropy compensation has been commonly observed in weak binding interactions (*91*). Also, this phenomenon suggests that water may be playing a role in binding reactions (*89, 90*).

Table 9: Comparison of water molecules involved in the DHF and/or NADPH binding and the heat capacity change associated with each binding process.

Ligand	Δn_w	ΔC_p (cal/^{o}K.mol)
DHF binding to enzyme●$NADP^+$	29 ± 3	-199 ± 16
NADPH binding to enzyme (K_{a1})	–38 ± 6	-178 ± 15

A theoretical approach to determine heat capacity is by utilizing the correlation between heat capacity change and changes in solvent accessible polar and non-polar surface areas upon binding. The heat capacity change involving the folding of various proteins as well as the transfer of hydrocarbons and amides from water to pure liquid phase has been characterized using equation 18. However, varying coefficients have been generated by different groups, with the Spolar and Record coefficient being the most commonly used ($C_{nonpolar}$ = 0.32 ± 0.04 and C_{polar} - 0.14 ± 0.04 (*92*)). Using these coefficients results in a positive ΔC_p (10 ± 23). Therefore the coefficients from Robertson and Murphy were used (*93*) and are shown in the equation below:

$$\Delta Cp\ (cal/mol^oK) = (0.16 \pm 0.05)\ \Delta A_{NP} + (0.12 \pm 0.08)\ \Delta A_P \qquad (18)$$

where ΔA_{NP} and ΔA_P describe the change in solvent accessible non-polar and polar areas respectively.

As mentioned, earlier we are only able to perform surface area calculations for the R67 DHFR·$NADP^+$ complex. The access_surf command of the NMR refine module of Insight II was used to calculate non-polar and polar solvent accessible surface areas of -207 $Å^2$ and -547 $Å^2$, respectively. Incorporating these values in the above equation, a heat capacity change of –101 ± 43 cal/ ^oK mol is calculated (error obtained using the online tool: www.colby.edu/chemistry/Pchem/scripts/error.html), which (within error) agrees with the experimentally determined value of -178 ± 15 cal / ^oK mol.

These values of ΔC_p observed are small as compared to those mentioned in the literature (*35*) and hence further analysis was not pursued.

Conclusion

R67 DHFR is a primitive enzyme possessing an unusually large active pore with a volume of 2938 $Å^3$ (as calculated by CASTp) (*8*), which provides a binding site for both DHF and NADPH. Of the two ligands, NADPH prefers binding to the enzyme first, followed by DHF (*5*). Also it forms contacts with the enzyme via its carboxamide moiety and phosphate groups as well as hydrogen bonds and van der Waals contacts, leading to a rigid structure with a fixed conformation (*4*). This agrees with our observations that binding of NADPH is tightened upon release of water. On the contrary, an opposite trend is observed for DHF wherein binding is weakened when water is squeezed out of the pore. In other words, water is required to stabilize DHF in the active site pore. This result can be explained from X-ray crystallography results, which show that the pteridine ring forms fixed contacts with the enzyme, however the pABA-glu tail is disordered (*3, 4, 9*). The change in conformation of the tail may lead to a change in the density of water, consequently resulting in uptake of water. The water present between the ligands may provide more hydrogen bonding contacts providing shape complementarity (*94-98*).

References

(1) Brisson, N., and Hohn, T. (1984) Nucleotide sequence of the dihydrofolate-reductase gene borne by the plasmid R67 and conferring methotrexate resistance. *Gene 28*, 271-274.

(2) Matthews, D. A., Smith, S. L., Baccanari, D. P., Burchall, J. J., Oatley, S. J., and Kraut, J. (1986) Crystal structure of a novel trimethoprim-resistant dihydrofolate reductase specified in Escherichia coli by R-plasmid R67. *Biochemistry 25*, 4194-4204.

(3) Narayana, N., Matthews, D. A., Howell, E. E., and Nguyen-huu, X. (1995) A plasmid-encoded dihydrofolate reductase from trimethoprim-resistant bacteria has a novel D2-symmetric active site. *Nat Struct Biol 2*, 1018-1025.

(4) Krahn, J., Jackson M., DeRose, E.F., Howell, E.E., and London, R.E. (Accepted) Structure of TypeII Dihydrofolate reductase ternary complex: use of identical binding sites for unrelated ligands. *Biochemistry*.

(5) Bradrick, T. D., Beechem, J. M., and Howell, E. E. (1996) Unusual binding stoichiometries and cooperativity are observed during binary and ternary complex formation in the single active pore of R67 dihydrofolate reductase, a D2 symmetric protein. *Biochemistry 35*, 11414-11424.

(6) Howell, E. E., Shukla, U., Hicks, S. N., Smiley, R. D., Kuhn, L. A., and Zavodszky, M. I. (2001) One site fits both: a model for the ternary complex of folate + NADPH in R67 dihydrofolate reductase, a D2 symmetric enzyme. *J. Comput. Aided Mol. Des. 15*, 1035-1052.

(7) Howell, E. E. (2005) Searching sequence space: two different approaches to dihydrofolate reductase catalysis. *ChemBioChem 6*, 590-600.

(8) Liang, J., Edelsbrunner, H., and Woodward, C. (1998) Anatomy of protein pockets and cavities: measurement of binding site geometry and implications for ligand design. *Protein Sci 7*, 1884-1897.

(9) Narayana, N. (2006) High-resolution structure of a plasmid-encoded dihydrofolate reductase: pentagonal network of water molecules in the D2-symmetric active site. *Acta Crystallogr D Biol Crystallogr 62*, 695-706.

(10) Li, D., Levy, L. A., Gabel, S. A., Lebetkin, M. S., DeRose, E. F., Wall, M. J., Howell, E. E., and London, R. E. (2001) Interligand Overhauser effects in type II dihydrofolate reductase. *Biochemistry 40*, 4242-4252.

(11) Brito, R. M., Rudolph, F. B., and Rosevear, P. R. (1991) Conformation of NADP+ bound to a type II dihydrofolate reductase. *Biochemistry 30*, 1461-1469.

(12) Pitcher, W. H., 3rd, DeRose, E. F., Mueller, G. A., Howell, E. E., and London, R. E. (2003) NMR studies of the interaction of a type II dihydrofolate reductase with pyridine nucleotides reveal unexpected phosphatase and reductase activity. *Biochemistry 42*, 11150-11160.

(13) Rand, R. P. (2004) Probing the role of water in protein conformation and function. *Philos Trans R Soc Lond B Biol Sci 359*, 1277-1284; discussion 1284-1275.

(14) Colombo, M. F., and Bonilla-Rodriguez, G. O. (1996) The water effect on allosteric regulation of hemoglobin probed in water/glucose and water/glycine solutions. *J Biol Chem 271*, 4895-4899.

(15) Kornblatt, J. A., and Hoa, G. H. (1990) A nontraditional role for water in the cytochrome c oxidase reaction. *Biochemistry 29*, 9370-9376.

(16) Chopra, S., Lynch, R., Kim, S. H., Jackson, M., and Howell, E. E. (2006) Effects of temperature and viscosity on R67 dihydrofolate reductase catalysis. *Biochemistry 45*, 6596-6605.

(17) Tartof, K., and Hobbs, C. (1987) Improved media for growing plasmid and cosmid clones. *BRL Focus 9* 12.
(18) Gornall, A. G., Bardawill, C. J., and David, M. M. (1949) Determination of serum proteins by means of the biuret reaction. *J. Biol. Chem. 177*, 751-766.
(19) Edsall, C. a. (1943) *Proteins, Amino acids and Peptides as Ions and Dipolar Ions*, Reinhold, New York.
(20) Howell, E. E., Warren, M. S., Booth, C. L., Villafranca, J. E., and Kraut, J. (1987) Construction of an altered proton donation mechanism in *Escherichia coli* dihydrofolate reductase. *Biochemistry 26*, 8591-8598.
(21) Ellis, K. J., and Morrison, J. F. (1982) Buffers of constant ionic strength for studying pH-dependent processes. *Methods Enzymol. 87*, 405-426.
(22) Blakley, R. L. (1960) *Nature 188*, 231-232.
(23) Horecker, B. L., and Kornberg, A. (1948) *Journal of Biological Chemistry 175*, 385-390.
(24) Baccanari, D., Phillips, A., Smith, S., Sinski, D., and Burchall, J. (1975) Purification and properties of *Escherichia coli* dihydrofolate reductase. *Biochemistry 14*, 5267-5273.
(25) Smiley, R. D., Saxton, A. M., Jackson, M. J., Hicks, S. N., Stinnett, L. G., and Howell, E. E. (2004) Nonlinear fitting of bisubstrate enzyme kinetic models using SAS computer software: application to R67 dihydrofolate reductase. *Anal. Biochem. 334*, 204-206.
(26) Smiley, R. D., Stinnett, L. G., Saxton, A. M., and Howell, E. E. (2002) Breaking symmetry: mutations engineered into R67 dihydrofolate reductase, a D2 symmetric homotetramer possessing a single active site pore. *Biochemistry 41*, 15664-15675.
(27) Nichols, R., Weaver, C. D., Eisenstein, E., Blakley, R. L., Appleman, J., Huang, T. H., Huang, F. Y., and Howell, E. E. (1993) Titration of histidine 62 in R67 dihydrofolate reductase is linked to a tetramer to two-dimers equilibrium. *Biochemistry 32*, 1695-1706.
(28) Royer, C. A., Mann, C. J., and Matthews, C. R. (1993) Resolution of the fluorescence equilibrium unfolding profile of trp aporepressor using single tryptophan mutants. *Protein Sci 2*, 1844-1852.
(29) Holland, J. C., Linn, C. E., DiGiammarino, E., Nichols, R., and Howell, E. E. (1993) Does R67 dihydrofolate reductase possess a proton donor? *Adv Exp Med Biol 338*, 493-498.
(30) Sweeney, T. E., and Beuchat, C. A. (1993) Limitations of methods of osmometry: measuring the osmolality of biological fluids. *Am J Physiol 264*, R469-480.
(31) Wyman, J., Jr. (1964) Linked Functions and Reciprocal Effects in Hemoglobin: a Second Look. *Adv Protein Chem 19*, 223-286.
(32) Wiseman, T., Williston, S., Brandts, J. F., and Lin, L. N. (1989) Rapid measurement of binding constants and heats of binding using a new titration calorimeter. *Anal. Biochem. 179*, 131-137.
(33) Prabhu, V., Lui, H., and King, J. (1997) *Arabidopsis* dihydropteroate synthase: general properties and inhibition by reaction product and sulfonamides. *Phytochemistry 45*, 23-27.
(34) Arumugam, S., Gao, G., Patton, B. L., Semenchenko, V., Brew, K., and Van Doren, S. R. (2003) Increased backbone mobility in beta-barrel enhances entropy gain driving binding of N-TIMP-1 to MMP-3. *J Mol Biol 327*, 719-734.
(35) Wright, E., Vincent, J., and Fernandez, E. J. (2007) Thermodynamic characterization of the interaction between CAR-RXR and SRC-1 peptide by isothermal titration calorimetry. *Biochemistry 46*, 862-870.
(36) Sambrook, J., Fritsch, E. F., and Maniatis, T. (1989) *Molecular Cloning: A Laboratory Manual*, Second ed., Cold Spring Harbo Laboratory Press, Cold Spring Harbor.

(37) Park, H., Zhuang, P., Nichols, R., and Howell, E. E. (1997) Mechanistic studies of R67 dihydrofolate reductase. Effects of pH and an H62C mutation. *J Biol Chem 272*, 2252-2258.
(38) Fried, M. G., Stickle, D. F., Smirnakis, K. V., Adams, C., MacDonald, D., and Lu, P. (2002) Role of hydration in the binding of lac repressor to DNA. *J Biol Chem 277*, 50676-50682.
(39) Jelesarov, I., and Bosshard, H. R. (1994) Thermodynamics of ferredoxin binding to ferredoxin:NADP+ reductase and the role of water at the complex interface. *Biochemistry 33*, 13321-13328.
(40) Andersson, B., and Olofsson, G. (1989) Calorimetric study of binary systems of tetraethyleneglycol octylether and polyethyleneglycol with water *J Solution Chemistry 18*, 1019-1035.
(41) Taylor, J. B., and Rowlinson, J. S. (1955) The thermodynamic properties of aqueous solutions of glucose. *Transactions of the Faraday Society 51*, 1183-1192.
(42) Wisniak, J., and Tamir, A. (1978) *Mixing and Excess Thermodynamic Properties*, Elsevier Scientific Publishing Co., New York.
(43) Harries, D., Rau, D. C., and Parsegian, V. A. (2005) Solutes probe hydration in specific association of cyclodextrin and adamantane. *J Am Chem Soc 127*, 2184-2190.
(44) Schellman, J. A. (2003) Protein stability in mixed solvents: a balance of contact interaction and excluded volume. *Biophys J 85*, 108-125.
(45) Larsen, J., Gasser, K., and Hahin, R. (1996) An analysis of dimethylsulfoxide-induced action potential block: a comparative study of DMSO and other aliphatic water soluble solutes. *Toxicol Appl Pharmacol 140*, 296-314.
(46) Vossen, K. M., Wolz, R., Daugherty, M. A., and Fried, M. G. (1997) Role of macromolecular hydration in the binding of the Escherichia coli cyclic AMP receptor to DNA. *Biochemistry 36*, 11640-11647.
(47) Vippagunta, S. R., Wang, Z., Hornung, S., and Krill, S. L. (2007) Factors affecting the formation of eutectic solid dispersions and their dissolution behavior. *J Pharm Sci 96*, 294-304.
(48) Xavier, K. A., Shick, K. A., Smith-Gil, S. J., and Willson, R. C. (1997) Involvement of water molecules in the association of monoclonal antibody HyHEL-5 with bobwhite quail lysozyme. *Biophys J 73*, 2116-2125.
(49) Csonka, L. N. (1982) A third L-proline permease in Salmonella typhimurium which functions in media of elevated osmotic strength. *J Bacteriol 151*, 1433-1443.
(50) Baskakov, I., and Bolen, D. W. (1998) Forcing thermodynamically unfolded proteins to fold. *J Biol Chem 273*, 4831-4834.
(51) Yancey, P. H., Clark, M. E., Hand, S. C., Bowlus, R. D., and Somero, G. N. (1982) Living with water stress: evolution of osmolyte systems. *Science 217*, 1214-1222.
(52) Garner, M. M., and Rau, D. C. (1995) Water release associated with specific binding of gal repressor. *Embo J 14*, 1257-1263.
(53) Cayley, S., and Record, M. T., Jr. (2003) Roles of cytoplasmic osmolytes, water, and crowding in the response of Escherichia coli to osmotic stress: biophysical basis of osmoprotection by glycine betaine. *Biochemistry 42*, 12596-12609.
(54) McLaggan, D., Logan, T. M., Lynn, D. G., and Epstein, W. (1990) Involvement of gamma-glutamyl peptides in osmoadaptation of *Escherichia coli*. *J Bacteriol 172*, 3631-3636.
(55) Baldwin, R. L. (1986) Temperature dependence of the hydrophobic interaction in protein folding. *Proc Natl Acad Sci U S A 83*, 8069-8072.
(56) Wood, J. M. (1999) Osmosensing by bacteria: signals and membrane-based sensors. *Microbiol Mol Biol Rev 63*, 230-262.

(57) Mildvan, A. S., Weber, D. J., and Kuliopulos, A. (1992) Quantitative interpretations of double mutations of enzymes. *Arch Biochem Biophys 294*, 327-340.
(58) Park, H., Bradrick, T. D., and Howell, E. E. (1997) A glutamine 67 to histidine mutation in homotetrameric R67 dihydrofolate reductase results in four mutations per single active site pore and causes substantial substrate and cofactor inhibition. *Protein Eng. Des. Sel. 10*, 1415-1424.
(59) Prabhu, N. V., and Sharp, K. A. (2005) Heat capacity in proteins. *Annu Rev Phys Chem 56*, 521-548.
(60) Ozen, C., Norris, A. L., Land, M. L., Tjioe, E., and Serpersu, E. H. (2007) Detection of Specific Solvent Rearrangement Regions of an Enzyme: NMR and ITC Studies with Aminoglycoside Phosphotransferase(3')-IIIa. *Biochemistry*.
(61) Ladbury, J. E., Wright, J. G., Sturtevant, J. M., and Sigler, P. B. (1994) A thermodynamic study of the trp repressor-operator interaction. *J Mol Biol 238*, 669-681.
(62) Kozlov, A. G., and Lohman, T. M. (2000) Large contributions of coupled protonation equilibria to the observed enthalpy and heat capacity changes for ssDNA binding to Escherichia coli SSB protein. *Proteins Suppl 4*, 8-22.
(63) Jen-Jacobson, L., Engler, L. E., and Jacobson, L. A. (2000) Structural and thermodynamic strategies for site-specific DNA binding proteins. *Structure Fold. Des. 8*, 1015-1023.
(64) Jackson, M., Chopra, S., Smiley, R. D., Maynord, P. O., Rosowsky, A., London, R. E., Levy, L., Kalman, T. I., and Howell, E. E. (2005) Calorimetric studies of ligand binding in R67 dihydrofolate reductase. *Biochemistry 44*, 12420-12433.
(65) Parsegian. (1995) Macromolecules and water: probing with osmotic stress. *Methods in Enzymology 259*, 43-94.
(66) Parsegian, V. A., Rand, R. P., Fuller, N. L., and Rau, D. C. (1986) Osmotic stress for the direct measurement of intermolecular forces. *Methods Enzymol 127*, 400-416.
(67) Parsegian, V. A., Rand, R. P., and Rau, D. C. (2000) Osmotic stress, crowding, preferential hydration, and binding: A comparison of perspectives. *Proc Natl Acad Sci U S A 97*, 3987-3992.
(68) Timasheff, S. N. (2002) Protein-solvent preferential interactions, protein hydration, and the modulation of biochemical reactions by solvent components. *Proc Natl Acad Sci U S A 99*, 9721-9726.
(69) Courtenay, E. S., Capp, M. W., Anderson, C. F., and Record, M. T., Jr. (2000) Vapor pressure osmometry studies of osmolyte-protein interactions: implications for the action of osmoprotectants in vivo and for the interpretation of "osmotic stress" experiments in vitro. *Biochemistry 39*, 4455-4471.
(70) Minton, A. P., and Wilf, J. (1981) Effect of macromolecular crowding upon the structure and function of an enzyme: glyceraldehyde-3-phosphate dehydrogenase. *Biochemistry 20*, 4821-4826.
(71) Schurr, J. M., Rangel, D. P., and Aragon, S. R. (2005) A contribution to the theory of preferential interaction coefficients. *Biophys J 89*, 2258-2276.
(72) Narayana, N., Matthews, D. A., Howell, E. E., and Nguyen-huu, X. (1995) A plasmid-encoded dihydrofolate reductase from trimethoprim-resistant bacteria has a novel D2-symmetric active site. *Nat. Struct. Biol. 2*, 1018-1025.
(73) Bhat, R., and Timasheff, S. N. (1992) Steric exclusion is the principal source of the preferential hydration of proteins in the presence of polyethylene glycols. *Protein Sci 1*, 1133-1143.
(74) Sidorova, N. Y., and Rau, D. C. (2004) Differences between EcoRI nonspecific and "star" sequence complexes revealed by osmotic stress. *Biophys J 87*, 2564-2576.

(75) Saunders, A. J., Davis-Searles, P. R., Allen, D. L., Pielak, G. J., and Erie, D. A. (2000) Osmolyte-induced changes in protein conformational equilibria. *Biopolymers 53*, 293-307.
(76) Fried. (2002) *Journal of Biological Chemistry 277*, 50676-50682.
(77) Bennion, B. J., and Daggett, V. (2003) The molecular basis for the chemical denaturation of proteins by urea. *Proc Natl Acad Sci U S A 100*, 5142-5147.
(78) Svergun, D. I., Richard, S., Koch, M. H., Sayers, Z., Kuprin, S., and Zaccai, G. (1998) Protein hydration in solution: experimental observation by x-ray and neutron scattering. *Proc Natl Acad Sci U S A 95*, 2267-2272.
(79) Merzel, F., and Smith, J. C. (2002) Is the first hydration shell of lysozyme of higher density than bulk water? *Proc Natl Acad Sci U S A 99*, 5378-5383.
(80) Chandler, D. (2005) Interfaces and the driving force of hydrophobic assembly. *Nature 437*, 640-647.
(81) Tanaka, H. (2000) Simple physical model of liquid water. J Chem Phys 112, 799-809 (2000). Simple physical explanation of the unusual thermodynamic behavior of liquid water. Phys Rev Letts 80, 57. *J Chem Phys 112*, 799-809.
(82) Tanaka, H. (1998) Simple physical explanation of the unusual thermodynamic behavior of liquid water. *Phys Rev Letts 80*, 5750-5753.
(83) Hicks, S. N., Smiley, R. D., Hamilton, J. B., and Howell, E. E. (2003) Role of ionic interactions in ligand binding and catalysis of R67 dihydrofolate reductase. *Biochemistry 42*, 10569-10578.
(84) Hicks, S. N., Smiley, R. D., Stinnett, L. G., Minor, K. H., and Howell, E. E. (2004) Role of Lys-32 residues in R67 dihydrofolate reductase probed by asymmetric mutations. *J. Biol. Chem. 279*, 46995-47002.
(85) Sidorova, N. Y., Muradymov, S., and Rau, D. C. (2006) Differences in hydration coupled to specific and nonspecific competitive binding and to specific DNA Binding of the restriction endonuclease BamHI. *J Biol Chem 281*, 35656-35666.
(86) Fersht, A. (1985) *Enyzme Structure and Mechanism*, W.H. Freeman and Company, New York.
(87) Dzingeleski, G. D., and Wolfenden, R. (1993) Hypersensitivity of an enzyme reaction to solvent water. *Biochemistry 32*, 9143-9147.
(88) Smith, P. E., and Tanner, J. J. (2000) Conformations of nicotinamide adenine dinucleotide (NAD(+)) in various environments. *J Mol Recognit 13*, 27-34.
(89) Cooper, A. (2005) Heat capacity effects in protein folding and ligand binding: a re-evaluation of the role of water in biomolecular thermodynamics. *Biophys Chem 115*, 89-97.
(90) Holdgate, G. A., Tunnicliffe, A., Ward, W. H., Weston, S. A., Rosenbrock, G., Barth, P. T., Taylor, I. W., Pauptit, R. A., and Timms, D. (1997) The entropic penalty of ordered water accounts for weaker binding of the antibiotic novobiocin to a resistant mutant of DNA gyrase: a thermodynamic and crystallographic study. *Biochemistry 36*, 9663-9673.
(91) Dunitz, J. D. (1995) Win some, lose some: enthalpy-entropy compensation in weak intermolecular interactions. *Chem Biol 2*, 709-712.
(92) Spolar, R. S., and Record, M. T., Jr. (1994) Coupling of local folding to site-specific binding of proteins to DNA. *Science 263*, 777-784.
(93) Robertson, A. D., and Murphy, K. P. (1997) Protein Structure and the Energetics of Protein Stability. *Chem Rev 97*, 1251-1268.
(94) Ladbury, J. E. (1996) Just add water! The effect of water on the specificity of protein-ligand binding sites and its potential application to drug design. *Chem Biol 3*, 973-980.
(95) Quiocho, F. A., Wilson, D. K., and Vyas, N. K. (1989) Substrate specificity and affinity of a protein modulated by bound water molecules. *Nature 340*, 404-407.

(96) Petrone, P. M., and Garcia, A. E. (2004) MHC-peptide binding is assisted by bound water molecules. *J Mol Biol 338*, 419-435.
(97) Levy, Y., and Onuchic, J. N. (2006) Water mediation in protein folding and molecular recognition. *Annu. Rev. Biophys. Biomol. Struct. 35*, 389-415.
(98) Sleigh, S. H., Seavers, P. R., Wilkinson, A. J., Ladbury, J. E., and Tame, J. R. (1999) Crystallographic and calorimetric analysis of peptide binding to OppA protein. *J Mol Biol 291*, 393-415.

Part IV: Conclusions And Future Objectives

Introduction

R67 DHFR is a homotetrameric enzyme possessing 222 symmetry in its active site pore. The active site is 25 Å long and 18 Å wide and it binds to both DHF and NADPH to facilitate catalysis. The substrate (DHF) and cofactor (NADPH) enter from opposite sides of the pore and assume an *endo* geometry to facilitate hydride transfer from the C4 of the nicotinamide ring to the C6 position of the pteridine ring (*1*). Site directed mutagenesis studies have been used to identify critical residues involved in ligand binding (*2-5*). Also, analogs of substrate and cofactor have been utilized to determine the critical regions on the substrate and cofactor that are important for binding (*6*). However, information on the ground state and transition state in the R67 DHFR reaction is lacking. The research presented and discussed in this thesis addresses these issues in more detail. Additionally, our research conducts an investigation into the role of water molecules in the ligand binding.

Interactions Formed By NADPH And DHF With The Protein

The ligands enter the pore and the carboxamide group of NADPH and the N3-O4 atoms of folate help position the substrate and cofactor for hydride transfer (*6*). The pteridine ring of folate is in a fixed position, while the tail regions are mobile. MD simulations predict that the tail forms intermittent contacts with the K32 residues (Robert Beahm and Hong Guo, personal communication). Mutagenesis and salt dependence studies also show that the interactions of the folate tail with the K32 residues are important (*4, 7*). Another approach to determine the importance of the tail is to use folate analogs with shorter tails. Two different truncated species have been used: 1) dihydrobiopterin (lacking the pABA-glu tail) and 2) dihydropteroic acid (lacking only the glutamate tail) (*6*). ITC binding studies and K_i studies show that removal of these groups weakens binding indicating these moieties provide important interactions. Also,

removal of these groups result in reduced binding enthalpies. Therefore, the charged groups on folate likely contribute to the binding enthalpy. Other studies in which the length of the glutamate tail is increased by polyglutamylation suggest that binding is not improved by increasing the negative charge on the substrate (*6*). Overall, results using folate and NADPH analogs suggest that two common features of the substrate and cofactor, i.e. the negative charge in the tail and the (N-C=O) groups in the head of the molecule, are essential for binding to the symmetric active site of R67 DHFR.

Thermodynamics Of Ligand Binding In The Ground And Transition States

The goal of chapter 2 was to shed light on the energetics of ligand binding in the ground state and transition state. By determining k_{cat} and k_{cat}/K_m for the DHFR reaction at different temperatures, both van't Hoff and Arrhenius plots were obtained and the activation energy of substrate binding in the ground state and transition state were calculated (*8*). From this, the change in enthalpy was also obtained. Additionally the entropy and free energy of substrate binding in both the ground state and transition state were calculated. Results indicated that the ΔH is more negative in the ground state than the transition state. A second observation was that the $T\Delta S$ associated with ground state was –5.4 kcal/mol. This value of $T\Delta S$ is less negative as compared to the $T\Delta S$ in the transition state (-11.3 kcal/mol), consistent with a reorientation of the substrate in the transition state.

Importance Of The Glutamate Tail Of DHF In Binding And Catalysis

Dihydropteroate (DHP), an analog of DHF, lacks the glutamate tail. As compared to DHF, DHP has only a single negative charge. The K_i of DHP is ~25 μM and the ternary complex K_d is 20μM (*6*). Therefore, loss of the glutamate tail results in weaker binding. Additionally, k_{cat} of the

DHFR reaction using DHP as a substrate showed an approximately 1600 fold reduction in k_{cat} as compared to DHF reduction (*8*). This suggested that the pABA glu tail is important in interacting with the K32 residue and consequently for correctly positioning the substrate in the active site.

Role Of Water In Ligand Binding In R67 DHFR

The active site pore of R67 DHFR is large with a volume of 2938 $Å^3$ (as calculated by CASTp) (*9, 10*). Water molecules have also been observed in the apo and ternary complex crystal structures of R67 DHFR (*11, 12*). Therefore, the ligands (DHF and NADPH) are not able to occupy the entire space in the pore and water must fill the remaining space. Figure 1 illustrates water molecules in the ternary complex structure of R67 DHFR•DHF•NADP(H).

To further probe the role of water in ligand binding and catalysis in R67 DHFR, osmolytes such as sucrose, betaine, DMSO, TMAO, ethylene glycol and glycerol were employed. It was observed that as the osmolyte concentration increased (i.e. osmotic pressure was increased), the K_m and/or K_d of NADPH decreased (based on results from kinetics and ITC experiments) (Chopra et al., manuscript submitted). This suggested that binding of NADPH is tightened upon release of water. Using this approach, the net change in number of water molecules (Δn_w) upon NADPH binding was estimated to be –38 ± 6 water molecules. Similarly, increasing concentrations of osmolytes were used to determine the effect on DHF binding. An opposite effect was observed, in which the binding of DHF weakened as the water concentration was decreased due to addition of osmolytes. Overall, the DHF data suggest that water uptake is required to stabilize DHF in the active site. Thus, osmolyte studies indicate that NADPH interacts with the protein through more direct contacts (via a 'dry' surface) as proposed by Janin (*13*) , while interactions of DHF with the protein are mediated by water molecules (using a 'wet' surface).

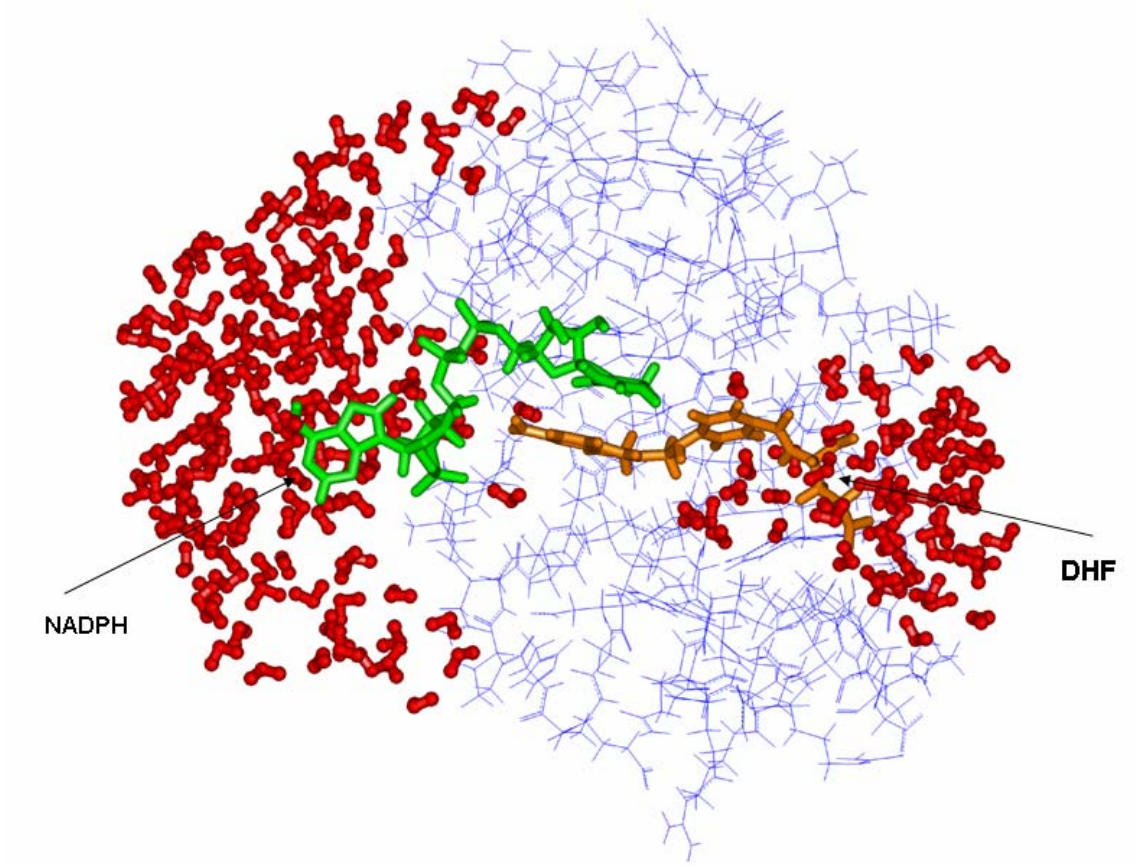

Figure 1: Water molecules in the ternary structure of R67 DHFR. The crystal structure of R67 DHFR with bound folate and $NADP^+$ was used as a template (Joe Krahn and Bob London; manuscript accepted) (*12*). Hydrogens were added to all residues and the bound folate was reduced to the protonated form of DHF using molecular modeling. Using a similar approach, the bound $NADP^+$ was converted to NADPH. A 5ns molecular dynamic simulation was then carried out and the resultant structure is shown with water molecules. DHF and NADPH are shown in orange and green respectively and half slice of the protein backbone is represented in blue. Water molecules around each ligand are represented in red.

Net uptake of water molecules was variable, depending on osmolyte identity and the observed range was 16 to 70 water molecules. This variation in the determination of Δn_w is usually attributed to several factors such as volume exclusion, preferential binding or preferential exclusion. *In vivo* experiments using media containing increasing concentrations of sorbitol as an osmolyte showed that the growth of *E.coli* containing wild type R67 DHFR and its mutant clones was arrested. This also indicated that water is required for substrate binding by R67 DHFR and can be considered a co-substrate. Therefore involvement of water in both DHF and NADPH binding suggests that water may provide shape complementarity upon binding of ligands.

As described in chapter 3, various models can perhaps explain the different sensitivities of NADPH and DHF binding to osmolytes. These models are based on the hydration of the protein and/or ligand, as well as on the density of the hydration shell.

One model proposed by Tanaka suggests that H_2O can be present in two phases (*14*). The first phase is an ordered phase, which other molecules do not penetrate, thereby making it less dense. The second phase is a more disordered phase and of higher density. In the case of R67 DHFR, uptake of water by DHF binding to the enzyme can possibly be explained by the Tanaka model. Prior to binding, water molecules in the enzyme active site are highly ordered (as shown in a recent crystal structure of the apo enzyme by Narayana) (*11*). When DHF binds to R67 DHFR, the mobile pABA-glu tail forms intermittent contacts with the K32 residues on either side of the pore (*4, 7*) resulting in a disordering of local water molecules. This may lead to an increase in density of water in the active site as compared to the density of ordered water in the apo enzyme pore. As a result, there is an uptake of water upon DHF binding.

Another model proposed by Dashnau et al. (*15, 16*) and Sidorova et al. (*15, 16*) suggests that variations in hydration of ligands can explain the differences in NADPH and DHF binding upon addition of osmolytes. Sidorova et al also proposed that water molecules can get sequestered in cavities or channels associated with the protein surface and are difficult to remove. Thus determination of the net change in water molecules is much easier on such surfaces as compared to exposed surfaces (*16, 17*).

A third possibility proposed by Bennion et al. and Beck et al. is that different hydration levels of the protein may be contributing to the differences in solvation induced by osmolytes (*18, 19*). Dzingeleski and Wolfenden proposed that there is a equilibrium between the hydrated and dehydrated forms of the protein. For some proteins, the hydrated form is more favorable for formation of the enzyme-substrate complex. Energetically, this can be explained as the stabilization of the enzyme by water and hence the requirement of more energy to reach the transition state.

Finally, it is also possible that more that one hydration layer is present between the glutamate tail and the K32 residue of the protein. Since osmolyte studies mainly describe the first hydration shell, it is possible that the bound DHF is more sensitive to osmolyte addition. From the energetic point of view, the formation of the enzyme-substrate complex would require more energy. This would result in an increase in the energy required for the formation of the transition state by the same amount (as k_{cat} of the reaction is not affected) and a consequent increase in the total barrier height to go from the ground state to the transition state.

As we can see, a number of different models can be invoked to explain binding of ligands to R67 DHFR. A stepwise analysis of each model may help evaluate the differences on NADPH and

DHF binding to R67 DHFR. Therefore, to obtain a clearer picture on the role of water in ligand binding to R67 DHFR, further experiments should be considered. For example:

1. ***Determination of ligand solvation:*** The difference in solvation of Bovine serum albumin (BSA) (upon osmolyte addition) has been investigated by Courtenay et al (*20*). A plot of osmolality (of particular osmolyte/ cosolute) versus concentration of the osmolyte was studied. This data was then compared to plot of buffer osmolality (without osmolyte) versus osmolyte concentration. The difference in the slopes of the two plots will indicate the degree of exclusion of the osmolyte from the protein. A similar approach can also be used in the case of R67 DHFR to determine the solvation of ligands (DHF and NADPH) in presence of different osmolytes. These studies may therefore explain if any differences in ligand solvation (upon osmolyte addition) are responsible for the different binding behavior of DHF and NADPH.

2. ***Evaluation of osmolyte addition with the Q67H mutant:*** Addition of osmolytes to wild type enzyme resulted in weaker binding of DHF and a tighter binding of NADPH. The Q67H mutant exhibits a 110 fold lower $K_{m(NADPH)}$ and a 36 fold lower $K_{m(DHF)}$ as compared to the wild type enzyme (*5*). In addition to a slight increase in catalytic efficiency, this mutant also has substrate and cofactor inhibition. Therefore, if osmolytes are used to study the binding of DHF to this mutant, we would predict a weakening of DHF binding as well as a decrease in DHF inhibition. Further, since addition of osmolytes tightens NADPH binding, we may expect to see very tight binding of NADPH to the Q67H mutant upon addition of osmolytes. Furthermore, we may also observe an increased level of cofactor inhibition as the concentration of osmolytes is increased. This

experiment could help support our findings that binding of DHF involves uptake of water, while binding of NADPH is associated with release of water.

Heat Capacity Changes For DHF And NADPH Binding?

The energetics of ligand binding to R67 DHFR was also evaluated at different temperatures. The data obtained were used to determine the heat capacity of the system ($\Delta C_p = \partial\Delta H/\partial T$). This parameter can provide information on the exposure/ burial of solvent accessible areas in the protein, protonation, conformational change, changes in internal vibrations or solvent reorganization during a binding reaction.

Using ITC, the enthalpy change for the binding of DHF and/or NADPH to R67 DHFR was determined at different temperatures (5^{o}C to 30^{o}C). The heat capacity for DHF binding (to form a ternary complex of DHF•$NADP^{+}$•enzyme) was found to be –199 cal/mol^{o}K, while the heat capacity for NADPH binding to form E·NADPH is –177 cal/mol^{o}K. These values for heat capacity are much smaller than those usually observed (in the range of -1000 cal/mol^{o}K). Also, the question that arises is: *What contributes to the heat capacity for DHF and NADPH binding?* Since several factors may be contributing to the observed heat capacity, these possibilities may need to be evaluated as described below:

1. ***Heat Capacity studies using analogs of DHF:*** In the case of DHF binding, there is a possibility that the interaction of the glutamate tail of DHF with the K32 residue of the enzyme may be contributing to the observed enthalpy of –13.3 kcal at 25^{o}C (chapter 2, (*8*)). When DHP (analog of DHF lacking the glutamate tail) is used as a substrate, the enthalpy change was decreased (-9.5 kcal) (*8*). This suggested that the glutamate tail was

contributing to the more negative enthalpy. Therefore, it would be interesting to determine the heat capacity change for binding of DHP to enzyme•NADPH complex. If a lower heat capacity is obtained, it will suggest that interactions of the glutamate tail of DHF with the K32 residues on the protein or restructuring of water molecules around the pABA-glu tail of the ligand are contributing to the heat capacity.

2. ***Contribution to Heat Capacity from Solvent Reorganization:*** Various examples can be seen in the literature where the contribution of heat capacity upon ligand binding is due to reorganization of water. For example Chervenak and Toone studied the thermodynamics of association of different systems such as protein-carbohydrate, protein-peptide, protein-nucleic acid and small molecule-small molecule interactions in both H_2O and D_2O (*21*). They observed that in each interaction the enthalpy of binding in D_2O was decreased relative to H_2O, with $\Delta\Delta H$ ranging from 0.4 to 1.8 kcal/mol. This experiment was performed at different temperatures and a linear relationship between the $\Delta\Delta H$ observed for binding in H_2O and D_2O suggested that solvent reorganization is responsible for part to all of the observed heat capacity change.

In R67 DHFR, osmolyte experiments have shown that water is involved in ligand binding. Also, results from earlier experiments indirectly suggest that water molecules in R67 DHFR may be providing some of the binding enthalpy. For example, a study was performed by Hicks et al., in which folate was titrated into an enzyme•NADPH mixture in the presence of various concentrations of NaCl (*4*). A titration in enthalpy was observed, but no change was observed in ΔG. This strongly suggested that water may be involved. Recently, experiments performed by Feng and Howell (manuscript accepted) also show similar results. In brief, the experiment involved titration of DHF into a

mixture of $NADP^+$ and a Q67H: 1+2+3+4 plus K32M: 1+3 mutant. It was surprising to see no significant change in the enthalpy as mutation of K32 to methionine has removed the possibility of an ionic interaction with the glutamate tail of DHF. This again supports the earlier observation that solvent molecules and/ or ring stacking could be contributing to the binding enthalpy.

To investigate this, a similar approach (as used by Chervenak and Toone) can be taken in R67 DHFR where enthalpy binding is monitored in D_2O as well as H_2O. However, before performing such experiments one assumption that needs to be made is that neither the protein nor the protein-ligand complex change conformation in the presence of H_2O or D_2O.

3. ***Molecular Dynamic Simulations:*** MD simulation is a powerful tool for monitoring binding and catalytic events. Using a suitable model, a time series of structures and their trajectories can be examined to look for clues as to what is occurring in solution experiments. In the case of ligand binding to enzyme, MD simulations provide a window for observing the conformations of enzyme that are most conducive to ligand binding. For example, MD simulations have been performed in the case of pig heart lactate dehydrogenase (LDH) to explore the variation in enzyme structure upon binding of the substrate and cofactor (*22*). Solvated binary (enzyme + cofactor) and ternary (enzyme + substrate + cofactor) complexes were studied using 2.48 ns simulations. Results obtained indicated both open and closed conformations, which suggested subtle protein and water rearrangements. Additionally, a large ΔC_p was observed that could be attributed to rearrangements taking place for ligand binding into the deep binding pocket of the protein.

MD simulations also have been carried starting with the R67 DHFR•folate•$NADP^+$ structure (Beahm and Guo, personal communication). The folate was reduced to DHF *in silico* and to this, a proton was added to the N5 position to obtain HDHF (using the parameters by Garcia-Vilocia) (*23*). Similarly, $NADP^+$ was changed to NADPH. The resultant R67 DHFR•HDHF•NADPH complex was then solvated and energy minimizations were performed to obtain a stable structure. A set of atoms was treated by the quantum mechanics (QM) approach, while the rest of the molecule was treated by a molecular mechanics (MM) force field. An umbrella sampling method (*24*) (used in CHARMM) (*25*) along with the weighted histogram analysis method (WHAM) (*26*) can help determine changes in free energy (potential of mean force) for the hydride transfer step. Therefore, this structure can be used to help determine the involvement of water molecules in ligand binding in R67 DHFR. Simulations using the binary complex of enzyme•NADPH as well as the ternary complex of enzyme•HDHF•NADPH could provide a clue on the role of water molecules in the binding of NADPH and DHF respectively.

Is There A Direct Interaction Between K32 Or K33 Residues With Folate?

X-ray and NMR studies indicate that the pABA-glu tail of DHF is disordered (*11, 27, 28*). Additionally, docking of DHF and molecular dynamic simulations (personal communication, Robert Beahm and Hong Guo) also predict the pABA-glu tail is mobile and can have transient interactions with symmetry related K32 residues on either side of the pore. Mutagenesis and salt effect studies have also suggested that the carboxylate residues on the glutamate tail of the substrate dihydrofolate can interact ionically with the lysine residue(s) (*4*). There is no direct evidence that the interaction involves K32 or (even possibly K33). Additionally, whether this

interaction is an ionic interaction and/ or a solvent separated ion pair (SSIP) is not well understood. Knowledge of these interactions is essential as enzyme efficiency is usually correlated with the correct positioning of the substrate in the ground state (*6, 8*).

One approach to investigate whether a direct interaction occurs between K32 and the glutamate tail of folate would be to chemically crosslink folate with the enzyme. Once crosslinked, the amino acid residue participating in the crosslink could be identified. These studies are currently being undertaken in the laboratory using a zero length crosslinker, EDC (1-ethyl-3- (3-dimethylaminopropyl) carbodiimide). This compound links the primary amine group to form an acylisourea intermediate, which then targets the carboxylic acid group (*29*). The primary amine groups that can be targeted in R67 DHFR are the K32, K33 residues and the N-terminus. Since the N-terminus can be deleted without any loss of activity and does not play any role in ligand binding, N-terminal truncated R67 DHFR can be generated after crosslinking to show involvement of the N-terminus. The crosslinking between the K32 residue and folate or between the K33 residue and folate can potentially be determined using mass-finger printing analysis or by sequencing the amino acids using Edman degradation.

These experiments will help evaluate if direct ionic interactions can form between the amino group of lysine and the carboxylate group of the folate. Alternatively, crosslinking experiments can be performed with the K33M mutant of R67 DHFR. If crosslinking of folate is observed, it will indirectly indicate that folate interacts with the K32 residue.

Stoichiometry Of Binding Of Folate To R67 DHFR

An advantage of the crosslinking experiments is that the number of folates crosslinked to the enzyme can also be determined. One method would be to incorporate radiolabeled folate (^{3}H or ^{14}C) during the crosslinking reaction with DHFR. The amount of folate crosslinked to the protein can then be determined on the basis of the radioactivity count. In summary, our preliminary crosslinking studies strongly suggest that there is an interaction between folate and K32, which is (at least part of the time), direct in nature. These studies combined with mass spectrometry can provide valuable information on the specific interaction of the glutamate tail with the lysine residue of R67 DHFR and also the stoichiometry of folate binding in a binary complex.

Future Experiments To Understand The Structure-Function Of The Glutamate Tail Of Dihydrofolate

The crystal structure of R67 DHFR bound to folate is available and provides information on the orientation of the pteridine ring (*27*). However, no electron density is observed for the pABA-glutamate moiety of folate, indicating that the tail is disordered. Another crystal structure by Krahn et al is also available that contains $NADP^{+}$ and DHF bound to the enzyme (*12*). This structure proposes that the cofactor forms hydrogen bonds with the backbone atoms of symmetry related I68 residues via a carboxamide group, while the N3 and O4 atoms of the substrate form interactions with I68 residues. Results from NMR studies also provide information on the residues involved in ligand binding. Information on how ligands bind is also available from ligand binding studies using the various analogs of folate and NADPH (*6*). However, certain features of ligand binding are not completely understood. We will discuss these aspects with a possible approach to understanding them as described below:

1. NADPH bound to R67 DHFR possesses a *syn* conformation between the nicotinamide and ribose rings, which is in contrast to the orientation observed for all other reductases. Therefore, it would be interesting to perform MD simulations of the cofactor with the nicotinamide ring and ribose rings locked in an *anti* conformation (when bound to the enzyme) and the energetics of binding can be determined.
2. Results from X-ray crystallography, NMR and MD simulations suggest that the pABA-glu tail is disordered. Also, the glutamate moiety of the pABA glu tail is present in the L-conformation. Therefore, it would be interesting to investigate if replacing the L-form of glutamate with the D-form has any effect on the binding of DHF. Additionally, MD simulations with the modified substrate can also be performed to determine the contact made by this substrate versus the natural substrate with the glutamate tail in the L-form.
3. Another experiment that can be performed with the glutamate tail is to decrease the length of the tail, while maintaining the total charge of -2. This can be achieved by using an analog in which the glutamate is replaced by aspartate. Evaluation of the binding properties of this substrate as well as effect on enzyme catalysis would provide information on the importance of the length of the pABA glu tail for binding and catalysis.

Importance Of The Carboxylate Moieties Of Glutamate In DHF Binding And Catalysis

The glutamic acid tail of DHF possesses two carboxylate moieties and R67 DHFR possesses 2 lysines in or near the active site pore (K32 and K33) on each monomer. Docking, molecular dynamic simulations, crystal structure analysis, salt effect and mutagenesis studies have proposed K32 is the important contact for binding and K33 helps establish a positive electrostatic potential

that aids binding (*30*). Inhibition studies using folate-histidine and folate-ornithine show minimal effects on the K_i of folate, suggesting that the α-carboxylate moiety of the glutamic acid tail of folate may be important in interacting with the lysine residue(s) (6). On the other hand, molecular dynamic simulations predict that both the carboxylate moieties form intermittent contacts with the lysine residues (Robert Beahm and Hong Guo, personal communication) (figure 2). Another avenue for investigating how the DHF tail interacts with R67 DHFR is to utilize folate derivatives. Folate can be modified at either the α- or the γ-carboxylate positions by various amines such as a non-charged molecule of methylamine (MA). The resultant modified folates would therefore include singly modified folates as well as doubly modified folates. Of these, the singly modified folate would include two isomers: one in which the α-carboxylate position of glutamic acid is conjugated to MA and the other in which the γ-carboxylate position of the glutamic acid is conjugated to MA (*31*). The three different species of modified can be identified and separated (from each other and the unmodified folate) on the basis of their pK_as using ion exchange chromatography. The effect of these isoforms on the binding and catalysis of R67 DHFR can then be monitored using kinetics. Specifically, K_i experiments will help determine if one carboxylate group is more critical than the other in forming interactions with the lysine residue. The singly modified folates can further be reduced to their respective dihydro forms and used as substrates to determine the K_m and k_{cat} of the reaction.

In contrast to the singly modified folate, the doubly modified will be devoid of any negative charge on the glutamic acid tail. This should result in decreased interactions with the lysine residues on the protein leading to weaker binding of the substrate. As discussed earlier, the Q67H: 1+2+3+4 K32M: 1+3 asymmetric multimutant (Feng and Howell, manuscript accepted) shows tighter binding of DHF as compared to the parent K32M: 1+3 asymmetric mutant. Even though, lysine 32 residues (in gene copies 1 and 3) are no longer present to form contacts with DHF, the Q67H mutation allows

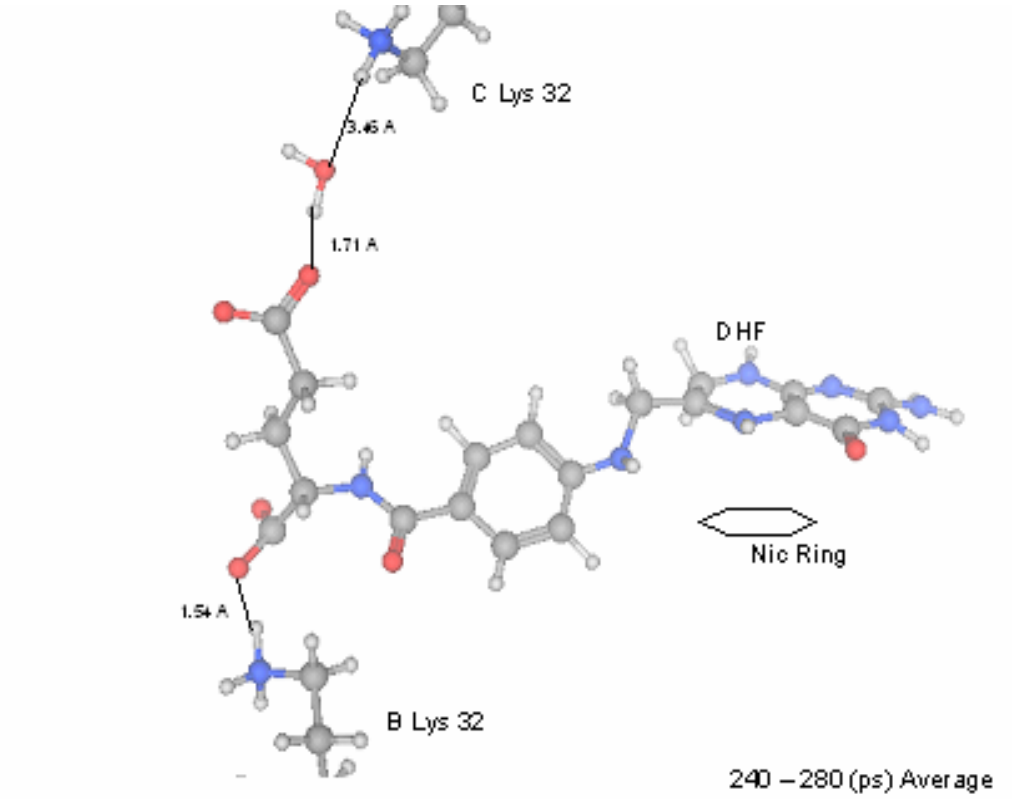

Figure 2: Molecular dynamic simulation describing the interaction of the glutamate tail of dihydrofolate with lysine residues from different monomers. A snapshot at 240-280 pico seconds is shown wherein the α and γ carboxylate groups of the glutamate tail of DHF form contacts with the lysine 32 residues of monomer B and C of R67 DHFR. The distance between the α- carboxylate group and lysine 32 (of monomer B) is 1.54Å. On the other hand, the distance between the γ-carboxylate to the bridging water is 1.71Å and that between lysine 32 (of monomer C) and the bridging water is 3.46Å at this time point in the MD simulation (Robert Beahm and Hong Guo, personal communication).

additional ring stacking between the Q67H residues and the pteridine ring, resulting in tighter binding of DHF. When folate lacking the negatively charged groups is isolated, it can be reduced to the dihydro form. This can then be used as a substrate with the wild type enzyme and/ or the Q67H: 1+2+3+4 mutant. We may expect to see similar results as for binding of unmodified DHF to the K32M: 1+3 mutant and/ or the Q67H: 1+2+3+4 plus K32M: 1+3 mutant.

Redesigning The Active Site Of An Enzyme

The van't Hoff, Arrhenius plots and osmolyte experiments reported in this thesis provide information on how the ligands and transition state bind and the role of water in ligand binding. Since R67 DHFR has a single active site pore that can bind both ligands, the binding surface is promiscuous in nature. Using steady state kinetics, the catalytic efficiency of R67 DHFR has been determined to be $1.8 * 10^5$ s^{-1} M^{-1} (for $k_{cat}/K_{m(NADPH)}$) and $1.2 * 10^5$ s^{-1} M^{-1} (for $k_{cat}/K_{m(DHF)}$) (*32*) These values are lower than diffusion limited enzymes which possess k_{cat}/K_m values in the range of 10^7 to 10^8 s^{-1} M^{-1} (*33*).

Enzyme engineering involves improving or modifying enzymes to obtain desired binding and catalytic properties. Penning and Jez have discussed the following factors that must be considered for redesigning an enzyme (*34*): (1) Can the substrate specificity be changed without altering the catalytic efficiency and the overall reaction mechanism of the enzyme? (2) Can the stereochemistry of the substrate, cofactor or product be inverted? (3) Can alteration of the active site introduce catalysis of a new chemical reaction? (4) And finally, can the cofactor specificity be changed (for example from NADPH to NADH)?

In order to achieve the desired result (as described above), two complementary strategies are available: rational design and directed evolution. Rational design involves making changes in the amino acid sequence based on detailed knowledge of the protein structure (substitution of amino acids or changes in secondary structure to generate enzymes with desired properties). (*35*). This approach has been used for the generation of a superoxide dismutase with high catalytic efficiency (*36*). In the case of isocitrate dehydrogenase and isopropylmalate dehydrogenases, coenzyme specificities have been reversed using the rational design approach (*37-40*). Other examples involving redesign of the enzyme to attain better substrate specificity and /or catalytic efficiency are aspartate aminotransferase (*41*) and lactate dehydrogenase (*42*). However, many attempts using this approach have failed indicating that amino acid replacements should not be the only criterion when redesigning enzymes. Chen et al., have proposed that many cycles of mutagenesis are required to improve the properties of enzymes (*39*).

The site directed mutagenesis approach has been used in R67 DHFR (as described earlier) to identify the critical residues involved in ligand binding and catalysis (*2-5, 7, 9, 43*). One such example is the asymmetric K32M: 1+3 mutant which places two mutations on the same side of the pore (*7*). This mutant shows an increased K_m for DHF as well as NADPH binding. This likely indicates that NADPH has a preference for binding to the wild type side of the pore, while DHF binds to the mutant half of the pore. Therefore, addition of the K32M: 1+3 mutations results in the generation of different specificities for the substrate and cofactor for binding to half of the pore. Another example is that of the Q67H: 1+2+3+4 plus K32M: 1+3 multimutant in which the addition of the Q67H: 1+2+3+4 mutations to the K32M: 1+3 mutant resulted in tighter binding of DHF (table 1). Therefore the $Q67H_{full}K32M_{half}$ mutant rescues the weak binding of DHF (Feng and Howell, manuscript accepted).

Table 1. Comparison of kinetic parameters for Q67H, Y69F and K32M asymmetric mutants of Quad3 DHFR.

R67 DHFR Variant	k_{cat} (sec^{-1})	$K_{m\ (DHF)}$ (μM)	$K_{m\ (NADPH)}$ (μM)
Quad3	0.81 ± 0.02	6.7 ± 0.4	3.4 ± 0.4
Q67H: 1+4	0.15 ± 0.01	2.6 ± 0.5	0.95 ± 0.14
Q67H: 1+2+3+4	0.10 ± 0.01	0.13 ± 0.02	0.026 ± 0.004
K32M: 1+3	≥3.7	≥ 400	≥ 145
[a] $Q67H_{half}K32M_{half}$	1.7 ± 0.04	11 ± 0.7	29 ± 2
[b] $Q67H_{full}K32M_{half}$	0.49 ± 0.01	14 ± 0.9	9.6 ± 2.8

[a] $Q67H_{half}K32M_{half}$ = Q67H: 1+2+3+4 plus K32M: 1+3

[\b] $Q67H_{half}K32M_{half}$ = Q67H: 1+4 plus K32M: 1+3

Directed evolution, on the other hand, does not require information on how enzyme structure relates to its function. In this technique, error-prone PCR is used to create a library of mutagenized genes. Another technique that can be used is phage display. Genetic screening can then be employed to select for mutants with new and improved properties. In other words, this technique involves mimicking the natural evolution process. The usefulness of this technique is that it searches through sequence space to obtain the desired result. This is advantageous in proteins where a clear prediction on how to engineer a protein cannot be made due to lack of structural or mechanistic information. One limitation of this technique is the requirement of an efficient screening method to identify a large number of potential mutants.

In R67 DHFR, combinatorial mutagenesis has been carried out, where 16 principal amino acids (encoded by residues 66 to 69 in all four monomers) that constitute the active site were mutated. Out of 5000 combinatorially mutated active site variants, three variants were selected due to their ability to confer TMP resistance (*44*). When they were kinetically characterized, it was observed that the k_{cat} and K_m values were similar to those of the wild type enzyme, indicating that the catalytic efficiency was not affected despite many mutations. This effect is in contrast to that obtained by single point mutations. Directed evolution can also be applied to other R67 DHFR variants such that an enzyme with a higher catalytic efficiency is generated. For example, the Q67H mutant has a good catalytic efficiency and tight DHF and NADPH binding (*3, 43*). Can random mutations be introduced around at valine 66, isoleucine 68 and tyrosine 69, such that a mutant with a higher catalytic efficiency is obtained? In this way, evolution in nature can be mimicked to obtain a more efficient enzyme.

Drug Design

Structure based drug design methods identify favorable and unfavorable interactions between the ligand and protein so as to maximize beneficial interactions that increase binding affinity. Therefore based on the structural determinants for ligand binding, we can design ligands that can inhibit the catalytic reaction of R67 DHFR. For example, since the pABA-glutamate tail of DHF is disordered, we can perhaps replace it by a moiety that is more rigid and also makes contacts with the lysine residue. One such moiety can be the NADPH tail region itself. This moiety contains phosphate groups that form ionic interactions with the lysine residues in the enzyme. Therefore, a chimeric substrate can be generated with potentially improved binding characteristics. Chimeric substrates have been employed in other instances in designing inhibitors that can effectively inhibit the enzyme (*45*).

From Chapter 2, temperature dependent studies have been performed to determine the energetics of ligand binding in the ground state and transition state. Results from these studies suggest that the entropy of binding is increased in the transition state as compared to the ground state. Therefore, the ligands likely reorient themselves to gain access to the transition state. Analogs mimicking the transition state can serve as potent inhibitors as they bind more tightly to the enzyme (*46*). For example, immucillin-H is a transition state analogue of the enzyme purine nucleoside phosphorylase (PNP) (*47, 48*). Using kinetic isotope effects Vern Schramm demonstrated that DADMe-immucillin-H is a more potent inhibitor of human-PNP as compared to immucillinH (*47, 48*). Moreover, DADMe-immucillin-H is 8 times more specific towards human PNP as compared to bovine PNP. Therefore, kinetic isotope effects along with molecular dynamic simulations can aid in providing detailed information on the transition state, which can be used for designing inhibitors for R67 DHFR.

As discussed in chapter 3, water molecules are involved in DHF and NADPH binding in R67 DHFR. In general, water molecules involved in ligand binding can be classified into two categories: those that are readily displaced by binding of ligands and those that are 'conserved' and never displaced (*49*). The latter category of tightly bound, conserved water molecules can be considered as an integral part of the protein, which provide hydrogen-bonding contacts for ligand binding to the enzyme. Using this information, different types of inhibitors can be designed. An example of an inhibitor utilizing a water molecule for binding is KNI-272 (an inhibitor of HIV-1 protease), one of the key targets for the treatment of AIDS (*50*). KNI-272 makes contacts with HIV-1 protease to the enzyme via a bridging water molecule (as shown by the crystal structure). On the other hand, DMP450 is an inhibitor of HIV-1 protease which uses a carbonyl group to maintain its hydrogen-bonding network with the protein, and it does so by excluding water molecules. The displacement of a key water molecule by insertion of a carbonyl group should be entropically unfavorable (due to desolvation cost for the carbonyl group). However, this does not occur as DMP-450 contains two less carbonyl groups as compared to KNI-272. Thus, the overall desolvation cost for DMP-450 is low resulting in favorable binding.

In R67 DHFR, water is required for binding of DHF (chapter 3). Also MD simulations predict that one of the possible ways in which the disordered tail of DHF can interact with the K32 residue on the protein is via a solvent separated ion-pair (Beahm and Guo, personal communication). Moreover, weaker binding affinity as well as decrease in binding enthalpy has been observed when the length of the pABA-glu tail of DHF is shortened (*6*). A parallel study using the K32M: 1+3 asymmetric mutant also showed weak binding affinity of DHF (*7*). However, when Q67H mutations were added to the K32M: 1+3 construct (Q67H: 1+2+3+4 plus K32M: 1+3 multimutant), tighter binding of DHF was observed as well as a large, negative binding enthalpy (Feng and Howell, manuscript accepted). Observation of a binding enthalpy in

the absence of ionic interactions of the DHF tail with the K32 residue of R67 DHFR suggests that water and/or ring stacking may be providing the binding enthalpy. Overall, these observations indirectly suggest that water molecules are playing important role in interaction of DHF with the protein.

For drug design, it would be interesting to identify conserved water molecules involved in DHF and/ or NADPH binding. Crystallography studies have been performed in R67 DHFR and have provided information on water molecules involved in substrate and cofactor binding. For example, a crystal structure of the Q67H mutant of R67 DHFR in complex with $NADP^+$ shows a number of water molecules mediating interactions between the cofactor and the enzyme (*51*). Of these, binding of NADPH to the apo enzyme causes displacement of water 149. However, the symmetry related water 149 in the vacant paired site remains and is proposed to form hydrogen-bonding interactions with the O7 atom of NADPH. Thus the symmetry related water 149 plays an important role in mediating interactions of the NADPH with R67 DHFR. When the second molecule of NADPH binds, this water molecule is also displaced and hence the weaker binding affinity observed. Therefore, loss of hydrogen bonding interactions by water 149 in both bound cofactor molecules, may explain the negative cooperativity observed for binding of 2 NADPH molecules.

For designing a mimic of NADPH, water 149 can be considered. Ligands can be designed that will form interactions with this conserved water molecule so as to form tight interactions with the enzyme. Alternatively ligands can be designed that will mimic the hydrogen bonding interactions of the conserved water by excluding it. A similar approach can be used to design inhibitors mimicking the substrate, DHF.

References

(1) Pattishall, K. H., Acar, J., Burchall, J. J., Goldstein, F. W., and Harvey, R. J. (1977) Two distinct types of trimethoprim-resistant dihydrofolate reductase specified by R-plasmids of different compatibility groups. *J Biol Chem 252*, 2319-2323.

(2) Strader, M. B., Smiley, R. D., Stinnett, L. G., VerBerkmoes, N. C., and Howell, E. E. (2001) Role of S65, Q67, I68, and Y69 residues in homotetrameric R67 dihydrofolate reductase. *Biochemistry 40*, 11344-11352.

(3) Strader, M. B., Chopra, S., Jackson, M., Smiley, R. D., Stinnett, L., Wu, J., and Howell, E. E. (2004) Defining the binding site of homotetrameric R67 dihydrofolate reductase and correlating binding enthalpy with catalysis. *Biochemistry 43*, 7403-7412.

(4) Hicks, S. N., Smiley, R. D., Hamilton, J. B., and Howell, E. E. (2003) Role of ionic interactions in ligand binding and catalysis of R67 dihydrofolate reductase. *Biochemistry 42*, 10569-10578.

(5) Smiley, R. D., Stinnett, L. G., Saxton, A. M., and Howell, E. E. (2002) Breaking symmetry: mutations engineered into R67 dihydrofolate reductase, a D2 symmetric homotetramer possessing a single active site pore. *Biochemistry 41*, 15664-15675.

(6) Jackson, M., Chopra, S., Smiley, R. D., Maynord, P. O., Rosowsky, A., London, R. E., Levy, L., Kalman, T. I., and Howell, E. E. (2005) Calorimetric studies of ligand binding in R67 dihydrofolate reductase. *Biochemistry 44*, 12420-12433.

(7) Hicks, S. N., Smiley, R. D., Stinnett, L. G., Minor, K. H., and Howell, E. E. (2004) Role of Lys-32 residues in R67 dihydrofolate reductase probed by asymmetric mutations. *J. Biol. Chem. 279*, 46995-47002.

(8) Chopra, S., Lynch, R., Kim, S. H., Jackson, M., and Howell, E. E. (2006) Effects of temperature and viscosity on R67 dihydrofolate reductase catalysis. *Biochemistry 45*, 6596-6605.

(9) Howell, E. E., Shukla, U., Hicks, S. N., Smiley, R. D., Kuhn, L. A., and Zavodszky, M. I. (2001) One site fits both: a model for the ternary complex of folate + NADPH in R67 dihydrofolate reductase, a D2 symmetric enzyme. *J. Comput. Aided Mol. Des. 15*, 1035-1052.

(10) Liang, J., Edelsbrunner, H., and Woodward, C. (1998) Anatomy of protein pockets and cavities: measurement of binding site geometry and implications for ligand design. *Protein Sci 7*, 1884-1897.

(11) Narayana, N. (2006) High-resolution structure of a plasmid-encoded dihydrofolate reductase: pentagonal network of water molecules in the D2-symmetric active site. *Acta Crystallogr D Biol Crystallogr 62*, 695-706.

(12) Krahn, J., Jackson M., DeRose, E.F., Howell, E.E., and London, R.E. (Accepted) Structure of TypeII Dihydrofolate reductase ternary complex: use of identical binding sites for unrelated ligands. *Biochemistry*.

(13) Janin, J. (1999) Wet and dry interfaces: the role of solvent in protein-protein and protein-DNA recognition. *Structure 7*, R277-279.

(14) Tanaka, H. (1998) Simple physical explanation of the unusual thermodynamic behavior of liquid water. *Phys Rev Letts 80*, 5750-5753.

(15) Dashnau, J. L., Sharp, K. A., and Vanderkooi, J. M. (2005) Carbohydrate intramolecular hydrogen bonding cooperativity and its effect on water structure. *J Phys Chem B 109*, 24152-24159.

(16) Sidorova, N. Y., Muradymov, S., and Rau, D. C. (2006) Differences in hydration coupled to specific and nonspecific competitive binding and to specific DNA Binding of the restriction endonuclease BamHI. *J Biol Chem 281*, 35656-35666.
(17) Sidorova, N. Y., and Rau, D. C. (2004) Differences between EcoRI nonspecific and "star" sequence complexes revealed by osmotic stress. *Biophys J 87*, 2564-2576.
(18) Bennion, B. J., DeMarco, M. L., and Daggett, V. (2004) Preventing misfolding of the prion protein by trimethylamine N-oxide. *Biochemistry 43*, 12955-12963.
(19) Beck, D. A., Bennion, B. J., Alonso, D. O., and Daggett, V. (2007) Simulations of macromolecules in protective and denaturing osmolytes: properties of mixed solvent systems and their effects on water and protein structure and dynamics. *Methods Enzymol 428*, 373-396.
(20) Courtenay, E. S., Capp, M. W., Anderson, C. F., and Record, M. T., Jr. (2000) Vapor pressure osmometry studies of osmolyte-protein interactions: implications for the action of osmoprotectants in vivo and for the interpretation of "osmotic stress" experiments in vitro. *Biochemistry 39*, 4455-4471.
(21) Chervenak, M. C., and Toone, E. J. (1995) Calorimetric analysis of the binding of lectins with overlapping carbohydrate-binding ligand specificities. *Biochemistry 34*, 5685-5695.
(22) Pineda, J. R., Callender, R., and Schwartz, S. D. (2007) Ligand binding and protein dynamics in lactate dehydrogenase. *Biophys J 93*, 1474-1483.
(23) Garcia-Viloca, M., Truhlar, D. G., and Gao, J. (2003) Reaction-path energetics and kinetics of the hydride transfer reaction catalyzed by dihydrofolate reductase. *Biochemistry 42*, 13558-13575.
(24) Torrie, G. M., Valleau, J. P. (1974) Monle Carlo free energy estimates using non-Boltzmann sampling: application to the sub-critical Lennard-Jones fluid. *Chem. Phys. Lett 28* 578-581.
(25) Brooks, B. R. B., R. E.; Olafson, B. D.; States, D. J.; Swaminathan,, and S.; Karplus, M. J. (1983) CHARMM: A program for macromolecular energy, minimization, and dynamics calculations. *4*, 187-217.
(26) Kumar, M. B., D.; Swendsen, R. H.; Kollman, P. A.; Rosenberg, J., and M. (1992) The Weighted Histogram Analysis Method for Free-Energy calculations on Biomolecules. . *J. Comput. Chem 13*, 1011-1021
(27) Narayana, N., Matthews, D. A., Howell, E. E., and Nguyen-huu, X. (1995) A plasmid-encoded dihydrofolate reductase from trimethoprim-resistant bacteria has a novel D2-symmetric active site. *Nat Struct Biol 2*, 1018-1025.
(28) Pitcher, W. H., 3rd, DeRose, E. F., Mueller, G. A., Howell, E. E., and London, R. E. (2003) NMR studies of the interaction of a type II dihydrofolate reductase with pyridine nucleotides reveal unexpected phosphatase and reductase activity. *Biochemistry 42*, 11150-11160.
(29) Grabarek, Z., and Gergely, J. (1990) *Analytical Biochemistry 185*, 131-135.
(30) Hicks, S. N., Smiley, R. D., Stinnett, L. G., Minor, K. H., and Howell, E. E. (2004) Role of Lys-32 residues in R67 dihydrofolate reductase probed by asymmetric mutations. *J Biol Chem 279*, 46995-47002.
(31) Wang, S., Luo, J., Lantrip, D., Waters, D., Mathias, C., Green, M., Fuchs, P., and Low, P. (1997) Design and synthesis of [111In]DTPA-folate for use as a tumor-targeted radiopharmaceutical. *Bioconjugate Chemistry 8*, 673-679.
(32) Reece, L. J., Nichols, R., Ogden, R. C., and Howell, E. E. (1991) Construction of a synthetic gene for an R-plasmid-encoded dihydrofolate reductase and studies on the role of the N-terminus in the protein. *Biochemistry 30*, 10895-10904.
(33) Fersht, A. (1985) *Enyzme Structure and Mechanism*, W.H. Freeman and Company, New York.

(34) Penning, T. M., and Jez, J. M. (2001) Enzyme redesign. *Chem Rev 101*, 3027-3046.
(35) Chen, R. (2001) Enzyme engineering: rational redesign versus directed evolution. *Trends Biotechnol 19*, 13-14.
(36) Pinto, A. L., Hellinga, H. W., and Caradonna, J. P. (1997) Construction of a catalytically active iron superoxide dismutase by rational protein design. *Proc Natl Acad Sci U S A 94*, 5562-5567.
(37) Chen, R., Greer, A., and Dean, A. M. (1995) A highly active decarboxylating dehydrogenase with rationally inverted coenzyme specificity. *Proc Natl Acad Sci U S A 92*, 11666-11670.
(38) Hurley, J. H. (1996) The sugar kinase/heat shock protein 70/actin superfamily: implications of conserved structure for mechanism. *Annu Rev Biophys Biomol Struct 25*, 137-162.
(39) Chen, R. (1999) A general strategy for enzyme engineering. *Trends Biotechnol 17*, 344-345.
(40) Doyle, S. A., Fung, S. Y., and Koshland, D. E., Jr. (2000) Redesigning the substrate specificity of an enzyme: isocitrate dehydrogenase. *Biochemistry 39*, 14348-14355.
(41) Yano, T., Oue, S., and Kagamiyama, H. (1998) Directed evolution of an aspartate aminotransferase with new substrate specificities. *Proc Natl Acad Sci U S A 95*, 5511-5515.
(42) Nicholls, D. J., Davey, M., Jones, S. E., Miller, J., Holbrook, J. J., Clarke, A. R., Scawen, M. D., Atkinson, T., and Goward, C. R. (1994) Substitution of the amino acid at position 102 with polar and aromatic residues influences substrate specificity of lactate dehydrogenase. *J Protein Chem 13*, 129-133.
(43) Stinnett, L. G., Smiley, R. D., Hicks, S. N., and Howell, E. E. (2004) "Catch 222," the effects of symmetry on ligand binding and catalysis in R67 dihydrofolate reductase as determined by mutations at Tyr-69. *J. Biol. Chem. 279*, 47003-47009.
(44) Schmitzer, A. R., Lepine, F., and Pelletier, J. N. (2004) Combinatorial exploration of the catalytic site of a drug-resistant dihydrofolate reductase: creating alternative functional configurations. *Protein Eng. Des. Sel. 17*, 809-819.
(45) Shi, G., Blaszczyk, J., Ji, X., and Yan, H. (2001) Bisubstrate analogue inhibitors of 6-hydroxymethyl-7,8-dihydropterin pyrophosphokinase: synthesis and biochemical and crystallographic studies. *J Med Chem 44*, 1364-1371.
(46) Wolfenden, R. (1999) Conformational aspects of inhibitor design: enzyme-substrate interactions in the transition state. *Bioorg. Med. Chem. 7*, 647-652.
(47) Schramm, V. L. (2005) Enzymatic transition states: thermodynamics, dynamics and analogue design. *Arch Biochem Biophys 433*, 13-26.
(48) Schramm, V. L. (2007) Enzymatic transition state theory and transition state analogue design. *J Biol Chem 282*, 28297-28300.
(49) Essex, J. W., Hann, M. M., and Richards, W. G. (1994) Molecular dynamics simulation of a hydrated phospholipid bilayer. *Philos Trans R Soc Lond B Biol Sci 344*, 239-260.
(50) Li, Z., and Lazaridis, T. (2003) Thermodynamic contributions of the ordered water molecule in HIV-1 protease. *J Am Chem Soc 125*, 6636-6637.
(51) Divya, N., Grifith, E., and Narayana, N. (2007) Structure of the Q67H mutant of R67 dihydrofolate reductase-NADP+ complex reveals a novel cofactor binding mode. *Protein Sci 16*, 1063-1068.

Vita

Shaileja Chopra was born in 1976 in Mumbai (formerly Bombay), India. She attended Sacred Heart School and Father Agnel Junior College in Mumbai. She then obtained her Bachelor's degree in Microbiology from the University of Mumbai. After completing her Bachelor's degree, she went on to successfully pursue a Masters Degree in Analytical Chemistry from SNDT Women's University, Mumbai. Shaileja then joined the University of Tennessee, Knoxville to obtain her doctoral degree in Biochemistry, Cell and Molecular Biology. Upon completion of her doctoral degree, she plans to pursue post-doctoral research.